

Energy Harvesting by Using Piezoelectric Flag behind C- Cylinders in Side by Side Arrangement



Author

Muhammad Saad Idrees

Regn. Number

273730

Supervisor

Dr. Emad Uddin

DEPARTMENT OF MECHANICAL ENGINEERING
SCHOOL OF MECHANICAL & MANUFACTURING ENGINEERING
NATIONAL UNIVERSITY OF SCIENCES AND TECHNOLOGY
ISLAMABAD
SEPTEMBER, 2020

Energy Harvesting by Using Piezoelectric Flag behind C-Cylinders in
Side by Side Arrangement

Author

Muhammad Saad Idrees

Regn Number

273730

A thesis submitted in partial fulfillment of the requirements for the degree of
MS Mechanical Engineering

Thesis Supervisor:

Dr. Emad Uddin

Thesis Supervisor's Signature: _____

DEPARTMENT OF MECHANICAL ENGINEERING
SCHOOL OF MECHANICAL & MANUFACTURING ENGINEERING
NATIONAL UNIVERSITY OF SCIENCES AND TECHNOLOGY,
ISLAMABAD

September, 2020

THESIS ACCEPTANCE CERTIFICATE

It is certified that final copy of MS thesis written by Muhammad Saad Idrees (Registration No. 273730), of SMME (National University of science and Technology) has been vetted by undersigned, found complete in all respects as per NUST Statues/Regulations, is free of plagiarism, errors, and mistakes and is accepted as partial fulfillment for award of MS degree. It is further certified that necessary amendments as pointed out by GEC members of the scholar have also been incorporated in this dissertation.

Signature: _____

Name of Supervisor: Dr. Emad Uddin

Date: _____

Signature (HoD): _____

Date: _____

Declaration

I certify that this research work titled “*Energy Harvesting by Using Piezoelectric Flag behind C-Cylinders in Side by Side Arrangement*” is my own work. The work has not been presented elsewhere for assessment. The material that has been used from other sources it has been properly acknowledged / referred.

Signature of Student
Muhammad Saad Idrees
NUST-Ms-Mech-18

Plagiarism Certificate (Turnitin Report)

This thesis has been checked for Plagiarism. Turnitin report endorsed by Supervisor is attached.

Signature of Student

Muhammad Saad Idrees

Registration Number

273730

Signature of Supervisor

Copyright Statement

- Copyright in text of this thesis rests with the student author. Copies (by any process) either in full, or of extracts, may be made only in accordance with instructions given by the author and lodged in the Library of NUST School of Mechanical & Manufacturing Engineering (SMME). Details may be obtained by the Librarian. This page must form part of any such copies made. Further copies (by any process) may not be made without the permission (in writing) of the author.
- The ownership of any intellectual property rights which may be described in this thesis is vested in NUST School of Mechanical & Manufacturing Engineering, subject to any prior agreement to the contrary, and may not be made available for use by third parties without the written permission of the SMME, which will prescribe the terms and conditions of any such agreement.
- Further information on the conditions under which disclosures and exploitation may take place is available from the Library of NUST School of Mechanical & Manufacturing Engineering, Islamabad.

Acknowledgements

I am thankful to my Creator Allah Subhana-Watala to have guided me throughout this work at every step and for every new thought which You setup in my mind to improve it. Indeed I could have done nothing without Your priceless help and guidance. Whosoever helped me throughout the course of my thesis, whether my parents or any other individual was Your will, so indeed none be worthy of praise but You.

I am profusely thankful to my beloved parents Baba Jaan and Ammi who raised me when I was not capable of walking and continued to support me throughout in every department of my life.

I would also like to express special thanks to my supervisor Dr. Emad Uddin for his help throughout my thesis. I can safely say that I haven't seen so talented and yet so down to earth person in my whole life.

I would also like to pay special thanks to Ali Anjum for his tremendous support and cooperation. Each time I got stuck in something, he came up with the solution. Without his help I wouldn't have been able to complete my thesis. I appreciate his patience and guidance throughout the whole thesis.

I would also like to thank Dr Samiur Rahman, Dr. Zaib Ali and Dr. Muhammad Sajid for being on my thesis guidance and evaluation committee and express my special thanks to Usman Latif for his help. I am also thankful to Abdul Raheem and Ahmed Nawaz for their support and cooperation.

Finally, I would like to express my gratitude to all the individuals who have rendered valuable assistance to my study.

For my brother
Humzah,
who lived in me throughout

Abstract

Since the start of last half century people working on the power production and researchers in energy sector have started paying serious attentions towards the harms of power production from traditional methods such as burning of fuel, coal and oil. During these years, non-traditional ways of producing power such as from renewable energy sources like sun, wind, water etc. have gained a lot of attention due to its environment friendly procedure, less or no pollution, less cost, availability in excess and green nature of energy. The purpose of this study is the energy harvesting using piezoelectric eel behind two cylinders in side by side arrangement. The improvement in power generation by vibrations caused by vortices is studied by performing a series of water-tunnel experiments. Two side by side cylinders in a staggered arrangement, with varied center-to-center gaps are placed in the water tunnel with the fluid flowing uniformly and electrical power is obtained using the vibrating behaviour of the piezoelectric eel caused by vortices in the downstream region. The poor and optimal coupling of different flapping modes with wake flow is observed in the experimental results. It is also demonstrated that the streamwise distance between the fixed end of piezoelectric eel and the line joining the centers of the staggered cylinders, and the center-to-center gap between cylinders have a significant effect on the flapping frequency and amplitude, resulting variation of the output power of piezoelectric eel. The experiments are carried out for cylinder diameter, $D = 25 \text{ mm}$ and flag length, $L = 60 \text{ mm}$ resulting $L/D = 2.4$. Different cases with varying N/D values from 1.00 to 2.00 for different values of G_x from 2.0 to 4.0 were tested. The comparison of flapping and amplitude response at each point for all cases is made to understand the effects of system's variable parameters on the results and their trends. The power generated at each point was mainly focused for all cases and their comparative study to find optimal configuration. For the low given fluid speed and the cylinder arrangement with $N/D = 1.00 - 1.25$, the continues oscillations and higher output power persisting for a wide range $G_x = 2.0 - 4.0$ was observed, which makes its application in the real-life systems feasible, as air and water usually flow at lower speeds. It is observed that the output power increases with the increase in streamwise gap between cylinders and eel till $G_x = 4.0$, higher values were obtained at $G_x = 3.5 - 4.0$ for the velocity, $U_\infty = 0.31 \text{ m/s}$, with $N/D = 1.00 - 1.25$. The power generated by these configurations ranges from $5.15 \mu\text{W}$ to $5.50 \mu\text{W}$. Hence, the stated configurations with $N/D =$

1.00 – 1.25 gives a significant advantage over other arrangements as a vibration source of energy harvesting from the flowing water, and the generated power would gradually increase with the streamwise distance. The harvested power comes totally from the renewable sources of energy, does not have any harmful effect on the environment, atmosphere or ecosystem, and can replace small trickle charge and chemical batteries for powering micro electromechanical sensors like the sensors used for structural health monitoring in the remote areas. All in all, this study makes an effective contribution to the field of energy harvesting from striking vortices by setting the streamwise distance and center-to-center distance gap the staggered cylindrical bluff bodies.

Key Words: *Staggered cylinders, Piezoelectric flag, Piezoelectric eel, Energy harvesting, Shedding frequency, Wake flow, Water tunnel testing, Renewable energy, Vortex induced vibrations*

Table of Contents

Declaration	i
Plagiarism Certificate (Turnitin Report)	iii
Copyright Statement	iv
Acknowledgements	v
Abstract	vii
Table of Contents	ix
List of Figures	xii
List of Tables	xv
CHAPTER 1: INTRODUCTION	1
1.1 Overview and Motivation.....	1
1.2 General Goal of the Thesis.....	6
1.3 General Structure and Outline of the Thesis	6
CHAPTER 2: BASICS OF FLUID ENERGY CONVERSION AND FLUID MECHANICS	8
2.1 Energy Conversion.....	8
2.2 Renewable Energy Sources	8
2.2.1 Wind Energy	10
2.2.2 Hydropower	13
2.3 Characteristics of Fluid	16
2.4 Properties of Fluids	17
2.4.1 Density	17
2.4.2 Pressure	18
2.4.3 Viscosity	18
2.5 Pattern of Flow	19
2.5.1 Streamline	19
2.5.2 Path line	19
2.5.3 Streak line	20
2.6 Classification and Description of Fluid Flow	20
2.6.1 One, two- and three-dimensional flows	20
2.6.2 Internal and external flow	20

2.6.3	Laminar and turbulent flow	21
2.6.4	Viscous and inviscid flow	21
2.6.5	Steady and unsteady flow	22
2.6.6	Compressible and incompressible flow	22
2.7	Fluid Solid Interaction (FSI)	22
2.7.1	Boundary layer	22
2.7.2	Boundary layer separation	24
2.7.3	Vortex formation.....	24
2.7.4	Separation region	25
2.7.5	Bluff body shape effect.....	25
2.7.6	Vortex street.....	25
2.7.7	Basic terminologies.....	27
CHAPTER 3: VIBRATION ENERGY HARVESTERS AND PIEZOELECTRICITY		29
3.1	Introduction	29
3.2	Electromagnetic Energy Harvester.....	30
3.3	Electrostatic Energy Harvester.....	31
3.4	Piezoelectric Energy Harvester	32
3.5	Comparison of Different Harvesters	34
CHAPTER 4: ENERGY HARVESTING FROM ENERGY HARVESTING EEL BEHIND TWO SIDE BY SIDE SOLID CYLINDERS IN STAGGER ARRANGEMENT		36
4.1	Introduction	36
CHAPTER 5: EXPERIMENTAL SETUP		39
5.1	Apparatus Description.....	39
5.1.1	Low-speed closed-circuit water channel.....	39
5.1.2	Data acquisition	43
5.2	Experimental Setup	45
CHAPTER 6: RESULTS AND DISCUSSION		50
6.1	Piezoelectric Eel's Flapping, Amplitude and Frequency Response.....	50
6.2	Piezoelectric Eel's Non-Dimensional Amplitude and Frequency of Flapping	60
6.3	Voltage and Power Produced by the Piezoelectric Eel's Flapping	61
CHAPTER 7: CONCLUSION AND FUTURE RECOMMENDATIONS		65
7.1	Conclusion.....	65
7.2	Future Recommendations.....	66
APPENDIX A		68

A-1	Video Processing.....	68
A-2	Frequency and Amplitude Response Visualization	69
A-3	Measurement of Flapping Amplitude	71
REFERENCES.....		72

List of Figures

Figure 1.1: World's total primary energy supply in (a) 1973 (b) 2017, by source [1]	2
Figure 1.2: Global average temperature anomaly ($^{\circ}C$) relative to pre-industrial era, over the time span from 1850 to 2015 AD [1].....	3
Figure 1.3: Global CO_2 emission by source from 1800 to 2018 AD [1]	3
Figure 1.4: Prices of coal, oil and natural gas from 1950 to 2008 AD [1]	4
Figure 1.5: Rise in nuclear power production from 1970 to 2018 AD by region [1].....	4
Figure 2.1: Different types and forms of energy [9].....	9
Figure 2.2: Renewable and non-renewable sources of energy [11].....	9
Figure 2.3: Common types of VAWTs (a) Savonius (b) Darrieus-rotor (c) H-Darrieus (d) Helix shape [17].....	11
Figure 2.4: Types of HAWT (a) single-blade (b) double-blade (c) three-blade (d) five-blade [19]	12
Figure 2.5: Installation diagram for (a) low head (b) medium head (c) high head hydropower plant [25].....	14
Figure 2.6: Types of hydraulic turbines on the basis of mechanism, flow, speed and head [28]	15
Figure 2.7: Hydraulic turbine application chart [29]	16
Figure 2.8: The relationship between absolute and gauge pressure with reference to the atmospheric pressure [35]	18
Figure 2.9: Migration of molecules between two layers of fluid which causes the friction between layers (viscosity) [37]	19
Figure 2.10: Stream, path and streak lines in the fluid flow [38], [39].....	20
Figure 2.11: Types of flow (a) internal flow (b) external flow (c) streamline flow (d) turbulent flow [41].....	21
Figure 2.12: Boundary layer formation in the flow over a flat plate [41]	22
Figure 2.13: Boundary layer separation process [46]	23

Figure 2.14: Vortex formation (a) from a circular cylinder (b) from a sharp edge obstacle [44]	24
Figure 2.15: Separation region when fluid flow over a cylinder [41]	25
Figure 2.16: Vortex shedding from circular cylinder [41]	26
Figure 2.17: Basic terminologies in vortices (a) vorticity (b) vortex line (c) vortex tube (c) vortex filament (d) vortex sheet [51]	27
Figure 3.1: Types of vibration energy harvesters [57]	30
Figure 3.2: Schematic diagram of vibration based of electromagnetic energy harvester [58]	30
Figure 3.3: Types of vibration based electromagnetic energy harvesters [58]	31
Figure 3.4: Schematic diagram of vibration based electrostatic energy harvester [60]	31
Figure 3.5: Types of electrostatic energy harvester [59]	32
Figure 3.6: Schematic diagram of vibration based piezoelectric energy harvester [62]	33
Figure 3.7: Stages involved in piezoelectric effect (a) before, (b) during and (c) after the application of stress [64]	33
Figure 3.8: Types of piezoelectric effect [65]	34
Figure 5.1: A closed loop water tunnel by <i>AEROLAB</i> with nominal speed 9.1 m/sec [100]	40
Figure 5.2: Schematic diagram of a simple data acquisition setup consisting of a sensor, DAQ device and a computer, by National Instruments (NI) [101]	43
Figure 5.3: (a) Complete experimental setup, (b) Schematic diagram of the piezoelectric eel placed behind two staggered cylinders, and (c) Schematic diagram of the whole experimental setup [6]	45
Figure 5.4: Arrangement of piezoelectric eel/flag behind two staggered cylinders of diameter D and separated by distance N , place at the distance Gx * in the fluid moving with the free stream velocity U_{∞}	47
Figure 5.5: The circuit diagram showing a voltage source (piezoelectric eel/flag) connected with the load resistor RL with the voltage drop VL [6]	48
Figure 5.0.6: <i>LabVIEW</i> circuit of the data acquisition setup	49

Figure 6.1: The results of the experimental cases for a range of Gx with different values of N/D ,
(a) Non-dimensional amplitude of flapping (b) Normalized frequency of flapping 60

Figure 5.2: The instantaneous voltages produced by eel in the case with $N/D = 1.00$ and $Gx = 2.0$, as recorded by the DAQ setup 62

Figure 6.3: Voltages and power produced by the piezoelectric eel for the different cases of the experimentation..... 63

List of Tables

Table 2-1: Distinctions between fluids and solid [31]	17
Table 2-2: Distinctions between two different phases of fluids i.e. liquids & gases [32]	17
Table 2-3: Drag coefficients for different types of bluff bodies [48]	26
Table 3-1: Sources of vibrations [53]	29
Table 3-2: Comparison of the advantages and disadvantages of the vibration-based energy harvesters of different types [4], [66], [67].....	35
Table 5-1: Physical properties of piezoelectric eel and its material [6].....	47
Table 5-0-2: Experimental system's parameters	48
Table 6-1: The results for the flapping, amplitude and the normalized frequencies of the piezoelectric eel, obtained by processing the captured video shots of the different testing cases using the <i>MATLAB</i> codes available in the Appendix A.....	51

CHAPTER 1: INTRODUCTION

The research work in this dissertation deals with the “energy harvesting using piezoelectric flag behind two cylinders in side by side arrangement”. The study includes the holistic and comprehensive literature review of the topic, development of experimental and data acquisition setup, experimentation on different configurations of eel and cylinders under different conditions, visualization of result, discussion on the observed behavior of the system and obtained results, concluding remarks, future recommendations and a brief insight into the potential environmental and societal impact of the research work. This chapter of the dissertation gives an insight to the motivation behind the study, the goals of the research work and a general outline of the thesis.

1.1 Overview and Motivation

The natural form of energy contained in raw fuels such as oil, coal and natural gas, minerals such as uranium and thorium, and other resources such as solar radiations, wind, biomass, geothermal, waves, tides, falling and flowing water, may be referred as the primary energy. It is the form of energy that has not been subjected to any human engineered conversion process. It can be renewable or non-renewable.[1]

Fossil fuels are the most common sources of energy. They are usually formed by natural processes, such as decomposition of buried dead organism including plants and animals, under high pressure and temperature conditions.[2] They release energy during combustion, therefore, the energy demanding sectors like electricity, transportation, heating and industries rely on fossil fuels such as oil, natural gas and coal.[3] More than 75 % of world’s energy comes from these fossil fuels. According to the World Energy Balance statistics published by International Energy Agency (IEA) in 2019, world’s total primary energy supply (TPES) in 1973 was 6097 *Mtoe*¹ which increased by more than 100 % till 2017 and reached the value of 13972 *Mtoe*. In 1973,

¹ The tonne of oil equivalent (*toe*) is a unit of energy defined as the amount of energy released by burning one tonne of crude oil. It is approximately 42 gigajoules or 11.630 megawatt-hours, although as different crude oils have different calorific values, the exact value is defined by convention; several slightly different definitions exist. The *toe* is sometimes used for large amounts of energy.

86.8 % of world's TPES while in 2017, 81.3 % of world's TPES was obtained from common fossil fuels such as oil, natural gas and coal, as shown in the detailed pie chart given in figure 1.1 (a) & (b), respectively. [1], [3]

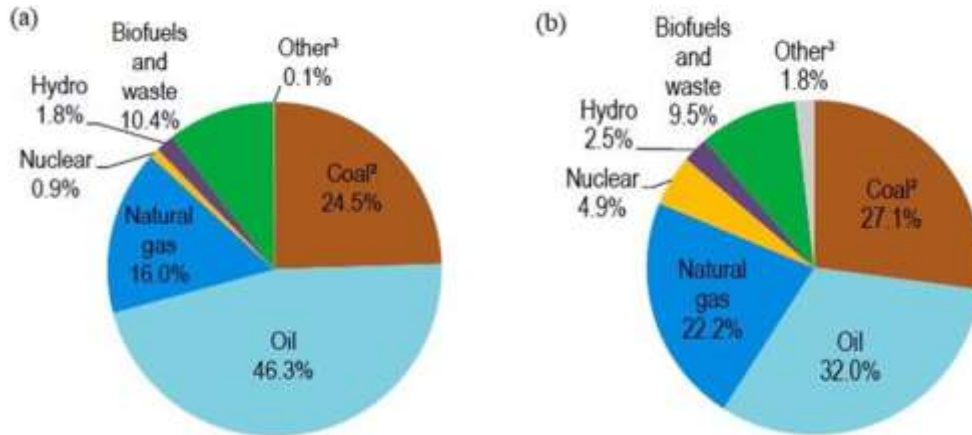


Figure 1.1: World's total primary energy supply in (a) 1973 (b) 2017, by source [1]

As, the demand for energy have increased immensely, hence the consumption of fossil fuels is increasing by the same rate. This fact has given rise to the new concerns especially that the world will run out of the all available reserves of the fossil fuels within the next one century. The data published by BP Statistical Review of World Energy 2016 shows that the world will run out of oil in 50 years, natural gas in 52 years and coal in 114 years from now on. Hence, fossil fuels are not sustainable and forever-lasting sources of energy. [1]

The harms of fossil fuels to environment such as air pollution, unpleasant incidents like mining accidents, and the longer run unsustainability related with them were not considered with much of the seriousness until the start of activism during 1970s. High temperature, changing rainfall, change in nature, melting sea ice, generation of pollutants, and greenhouse gases are some environmental issues associated with the non-renewable energy resources. [4] The global average temperature has increased by more than 1°C since pre-industrial times, as shown in figure 1.2.

Carbon dioxide emissions remain trapped in the atmosphere for long periods of time, building up an atmospheric stock that leads temperatures to rise. The main contribution of emission of CO_2

to the atmosphere is due to the burning of fossil fuel, as shown in figure 1.3. It is interesting to note that on the one hand fossil fuels are causing a major climate change, the effects of that global climate change are in turn responsible for limiting fossil fuel production. There is a need to reduce such emissions to prevent global climate change. [3]

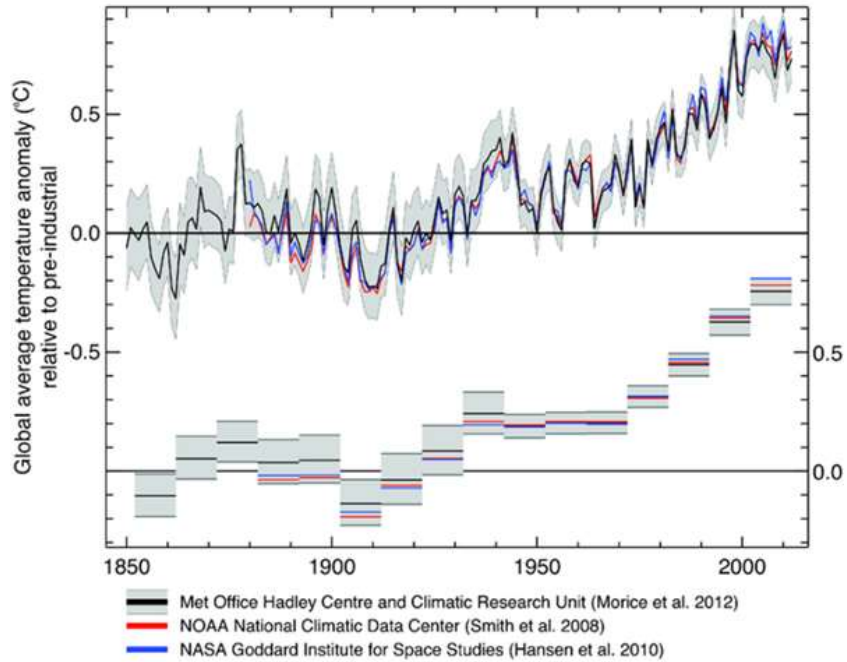


Figure 1.2: Global average temperature anomaly (°C) relative to pre-industrial era, over the time span from 1850 to 2015 AD [1]

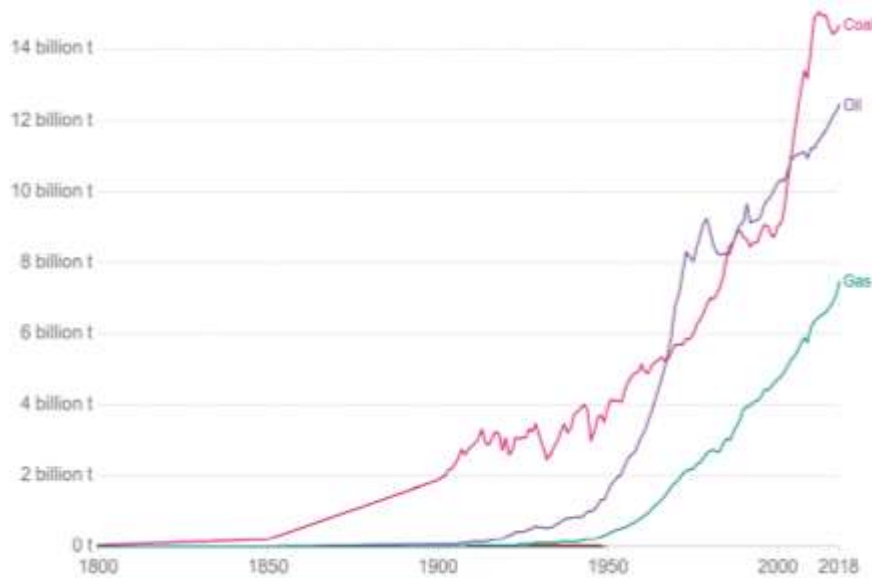


Figure 1.3: Global CO_2 emission by source from 1800 to 2018 AD [1]

The prices of fossil fuels started rising abruptly and at much higher rate after this period, and in parallel the environmental movements brought the harms related with fossil fuels and their longer-run consequences such as global climate change into light and the world started taking it seriously on governmental and social levels. [2]

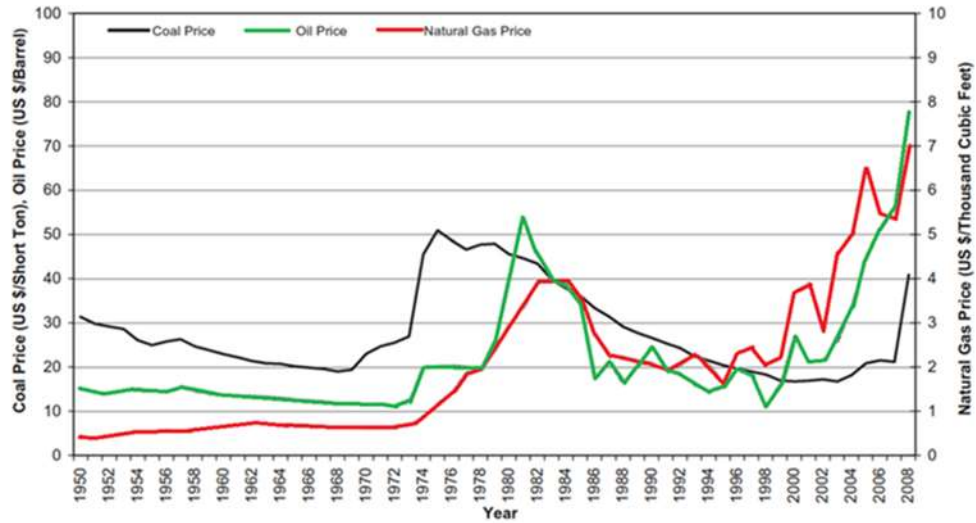


Figure 1.4: Prices of coal, oil and natural gas from 1950 to 2008 AD [1]

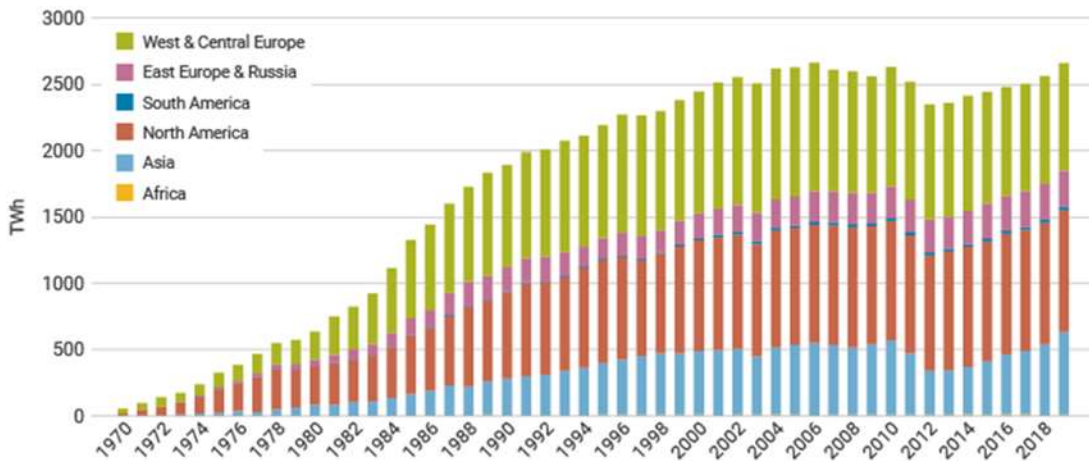


Figure 1.5: Rise in nuclear power production from 1970 to 2018 AD by region [1]

After 1950s, most of the countries in the world started working on the development of nuclear power as an alternative to the fossil fuels. It is the cheap and clean form of energy obtained by the fission reaction within large nuclear reactors, using minerals such as uranium as a fuel. Around 10 % of the world's electricity is generated by about 440 nuclear power reactors. About

50 more reactors are under construction, equivalent to approximately 15 % of existing capacity. In 2019 nuclear plants supplied 2657 *TWh* of electricity, up from 2563 *TWh* in 2018. The rise in nuclear power production from 1970 to 2018 *AD* by region is given in figure 1.5. Safety and waste management of the radioactive byproducts of the nuclear reactions are the big issues related with nuclear power production. Hence, they have slowed down the progress in this field. [2], [5]

In recent times, different forms of renewable energy have gained a lot of attention. These are untraditional ways of power generation which ensure the sustainable development, are eco- and environment friendly and do not involve any social or health-related harms. Only a few of the sources fulfill this ideal criterion. [3], [6]

The most common renewable power technologies include:

- Solar (photovoltaic, solar thermal)
- Wind
- Biogas (e.g., landfill gas/wastewater treatment digester gas)
- Geothermal
- Biomass
- Low-impact hydroelectricity
- Emerging technologies - wave and tidal power

Here are some of the environmental and economic benefits of using renewable energy:

- It causes no gas emission hence reduces the pollution.
- It diversifies energy supply and reduces dependence on imported fuels.
- It creates economic development and jobs in manufacturing, installation, and more.
- Renewable energy will not run out.
- It requires a way less maintenance than traditional power plants and have very low operational cost. Therefore, it saves money.

1.2 General Goal of the Thesis

This thesis is built around an experimental study of energy harvesting from fluid flow (a renewable energy). Energy harvesting eel made of piezoelectric polymer is used to convert flow energy into electrical energy. The energy is actually harvested by the flapping of the eel due to the turbulence in the fluid (water) caused by vortices, generated by introducing two side by side (staggered) solid cylinders before the eel. The main goal of this study is to produce green energy which will power small voltage devices.

The questions to be addressed in this study are:

1. How energy can be harvested from fluid flow using energy harvesting eel?
2. What is the effect of staggered cylinders on energy harvesting?
3. What is the effect of the distance between cylinders and their gap from eel on energy harvesting?

1.3 General Structure and Outline of the Thesis

This thesis documents different parts of the study on the “energy harvesting using piezoelectric flag behind two cylinders in side by side arrangement”. The general goals of the study are described in the **Section 1.2** of this chapter. This thesis is divided into seven chapters and an appendix. The general description of each chapter is outlined below.

Chapter 1 (the present chapter) deals with the introduction to the study. This chapter gives an insight into the motivation behind this research. The need, importance and vitality of this research work is the major part of this chapter. Moreover, this chapter defines the main research objectives of the study and outline the questions to be addressed through the research.

Chapter 2 deals with the basics of the fluid energy conversion and the fundamental concepts in fluid mechanics. This part of thesis gives an insight into two majors renewable energy sources: wind energy and hydropower. It explains the general process and different methods of power generation from these two sources. After explaining each source comprehensively, it explains the basics of the fluid mechanics including fundamental concepts and a brief introduction to different terminologies in the field.

Chapter 3 gives a detailed insight into the vibration energy harvesters and piezoelectricity. It describes the basics of energy harvesting from vibrations, its types and methods. This chapter also gives an understanding of the piezoelectricity and piezoelectric devices, used to harvest vibration energy. The present research work uses the piezoelectric flag/eel to harvest energy from the vibrations caused by the turbulence in the fluid (water) waked by bluff bodies (two side-by-side cylinders in a staggered arrangement) within the water tunnel.

Chapter 4 deals with the previous research work regarding piezoelectricity-based energy harvesting from the wake of bluff bodies in water flow and the cases similar to the energy harvesting from energy harvesting eel behind two side by side solid cylinders in stagger arrangement. This chapter includes the citations from the research articles published by different researchers working on the topic around the globe, in different journals.

Chapter 5 describes the experimental setup and methodology of the study. This chapter provides a detailed description of the apparatus used in the experimentation, experimental setup, system parameters and experimental conditions and methodology of the work. This chapter also includes the schematic description of the experimental setup and data acquisition setup highlighting the system parameters and the parameters to be measured.

Chapter 6 explains the measured results of experimentation and processed results of amplitude, voltage and power through *MATLAB* program and *Microsoft Excel* sheets. It also includes the graphical representation and plots of the results. This chapter mainly focuses on discussing the obtained values of the parameters including frequency, amplitude, voltage and power under different testing conditions and scenarios, and explains the trends of the obtained graphs.

Chapter 7 is the last chapter of thesis which concludes the whole study based on the concepts discussed in the previous chapters, reviewed literature, observations during experimentation and the results obtained. It also provides the future recommendations for further continuation and extension of the research work on the topic.

Appendix A contains the important *MATLAB* codes used to process the data obtained through experimentation using data acquisition setup according to the methodology explained in **Chapter 5** to get the results of different parameters, presented in **Chapter 6**.

CHAPTER 2: BASICS OF FLUID ENERGY CONVERSION AND FLUID MECHANICS

This chapter deals with the basics of the fluid energy conversion and the fundamental concepts in fluid mechanics. It gives an insight into two major renewable energy sources: wind energy and hydropower. It explains the general process and different methods of power generation from these two sources. After explaining each source comprehensively, it explains the basics of the fluid mechanics including fundamental concepts and a brief introduction to different terminologies in the field.

2.1 Energy Conversion

Any system involving the energy conversion follows the first law of thermodynamics. It is another form of the law of conservation energy. The first law of thermodynamics states that "total amount of energy remains unchanged in any conversion of energy from one form to another". [7] If we get a smaller output than input, then it means that energy is converted into another form. Some of the energy conversion includes: A wind turbine converts the kinetic energy of moving air into electrical energy, an engine converts chemical energy into heat and then into kinetic energy to run a vehicle. [8] Different types and forms of energy are given in figure 2.1. [9]

When one form of energy is converted into another form, the output is not always equal to the input. They are interconnected by a parameter known as efficiency. The efficiency of any system is defined as the ratio from output to the input of that system. [10]

$$Efficiency = \frac{Output}{Input}$$

2.2 Renewable Energy Sources

The technology of renewable energy exists in many forms, as presented in figure 2.2. Some of the common forms are: biomass, wind, wave, solar, tidal, hydropower and geothermal energy. Wind energy and hydropower are the largest sources of renewable energy. The fluid is considered as a system of energy carrying. The flow of energy can be used by converting it into

electrical energy in the form of power. [11] Some of the large-scale wind energy and hydropower systems are explained below.

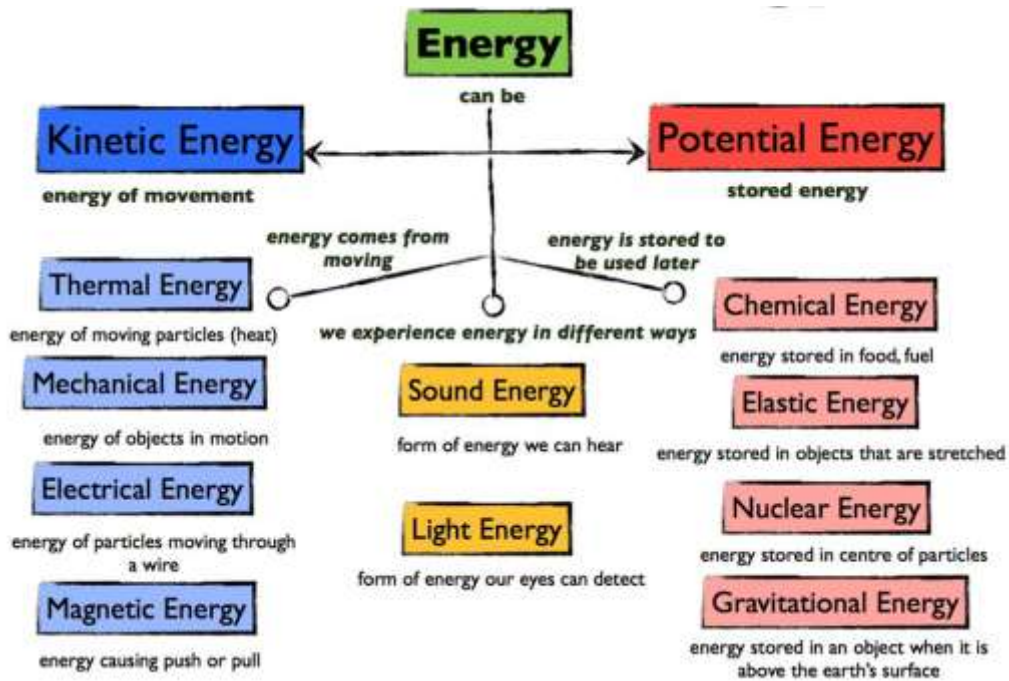


Figure 2.1: Different types and forms of energy [9]

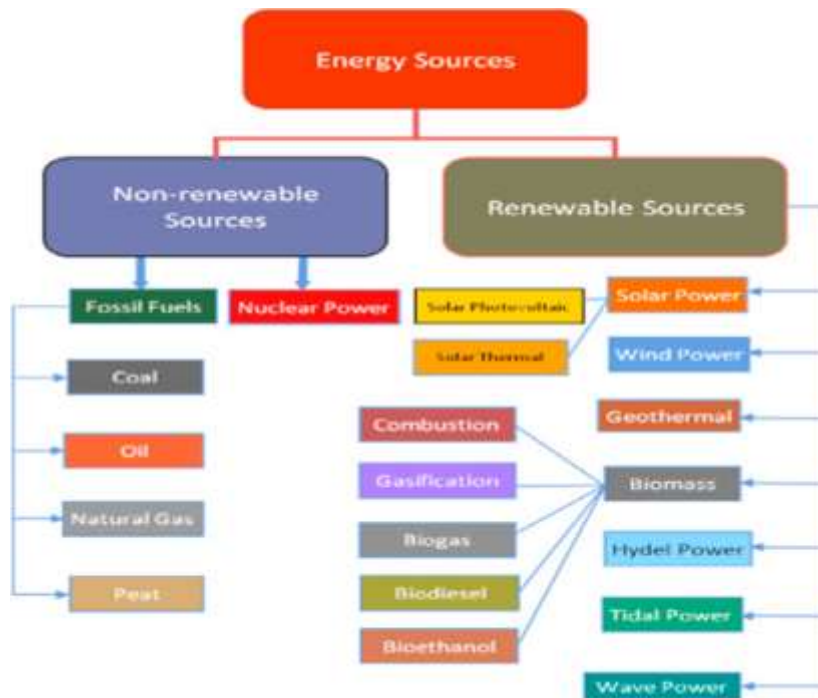


Figure 2.2: Renewable and non-renewable sources of energy [11]

2.2.1 Wind Energy

The ultimate source of all energy is the sun. 1 – 2 % of the energy out of energy radiated by the sun is converted into wind energy. Due to the lighter weight of hot air than cold air, hot air rises about 10 *km* into the sky and spread to the south and north. Bending forces are created due to the rotation of the globe force to move the air (generate wind). Wind contained kinetic energy which is due to motion. Wind energy has been used for many years in several applications like mechanical power, pumping water, etc. windmills also known as wind turbines are used to generate electricity. It involves many fields of knowledge including aerodynamics, meteorology, structural, civil, mechanical, electrical, and planning. [12]–[14]

Wind as a source of energy was exploited by early civilization. It was first used to propel sailing boats. Wind energy harvesting utilizing windmills takes place for about 4000 years. Windmills have been also used for different purposes like grinding spices, milling grain, making paper, etc. wind pumps also referred to as windmills were used to pump water. Many of them were of vertical types. [15]

Wind turbines are classified based on size, type, and sustainability. On the basis of general geometry, wind turbines are classified into two major types. [16]

2.2.1.1 Vertical axis wind turbine

In the vertical axis wind turbine (VAWT), the axis of rotation is perpendicular to the direction of the wind. They can harness wind energy from any wind direction without changing the position of the rotor concerning wind direction. VAWTs are further divided into following types. The rotor shapes for some common types of VAWTs are shown in figure 2.3. [17]

2.2.1.1.1 Darrius type VAWT

It consists of curved blades whose ends are attached to the vertical shaft. They are structural efficient but are difficult to manufacture, transfer, and install.

2.2.1.1.2 H-type VAWT

It consists of aero foil blades which are supported by two horizontal cross arms attached by the bob of the tower. Only limited development of H-type VAWT has taken place so far.

2.2.1.1.3 V-type VAWT

It consists of aero foil blades whose one end is attached to the bob of the vertical shaft and the other is inclined. It has several features that include a short tower, ground-level blade installation, and ground-mounted generator.

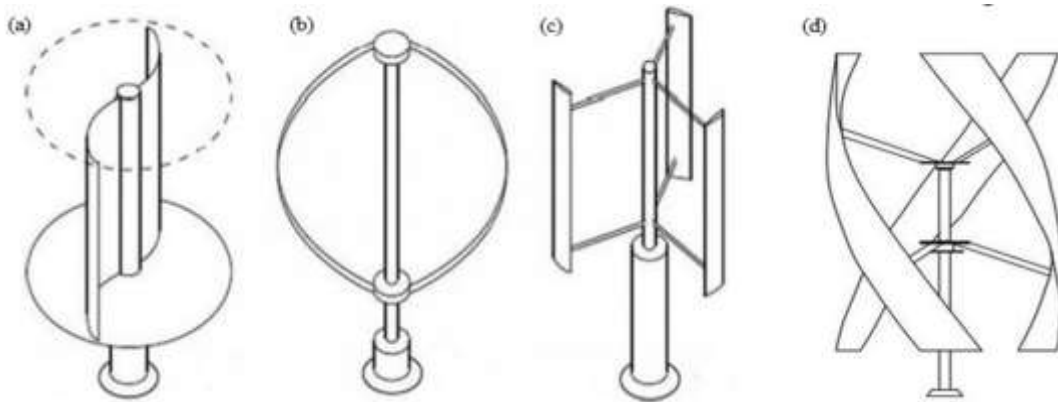


Figure 2.3: Common types of VAWTs (a) Savonius (b) Darrieus-rotor (c) H-Darrieus (d) Helix shape [17]

2.2.1.2 Horizontal axis wind turbine

Horizontal axis wind turbine (HAWT) is also known as a propeller wind turbine. It is consisted of blades. Efficiency will be increased by increasing the number of blades. Mechanical power extracted by wind turbines is a product of angular velocity and torque imported by the wind. Torque is the movement about the center of rotation. It depends on the driving force exerted by the wind on the rotor blades. So, to get higher efficiency, the rotor blade must fully interact with the wind. Vertical axis wind turbine is more efficient and nearly all the current wind turbines are vertical axis wind turbine. [18] HAWTs are usually divided on the basis of number of blades, into following types:

2.2.1.2.1 Single-blade HAWT

Single-blade wind turbines are not very commonly used, their use is limited to a few applications, only. Single-blade turbines usually requires one or two counterbalances for their smooth rotation. A single-blade wind turbine with two counterbalances is shown in figure 2.4 (a). The advantage of this type of wind turbine is the lower cost because of the use of only one turbine blade (and the small weight savings), but single-blade turbines must run at much higher

speeds to convert the same amount of energy from the wind as two-blade or three-blade turbines with the same size blades. [19]

2.2.1.2.2 Double-blade HAWT

Compared to three-blade turbines, two-blade wind turbines have the advantage of saving on the cost and the weight of the third rotor blade, but they have the disadvantage of requiring higher rotational speed to yield the same energy output. This is a disadvantage in terms of both noise and wear of critical bearings, shafts, and gearboxes. [19]

2.2.1.2.3 Three-blade HAWT

The majority of large horizontal-axis wind turbines use three blades, with the rotor position maintained upwind by the yaw control. Figure 2.4 (c) shows a three-blade wind turbine. The three blades provide the most energy conversion while limiting noise and vibration. The three blades provide more blade surface for converting wind energy into electrical energy than a two-blade or single-blade wind turbine. [19]

2.2.1.2.4 Five-blade HAWT

A few wind turbines have five blades to produce electrical energy efficiently from low-speed winds. Figure 2.4 (d) shows a five-blade wind turbine. A five-blade wind generator normally has narrower and thinner blades, which creates issues with strength. While they are excellent in low-speed winds, they become inefficient in high-speed winds and they are noisier. [19]



Figure 2.4: Types of HAWT (a) single-blade (b) double-blade (c) three-blade (d) five-blade [19]

Wind turbine extracts power due to the rotation of the rotor pushed by the motion of air. When air flows across blades of a wind turbine, it produces a lift force (a transverse force) that rotates turbine blades and a drag force which slows down the rotation speed by bending the blades. The kinetic energy of flowing fluid is proportional to the square of its velocity. When flowing fluid encounters the object placed in its path, its cross-sectional area reduces, and its energy is transformed to pressure against the object, and its velocity decreases. Power is force times velocity. Pressure gives the total force on the object. [12]

Some advantages of wind energy are: [20]

- No air pollution
- Low environmental impact
- Occupy small amount of land
- Available in greater amount
- Can offset the use of fossil fuel

2.2.2 Hydropower

Hydropower is a well-established technology, which is economic, non-polluting, and environmentally friendly. According to the report published by International Energy Agency (IEA) in 2015, it contributes about 16% of the Worlds electricity production. It is one of the oldest renewable energy technologies in which hydropower is converted into electrical power via a mechanical mechanism. [1]

Water at some height represents stored energy also known as potential energy. The main characteristic of hydropower is effective heads which is the height through which waterfalls and the flow rate. Power is 10 times the product of effective head and flow rate. A turbogenerator is used to convert the water-energy into electrical energy. The turbogenerator consists of a rotating turbine that is connected to a rotor of a generator by a shaft. During the conversion, water losses some of the energy due to frictional drag and turbulence. [21], [22]

No one knows how many years age the water wheel was invented but the system of irrigation existed at least 5000 years ago. Noria is the earliest device which was made for water rising

purpose. The paddle dips into the flowing stream and water was lifted by the rotating wheel. By the eighteenth century, three main types of wheels (overshoot, undershot, breast shot) were used. In overshoot, the wheel is driven by the water falling onto the blades from the closed side. In undershoot, the wheel is driven by water pressure on lower blades. In breast shot, the wheel is driven by the water when it strikes at about the level of the wheel axle. [21], [23], [24]

Hydropower plants are differentiated from each other depending on following factors: [25]

2.2.2.1 The effective head of water

An effective head is an important factor in determining the type of plant and installation. On the basis of effective head, the hydropower plants are further categorized as: [26]

2.2.2.1.1 Low head hydropower plant

Though there is no rule regarding water head height but the hydropower plant having effective water head below 30 m is considered as low head power plant. The installation diagram is shown in figure 2.5 (a). [23], [25], [26]

2.2.2.1.2 Medium head hydropower plant

The hydropower plant having effective water head above 30 m to 300 m is considered as medium head power plant. The installation diagram is shown in figure 2.5 (b). [25]

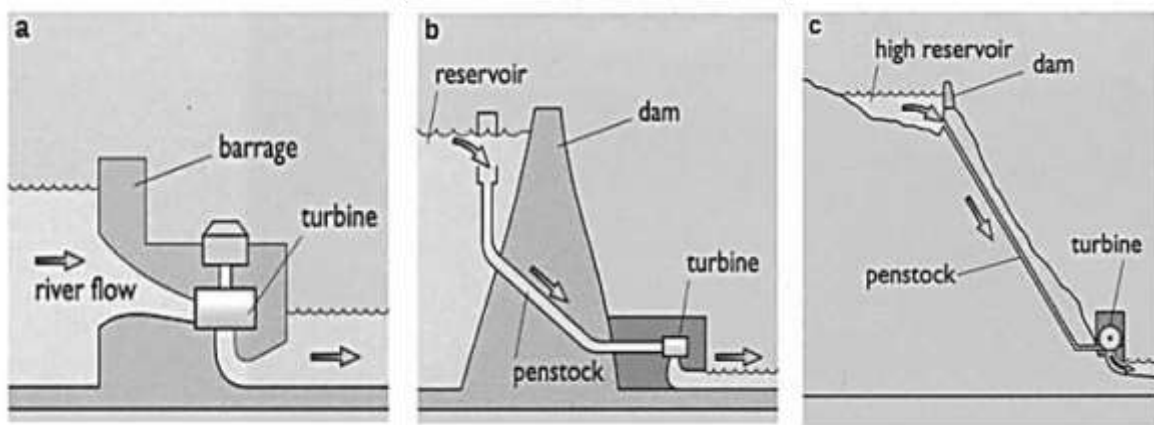


Figure 2.5: Installation diagram for (a) low head (b) medium head (c) high head hydropower plant [25]

2.2.2.1.3 High head hydropower plant

The hydropower plant having effective water head above 300 m is considered as high head power plant. The installation diagram is shown in figure 2.5 (c). [25]

2.2.2.2 The capacity/scale of the system

According to the Central Electrical Agency (CEA), on the basis of capacity (power generation), the power plants are classified as: [27]

2.2.2.2.1 Small scale

Plants having station capacity up to 15000 kW come under small-scale hydropower plants. They are further classified as: [27]

- Micro: Up to 100 kW
- Mini: 101 kW – 2000 kW
- Small: 2001 kW – 15000 kW

2.2.2.2.2 Large scale

Hydropower plants having station capacity more than 15000 kW comes under large-scale category. [27]

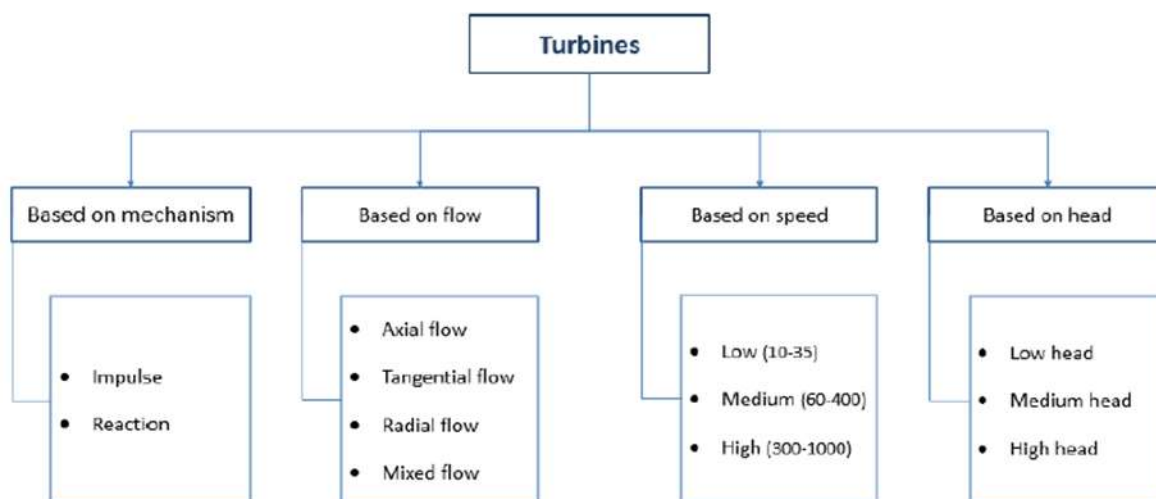


Figure 2.6: Types of hydraulic turbines on the basis of mechanism, flow, speed and head [28]

2.2.2.3 Type of hydro-turbine used

Figure 2.6 shows the classification of hydraulic turbines on the basis of mechanism, flow, speed and available hydraulic head. Figure 2.7 shows the types of turbines that can be used for any set of available water flow rate and hydraulic head. [28], [29]

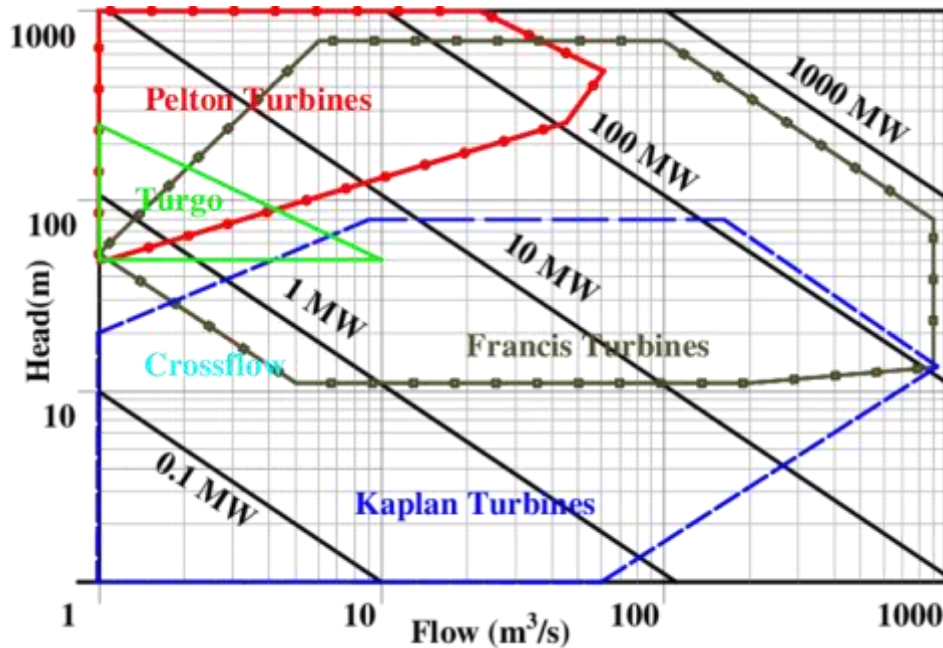


Figure 2.7: Hydraulic turbine application chart [29]

Some advantages of hydropower are: [30]

- It is clean as no burning of oil takes place
- No air pollution
- No greenhouse gases emission
- Efficient way of generating electricity
- Low operational cost

2.3 Characteristics of Fluid

The fluid is defined as a substance that can flow or can own the shape of the vessel containing it. Fluid deforms when acted tangential to the area by any force. Such force by which it acts tangential to the area is known as shear force. Shear stress is defined as the ratio of shear force to the area on which it acts.

In fluids, the opposition force between the layers exists when the movement between the layers is taking place due to the shear force applied. When this shear force is removed, fluid particles come to their original position. [31]

Table 2-1: Distinctions between fluids and solid [31]

Fluid	Solid
<ul style="list-style-type: none"> • At rest, no shear force and no shear stress occur 	<ul style="list-style-type: none"> • At rest, can resist shear force
<ul style="list-style-type: none"> • Shear forces are possible only when relative motion between layer takes place 	<ul style="list-style-type: none"> • Shear force may cause large displacement, but position of stable equilibrium is reached, and material does not move
<ul style="list-style-type: none"> • Fluid flows under the action of shear force 	<ul style="list-style-type: none"> • Does not flow until shear force exceed a certain value

Molecules are much closed to each other in liquids and solids as compared to gas. So, there is a sufficient attractive force to keep them together. In liquid when a shear force is applied, the molecules pass or slip over one another until the force is removed. This does not normally occur in solids. Table 2-1 shows the distinctions between fluids and solids, while table 2-2 shows the distinction between two different phases of fluids i.e. liquids & gases. [32]

Table 2-2: Distinctions between two different phases of fluids i.e. liquids & gases [32]

Liquid	Gases
<ul style="list-style-type: none"> • Has a definite volume which varies with temperature and pressure 	<ul style="list-style-type: none"> • Always expand until its volume equal to the volume of vessel in which it is closed
<ul style="list-style-type: none"> • Difficult to compress 	<ul style="list-style-type: none"> • Can be compressed
<ul style="list-style-type: none"> • High density 	<ul style="list-style-type: none"> • Low density

2.4 Properties of Fluids

2.4.1 Density

Density is defined as the ratio of the mass of a given substance per unit volume. [33]

$$Density = \frac{Mass}{Volume} \quad (2.1)$$

2.4.2 Pressure

Pressure results due to molecular collision when a normal compressive force acts on an area. The pressure is a scalar quantity and the SI unit of pressure is the pascal. Pressure can be measured using different scales. Conversion is carried out using equation: [34]

$$P_{absolute} = P_{gauge} + P_{atmospheric} \quad (2.2)$$

The pressure of the atmosphere is commonly used for reference, as shown by the schematic diagram in figure 2.8. [35]

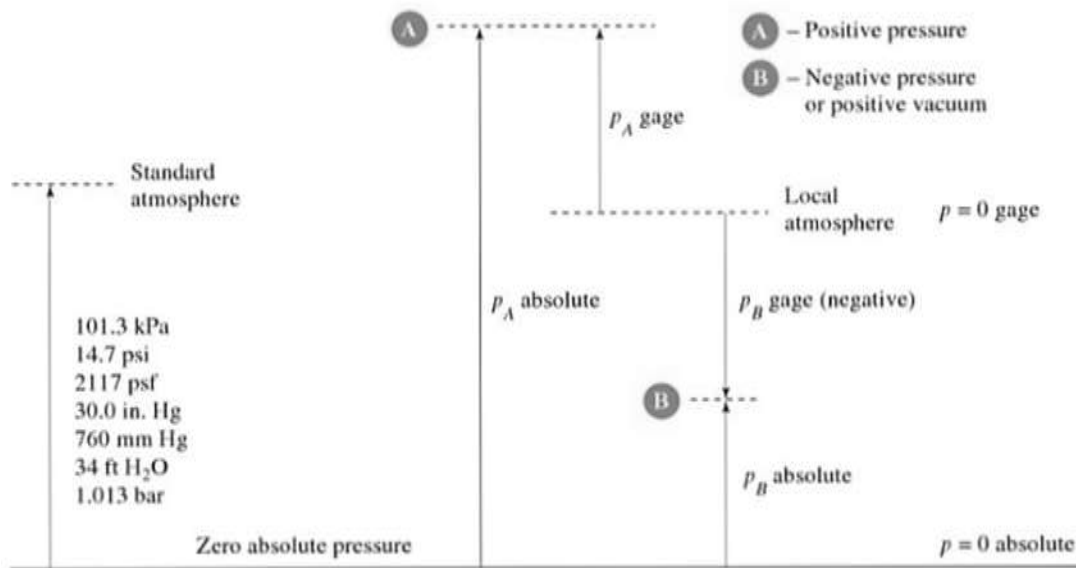


Figure 2.8: The relationship between absolute and gauge pressure with reference to the atmospheric pressure [35]

2.4.3 Viscosity

Viscosity can be defined as the resistance force between two layers of fluid. It comes in action during the motion of the fluid element. The fluid deformation rate is linked directly to the viscosity of the fluid. [36]

The force of attraction between molecules is considered one of the causes of viscosity. Consider straight and parallel flow as shown in figure 2.9. The layer $\bar{a}\bar{a}$ is moving at a greater speed than the layer $\bar{b}\bar{b}$. Due to continuous thermal agitation, some molecules of layer $\bar{a}\bar{a}$ taking momentum (because of velocity) migrate from layer $\bar{a}\bar{a}$ into the layer $\bar{b}\bar{b}$. This momentum is shared among the occupants of $\bar{b}\bar{b}$ due to collision with the molecules of layer $\bar{b}\bar{b}$. Thus, the speed of layer $\bar{b}\bar{b}$ increases. Similarly, when molecules of slower layer $\bar{b}\bar{b}$ cross molecules of layer $\bar{a}\bar{a}$ they tend to decrease the speed of layer $\bar{a}\bar{a}$. To eliminate the difference between layers velocity, forces of acceleration and deceleration are created due to molecules migration. Liquid molecules are very close and have intermolecular forces between them. These forces are modified due to relative motion between layers and cause a net shear force that resists relative motion. Viscosity depends on temperature and is independent of pressure. Hence, viscosity decreases with the increase of temperature. [37]

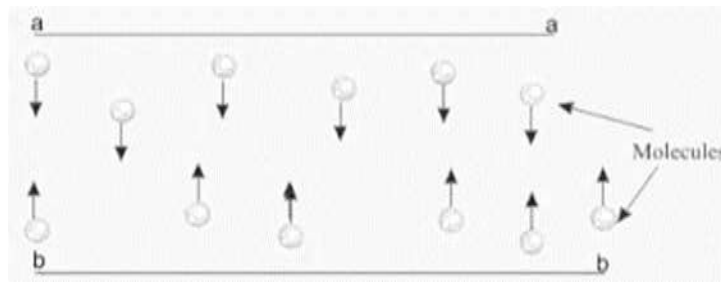


Figure 2.9: Migration of molecules between two layers of fluid which causes the friction between layers (viscosity) [37]

2.5 Pattern of Flow

2.5.1 Streamline

Streamline also known as flow line is an imaginary curve in the fluid across which no fluid is flowing at that instant of time. Each particle occupying a point on the streamline, its vector is tangent to streamline. [38], [39]

2.5.2 Path line

The path followed by a particle as it travels in the flow field for a certain period is known as the path line. It gives us the history of the location of the particle. [38], [39]

2.5.3 Streak line

The streak line is an imaginary line, whose points are occupied by all particles originating from a common point in the field flow. It gives an instantaneous picture which has passed through a common point. The schematic diagram of the comparison between stream, path and streak lines in the fluid is shown in figure 2.10. [38], [39]

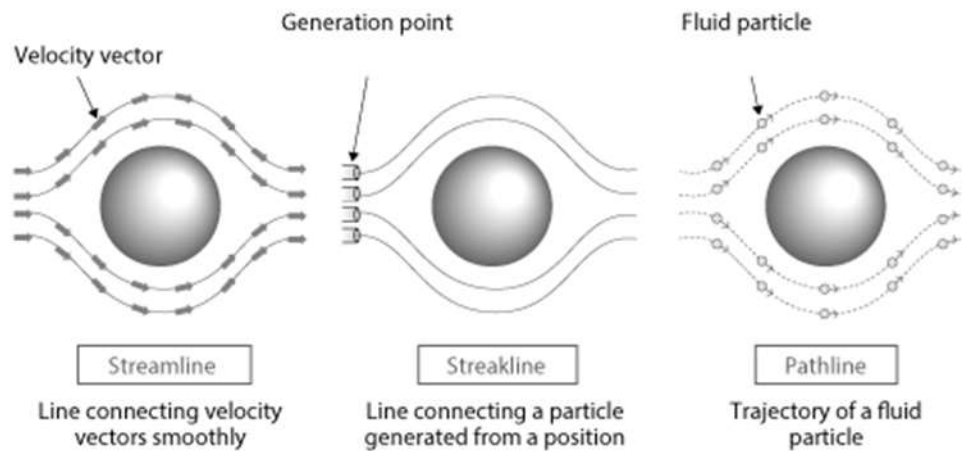


Figure 2.10: Stream, path and streak lines in the fluid flow [38], [39]

2.6 Classification and Description of Fluid Flow

2.6.1 One, two- and three-dimensional flows

In one dimensional flow, flow parameters are expressed as a function of time and one coordinate. In two-dimensional flow, flow parameters are expressed as a function of time and two coordinates. In three-dimensional flow, flow parameters are expressed as a function of time and three coordinates. [40]

2.6.2 Internal and external flow

The flow of fluid within the boundaries is known as internal flow. The flow of fluid around the immersed structure is known as external flow. The schematic diagram for internal and external flows and their respective boundary layers is shown in figure 2.11 (a) and (b), respectively. [41]

2.6.3 Laminar and turbulent flow

The highly ordered fluid motion which does not vary irregularly is known as laminar flow. They are characterized by a smooth streamline, as shown in figure 2.11 (c). The highly disordered fluid motion, as shown in figure 2.11 (d), which varies irregularly is known as turbulent flow. They are characterized by velocity fluctuation. [41]

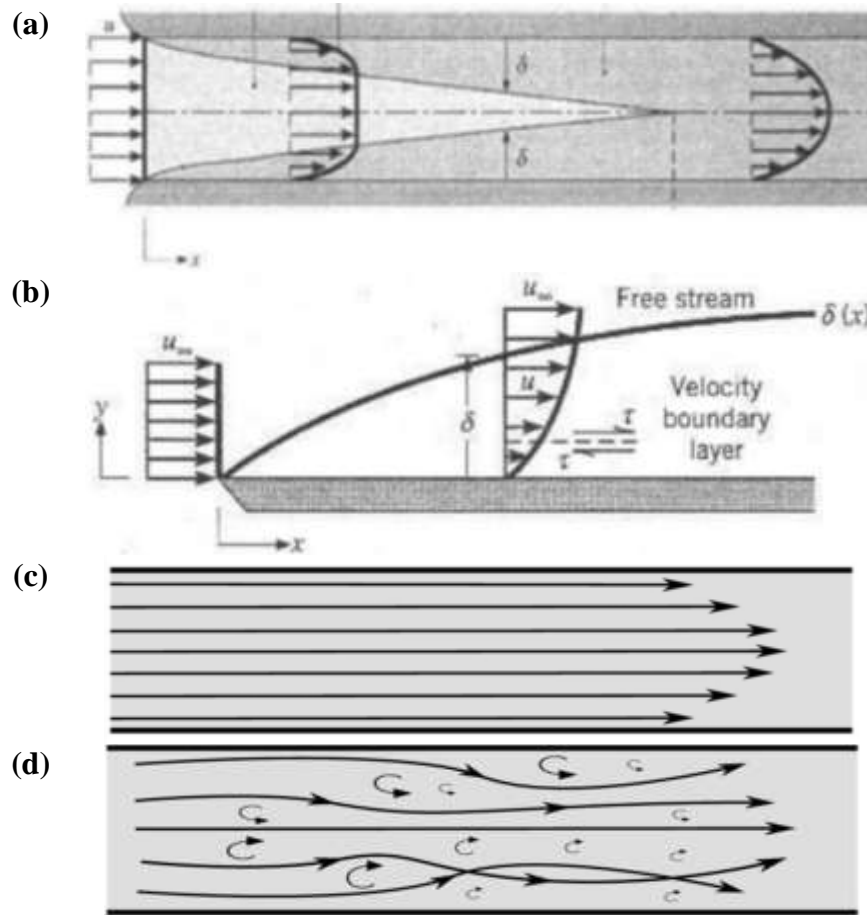


Figure 2.11: Types of flow (a) internal flow (b) external flow
(c) streamline flow (d) turbulent flow [41]

2.6.4 Viscous and inviscid flow

The flows in which the viscosity effect (the friction between the layers of fluid) is significant is known as viscous flow. The flow in which the viscosity effect is insignificant is known as inviscid flow. [42]

2.6.5 Steady and unsteady flow

The flow in which at any point, the parameter does not change with time is known as steady flow. The flow in which parameter changes with time is known as unsteady flow. [43]

2.6.6 Compressible and incompressible flow

If the density of fluid particles varies as it moves through the flow field, then it is called compressible flow. If the density of fluid particles does not vary, as it moves through the flow field, then they are called incompressible flows. [41]

2.7 Fluid Solid Interaction (FSI)

2.7.1 Boundary layer

The real fluid flow has two characteristics: one is no velocity discontinuity and second is during fluid solid interaction, the relative fluid velocity at the surface is zero known as a no-slip condition. The velocity increases from zero and approaches the velocity of the mainstream. The region between these two velocities is known as the boundary layer region. This indicates the presence of shear stresses. According to the suggestion given by German engineer Ludwig Prandtl in 1904, two parts are considered for the external flows. [44]–[46]

- Boundary layer where velocity gradient is important
- Outside the boundary layer where the velocity gradient is small

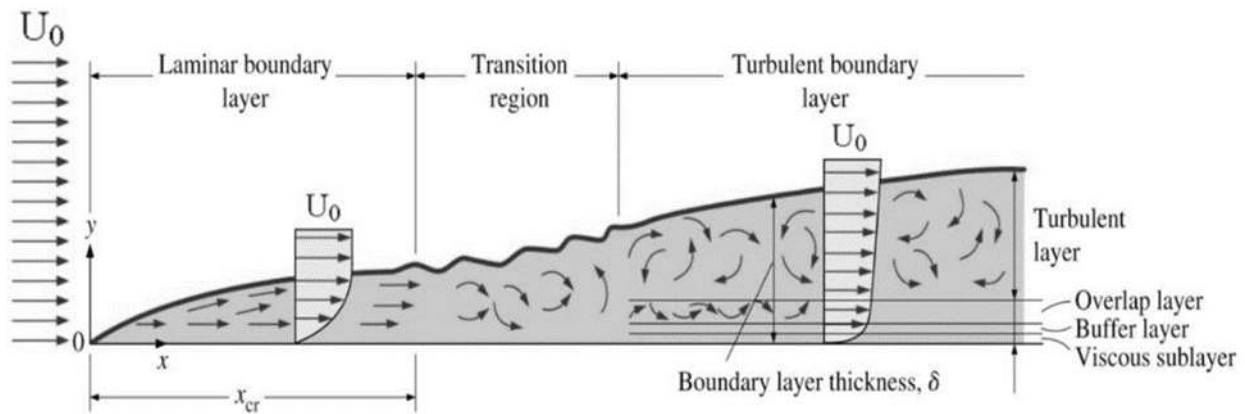


Figure 2.12: Boundary layer formation in the flow over a flat plate [41]

In real fluid, near the surface, the velocity gradient is due to viscous action. The boundary layer begins at the leading edge of the plate. The thickness of the boundary layer increases as more and more fluid is slowed down. The flow close to the leading edge is entirely laminar. The laminar layer becomes unstable with increasing thickness and flows develop into turbulence. The short length in which laminar to turbulent flow takes place is known as the transition region. Figure 2.12 shows the boundary layer formation on the flat plate. [41]

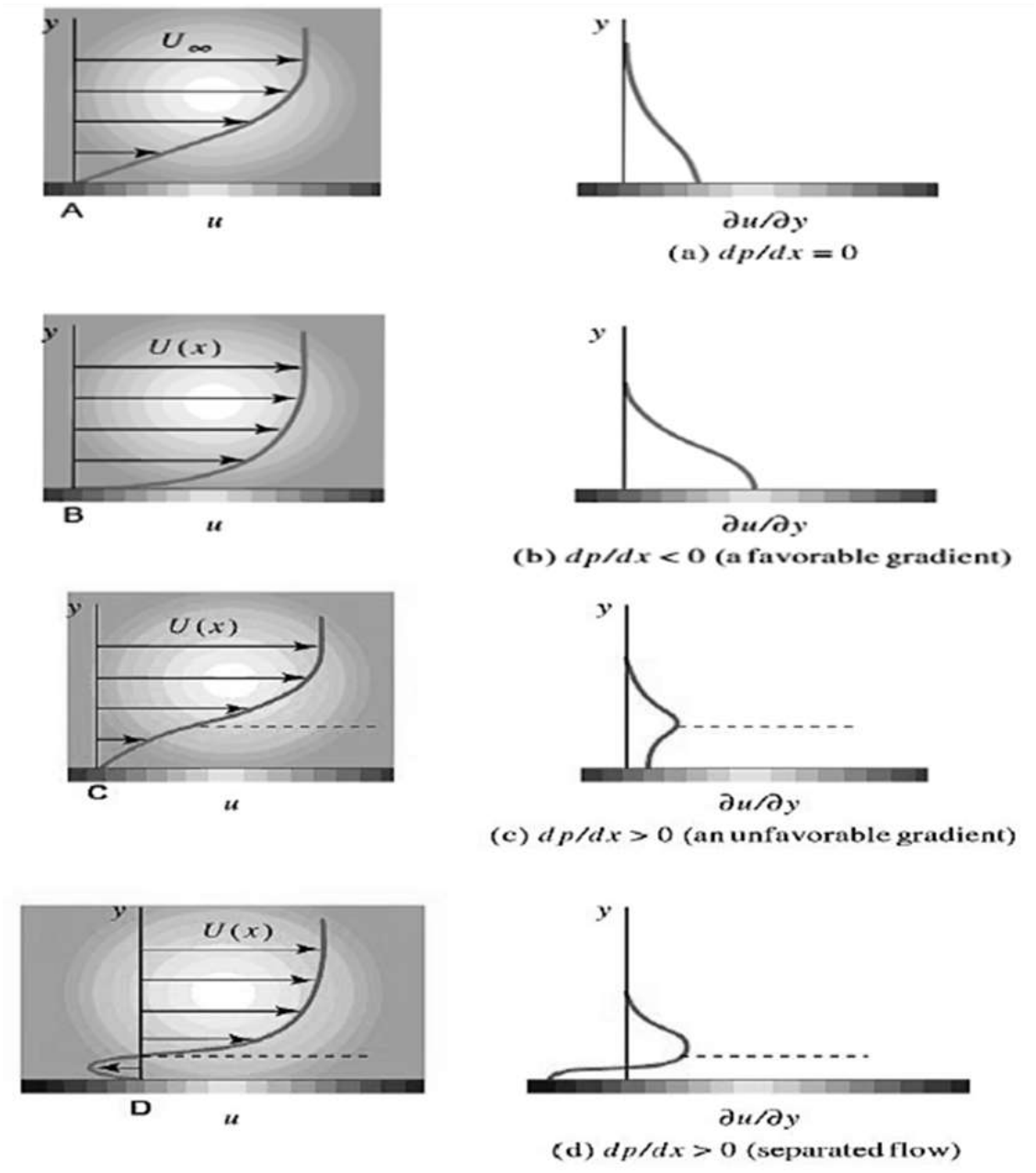


Figure 2.13: Boundary layer separation process [46]

2.7.2 Boundary layer separation

Outside the boundary layer until at point B shown in the figure 2.13, the velocity is maximum, and pressure is minimum. So, the pressure gradient is negative at point B as shown in the figure 2.13. Within the boundary layer, the net pressure force on an element is in the forward direction.

Beyond point B, the increase in pressure opposes the forward flow. The value of the pressure gradient is the same throughout the cross-section of the boundary layer. pressure gradient near to the surface has a significant effect due to the large difference of momentum of fluid near to the surface as compared to fluid further away. The momentum reduces until fluid is brought to a standstill near the surface.

Further, at point D, the flow becomes reversed forming a secondary boundary layer where the positive pressure gradient occurs. The separation develops due to an adverse pressure gradient (positive pressure gradient combines with reduction of velocity in the boundary layer) since it opposes the flow. [44]–[46]

2.7.3 Vortex formation

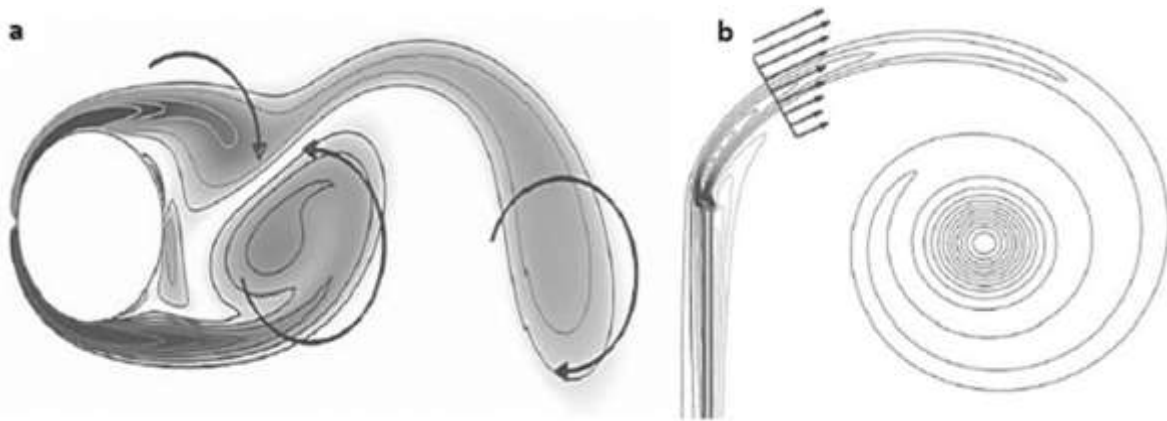


Figure 2.14: Vortex formation (a) from a circular cylinder (b) from a sharp edge obstacle [44]

Boundary layer separation represents the starting phase of the formation of a vortex. There is a velocity difference between the two sides of the shear layer. The shear layer farther side separated from the wall move with higher speed than the side close to the wall. So, it curves itself and the distance between the two-shear layers reduces during the rolling process. Vortex

formation from a circular cylinder and a sharp edge obstacle is shown in figure 2.14 (a) and (b), respectively. [44]–[46]

2.7.4 Separation region

Disturbed region behind a bluff body where the flow gets separated from the body, leaves the stream lines and becomes turbulent is termed as separation region, as shown in figure 2.15. [41]

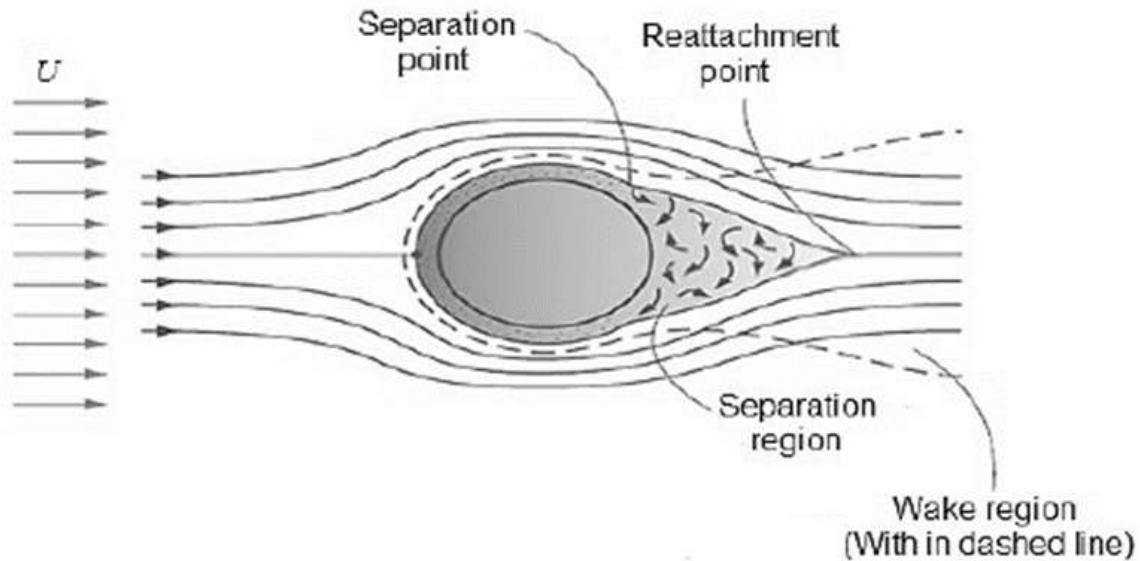


Figure 2.15: Separation region when fluid flow over a cylinder [41]

2.7.5 Bluff body shape effect

For bluff bodies, pressure drag is dominant and depends on bluff body shapes. Pressure drag and separation region are related to each other. If pressure drag is larger than separation region (disturbed region behind a bluff body) will be larger. Drag coefficient for various bluff bodies are shown in table 2-3. [47], [48]

2.7.6 Vortex street

Vortex is shed alternatively from the two sides of the cylinder. The figure 2.16 shows the vortex shedding forming two rows of vortices. Disturbed region behind Downstream flow resulting when a cylinder is placed normal to fluid flow is referred to as Karman Vortex street named after Theodor Von Karman. [41], [49], [50]

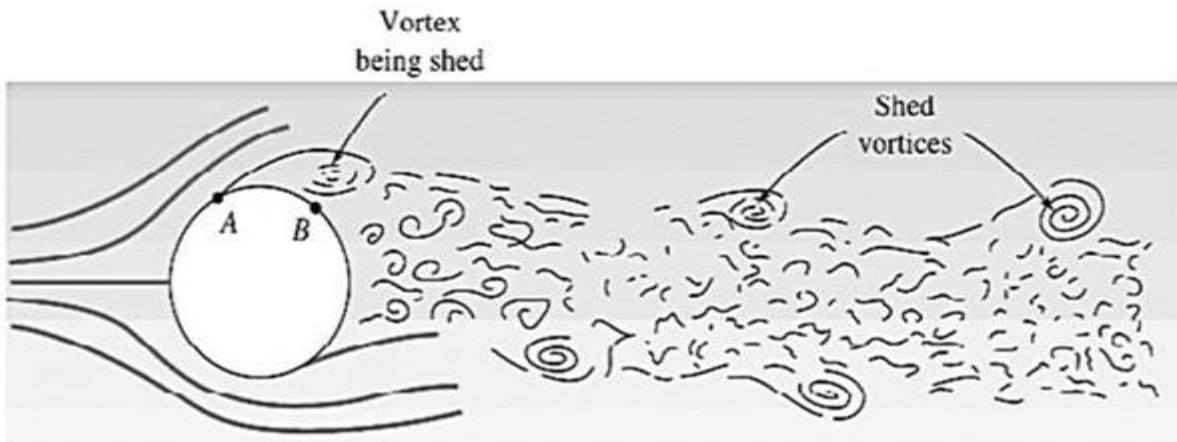


Figure 2.16: Vortex shedding from circular cylinder [41]

Table 2-3: Drag coefficients for different types of bluff bodies [48]

	$C_d = 1.98$		$C_d = 1.18$
	$C_d = 2.0$		$C_d = 1.0 \text{ to } 1.2$
	$C_d = 2.2$		$C_d = 1.7$
	$C_d = 1.4$		$C_d = 0.4$
	$C_d = 1.3$		$C_d = 1.1$
	$C_d = 2.0$		$C_d = 0.7$
Two-dimensional		Three-dimensional	

2.7.7 Basic terminologies

2.7.7.1 Vorticity

Rotation of a fluid particle, as shown in figure 2.17 (a), is known as vorticity. [51]

2.7.7.2 Vortex line

It is an imaginary line on which when tangent is drawn at any point gives the direction of the vorticity vector, as shown in figure 2.17 (b).

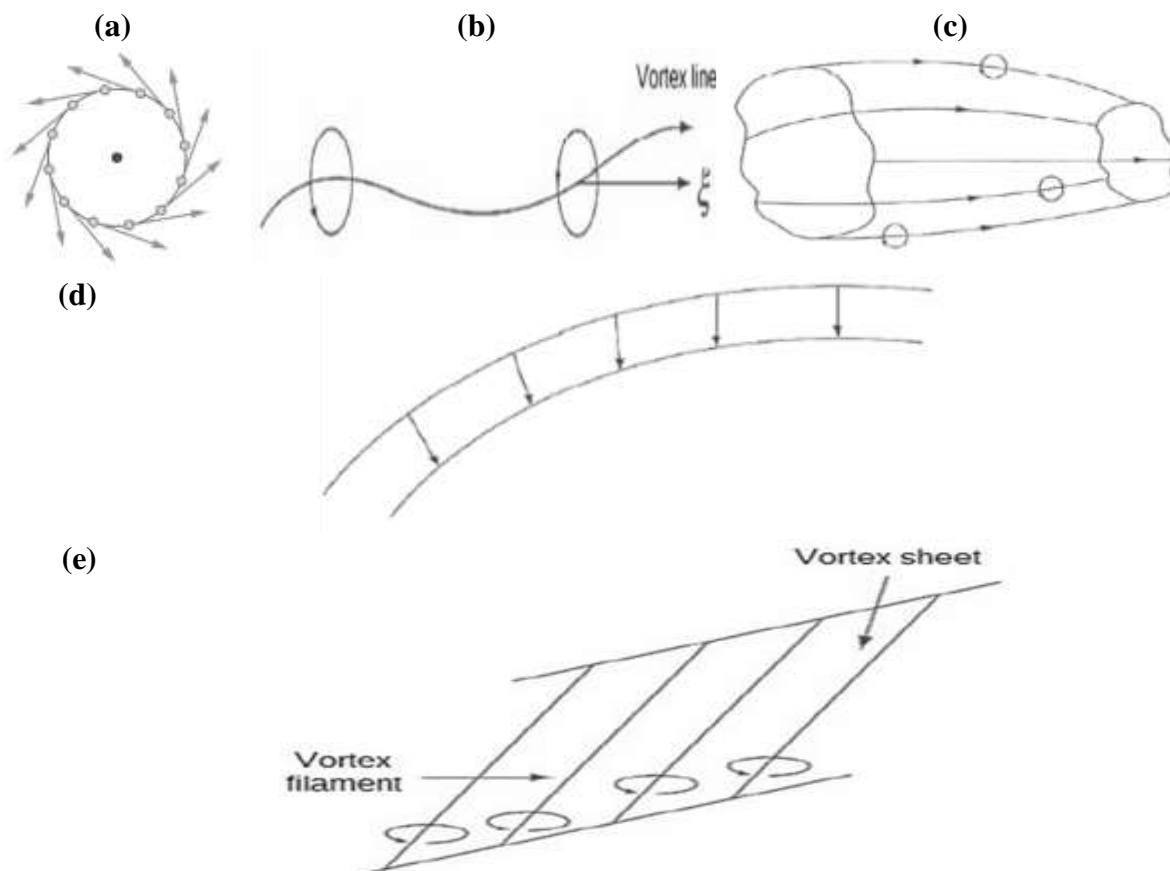


Figure 2.17: Basic terminologies in vortices (a) vorticity (b) vortex line (c) vortex tube (c) vortex filament (d) vortex sheet [51]

2.7.7.3 Vortex tube

A volume bounded by the vortex line, as shown in figure 2.17 (c), is termed as a vortex tube.

2.7.7.4 Vortex filament

An infinitesimally small cross-sectional area vortex tube, as shown in figure 2.17 (d), is termed as vortex filament.

2.7.7.5 Vortex sheet

A thin layer of the vortex, as shown in figure 2.17 (e), is known as the vortex sheet.

CHAPTER 3: VIBRATION ENERGY HARVESTERS AND PIEZOELECTRICITY

This chapter gives a detailed insight into the vibration energy harvesters and piezoelectricity. It describes the basics of energy harvesting from vibrations, its types and methods. It also imparts an understanding of the piezoelectricity and piezoelectric devices, used to harvest vibration energy. The present research work uses the piezoelectric flag/eel to harvest energy from the vibrations caused by the turbulence in the fluid (water) waked by bluff bodies (two side-by-side cylinders in a staggered arrangement) within the water tunnel.

3.1 Introduction

Vibration is mechanical energy that can be found in our surroundings in an excess amount such as ocean wave, vehicle, structure, industrial, and environment as shown in table 3-1. Vibration energy harvesting is a technique for harvesting energy from surplus vibration accruing in the environment. [52], [53]

Table 3-1: Sources of vibrations [53]

Vehicles	Structures	Industrial	Environment
Aircraft, uav, helicopter, automobiles, trains	Bridges, roads, tunnels, farm house structures	Motors, compressors, chillers, pumps, fans	Wind, solar, temperature gradient, daily temperature
Tires, tracks, peddles, brakes, shock absorbers, turbines	Control-switch, hvac systems, ducts, cleaners, etc.	Conveyors, cutting g and dicing, vibrating mach.	Ocean currents, acoustic waves, em waves, rf signal

Different types of energy harvesters have been designed by the researchers to convert these vibration energies into electrical energy. However, some of these harvesters do not meet the high-efficiency conversion. This is because harvester resonant frequency does not match with the vibration ambient frequency. Regardless of the harvester type, the conversion efficiency is of great importance. Vibration energy can be harvested to power self-powered devices like

microelectromechanical systems (MEMs), wireless sensor networks (WSN), and the internet of things (IoT). Some of the types of energy harvester are shown in figure 3.1. [54], [55]

3.2 Electromagnetic Energy Harvester

Electromagnetic energy harvester works on the principle of Faraday's law of electromagnetic induction. Change in the electric field results in voltage generation which can be used or stored to power low voltage devices. A schematic of electromagnetic energy harvester is shown in figure 3.2. [56]

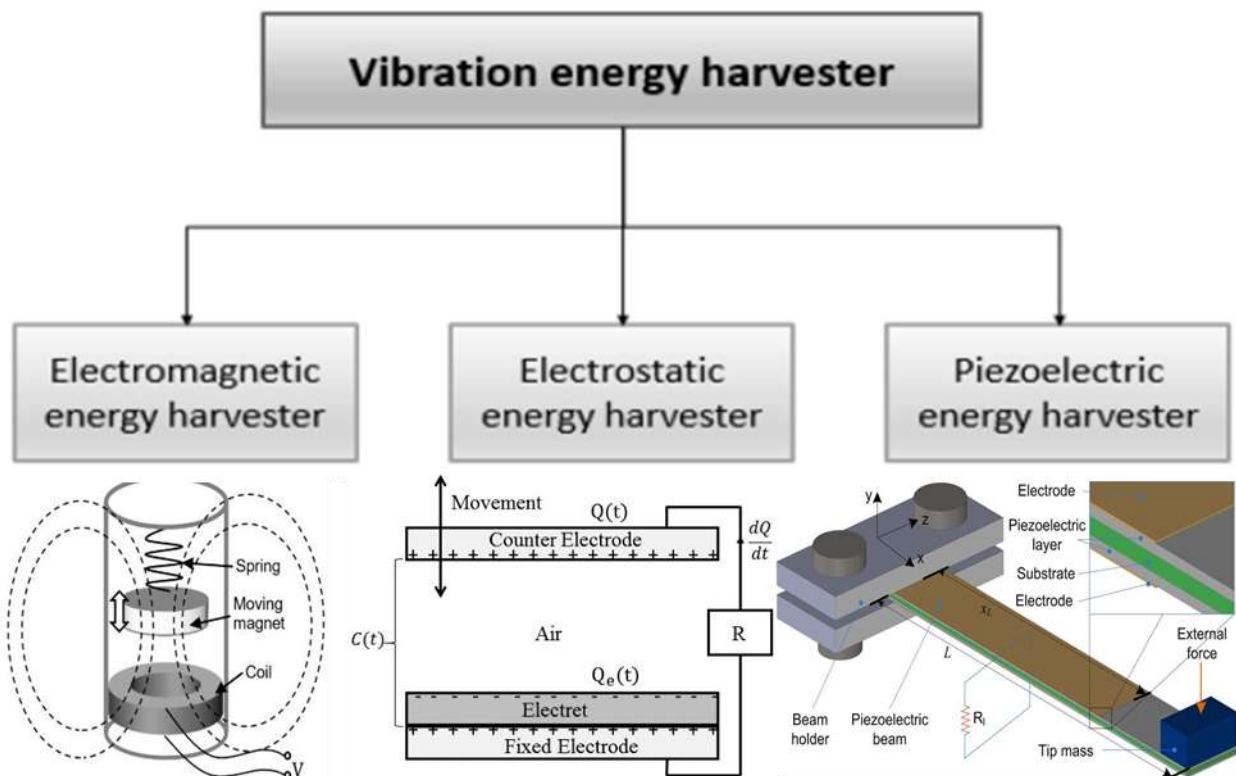


Figure 3.1: Types of vibration energy harvesters [57]

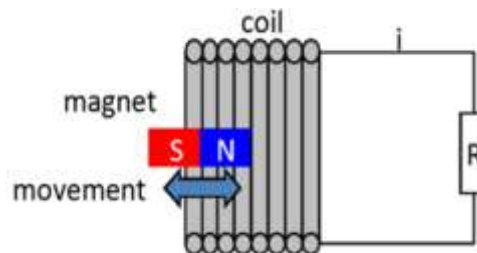


Figure 3.2: Schematic diagram of vibration based of electromagnetic energy harvester [58]

In an electromagnetic energy harvester, a magnetic circuit requires a magnetic field for the generation of power. A permanent magnet is more suitable as no power input is required. The permanent magnet contains ferromagnetic material that produces a strong magnetic field and has higher electrical resistance. The relative motion between the coil and the magnet produces electrical energy. The electromagnetic energy harvester is divided into three configurations. [57]

Moving magnet type has a significant over others. Output power also depends on the material properties and size of the transducer and coil resistance depends on the number of turns of the coil. Electromagnetic energy harvester has a certain advantage that the greater amount of energy can be harvested from weak vibration and there is no external input is required. [58]

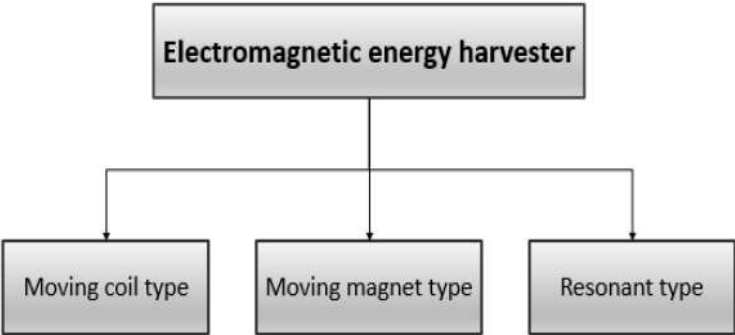


Figure 3.3: Types of vibration based electromagnetic energy harvesters [58]

3.3 Electrostatic Energy Harvester

In electrostatic energy harvester also known as triboelectric energy harvester, the relative motion between the two charged capacitor surfaces produces energy. A schematic of electrostatic energy harvester is shown in figure 3.4. [59], [60]

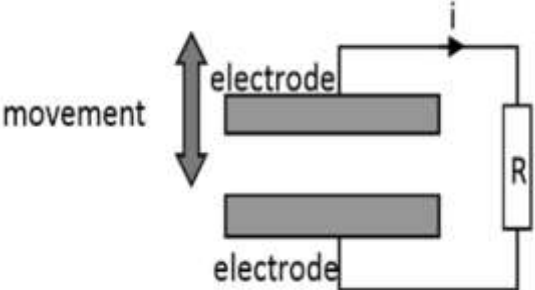


Figure 3.4: Schematic diagram of vibration based electrostatic energy harvester [60]

Electrostatic energy harvested performance depends on the configuration and nature of materials. It works on the triboelectric effect. Triboelectric material is arranged in series employing their tendency of losing and gaining electrons. The electrostatic charge flows to the surface when electrostatic energy harvesters are connected by the electrode and circuit impedance. The partially triboelectric potential layer is formed and due to triboelectric field, electrons flows and variation in capacitance occur. The triboelectric effect can be increased by changing surface structure. Types of electrostatic energy harvester are shown in figure 3.5. [59], [60]

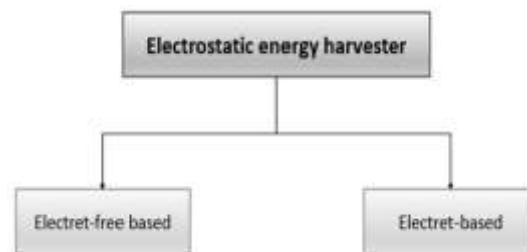


Figure 3.5: Types of electrostatic energy harvester [59]

In electret-free based electrostatic energy harvester, vibration energy is converted into electrical energy by energy conversion cycle. In electret based electrostatic energy harvester, the conversion of energy takes place due to the polarization of electret layers. [59], [60]

The configuration of electrostatic energy harvesting depends on: [59], [60]

- Vertical contact separation mode
- Lateral sliding mode
- Free-standing triboelectric layer mode
- Single electrode mode

To generate small energy density, an external source of voltage is required. The major advantage of it is the production of high voltage.

3.4 Piezoelectric Energy Harvester

Piezoelectric energy harvester works on the principle of the piezoelectric effect. It can be used as both a sensor and an energy harvester. A schematic of piezoelectric energy harvester is shown in figure 3.6. [61]

The piezoelectric effect is the ability of certain materials to generate an electric charge/deformation in response to applied mechanical stress/electric charge. When there is no mechanical stress applied, electrically neutral molecules appear, this is because of the reason that external effects of the charges are canceled when centers of positive and negative charges of each molecule coincide as shown in figure 3.7 (a). [62]

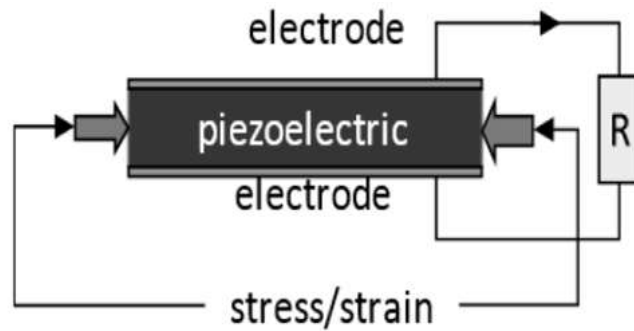


Figure 3.6: Schematic diagram of vibration based piezoelectric energy harvester [62]

When mechanical stress is applied, it alters the distance between centers of positive and negative charge of the molecule which causes separation between them, and the small dipole is generated as shown in figure 3.7 (b). [63], [64]

Facing poles are mutually canceled and polarization charge is induced on the material surface. The electric field is generated due to polarization and can be used to convert mechanical energy into electrical energy.

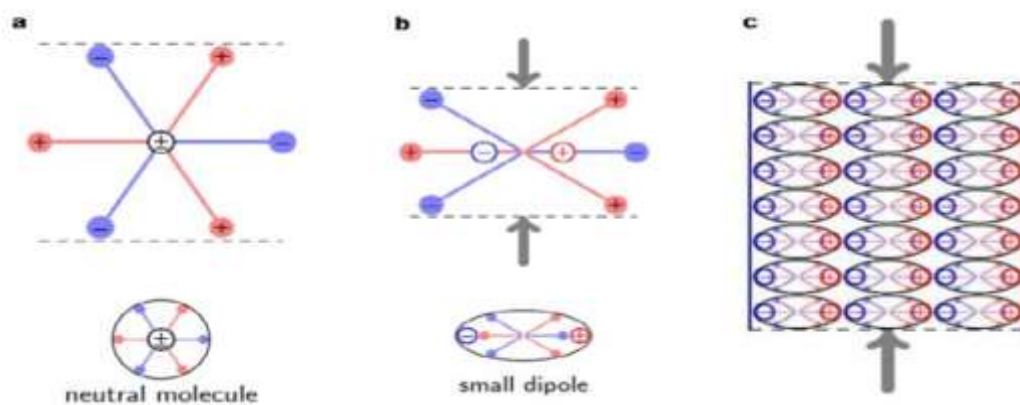


Figure 3.7: Stages involved in piezoelectric effect (a) before, (b) during and (c) after the application of stress [64]

The piezoelectric effect is divided into two types: direct and indirect, as shown in figure 3.8. In the direct piezoelectric effect, the electric field is produced due to mechanical load and in the inverse piezoelectric effect, deformation is produced due to the electric field applied as shown in figure 3.8. [65]

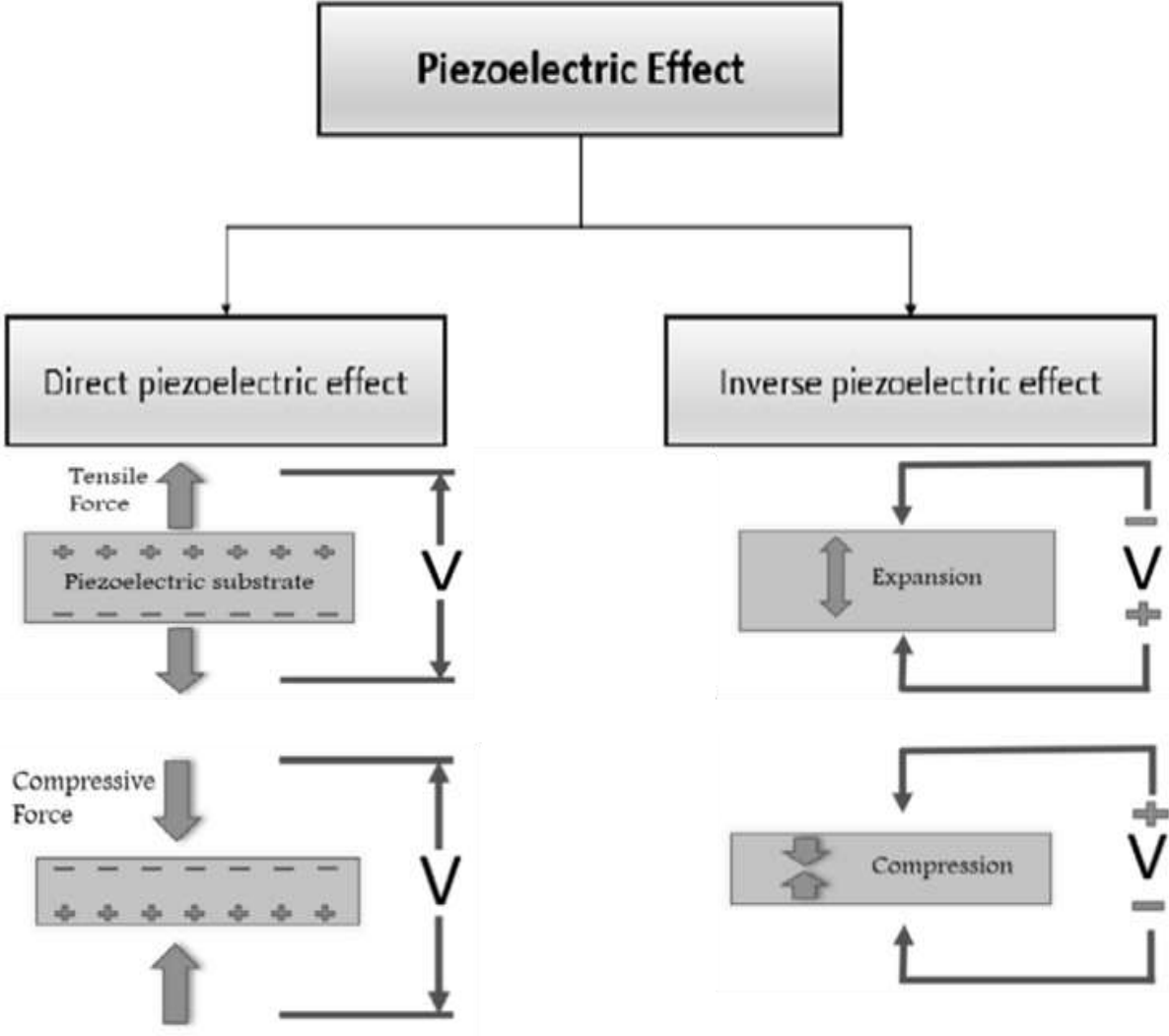


Figure 3.8: Types of piezoelectric effect [65]

3.5 Comparison of Different Harvesters

A comparison of electromagnetic devices, electrostatic devices, and piezoelectric devices is shown in table 3-2. [4], [66], [67]

Table 3-2: Comparison of the advantages and disadvantages of the vibration-based energy harvesters of different types [4], [66], [67]

Device type	Electromagnetic	Electrostatic	Piezoelectric
Advantages	<ul style="list-style-type: none"> ➤ High output current ➤ Long lifetime ➤ Robustness 	<ul style="list-style-type: none"> ➤ High output voltages ➤ Low-cost system ➤ High coupling coefficients reachable 	<ul style="list-style-type: none"> ➤ High output voltages ➤ High capacitance ➤ No need to control any gap
Disadvantages	<ul style="list-style-type: none"> ➤ Low output voltages ➤ Material may be Expensive ➤ Low efficiency 	<ul style="list-style-type: none"> ➤ Low capacitance ➤ No direct conversion ➤ High impact of parasitic capacitance 	<ul style="list-style-type: none"> ➤ Material is expensive ➤ Coupling coefficient linked to material properties

CHAPTER 4: ENERGY HARVESTING FROM ENERGY HARVESTING EEL BEHIND TWO SIDE BY SIDE SOLID CYLINDERS IN STAGGER ARRANGEMENT

This chapter deals with the previous research work regarding piezoelectricity-based energy harvesting from the wake of bluff bodies in water flow and the cases similar to the energy harvesting from energy harvesting eel behind two side by side solid cylinders in stagger arrangement. It includes the citations from the research articles published by different researchers working on the topic around the globe, in different journals.

4.1 Introduction

Self-powered instruments have gained growing attention from the researchers to make use of renewable energy sources present in our environment, as these are environmentally friendly and have become a part of the modern world. [6], [68], [69]. The technology of renewable energy exists in many forms (see Chapter 2). The choice of energy source depends on different factors: sensing lifetime, sensing load, amount of energy to be harvested, and storage. [55] Now a day's vibration energy harvesting has received significant attention as these are sustainable and can provide energy for a longer time. [70] The concept of vibration energy harvesting began with the growth of MEMS devices in the 2000's. [54], [55]. From the vibration source, kinetic energy is converted into electrical energy by vibration energy harvester. To convert vibration energy into electrical energy, different harvesting mechanism have been proposed. [71], [72]

Due to its simple structure and high efficiency, piezoelectric energy harvester has significant potential and are being evaluated. It can be used as both a sensor and an energy harvester. [5], [73], [74]

In the last several decades, the flow-induced fluttering of an energy harvesting eel has attracted interest. When a bluff body is placed in a constant fluid flow. At the interface of fluid and solid, the boundary layer is produced. [75], [76]. This boundary layer separates from the wall and becomes an independent vortex structure. Downstream flow resulting when a cylinder is placed normal to fluid flow is referred to as Karman Vortex street (see Chapter 2). [61], [77] Energy

harvesting eel made of piezoelectric polymer flutters when it is placed in the Karman Vortex street formed behind the bluff body. This results in electrical energy generation. [76], [78], [79]

There have been several studies of water tunnel and wind tunnel experiments. [68], [80] Alexandra et al. followed this approach to study energy harvesting from piezoelectric eels in the oceans. [75] Christophe et al. experimentally study the instability of a flexible plate in a uniform flow. [81]–[83] Dunmen et al. designed an experimental system to verify the theoretical aero elastic systems. [84] Dung et al. developed an analytical design method for energy harvesting. [85] The main contribution was to fabricate and test prototype energy harvester. LadHyx et al. showed how self-sustained oscillation resulting from fluid-structure interaction can be used for energy harvesting. [86] Daegyoun et al. experimentally study the flapping dynamics of an inverted flag for potential application of energy harvesting. [87], [88] Wenshang et al. investigate the dynamics of cantilever flexible plates in axial flow both by theoretically and experimentally. [89], [90] Jae et al. use the inverse boundary method to investigate the flapping dynamics of a flexible flag in a uniform flow. [91], [92] Chuang et al. tested the performance of the piezoelectric sensor in a small wind tunnel. [93] Hyeong et al. considered two designs for electromechanical coupling and investigate by varying flow passage and geometry experimentally. [72] Xiaobiao et al. numerically and experimentally investigate the ability of microfiber composite piezoelectric energy harvested when placed in a water vortex. [94], [95] Rujum et al. found that vortex-induced piezoelectric energy harvesting shows better performance with the attachment of a large diameter and lighter weight mass cylinder. [94], [95] Mehedi et al. conducted a computational study on piezoelectric transducer placed in a small channel fluid flow by varying fluid and flow characteristics. [96] Hidemi et al. study the effect on energy harvesting by optimizing the design of a flexible piezoelectric energy device. [5], [97] Hyeonseong et al. explored the effect of air and water flow on a conventional and inverted flag. [88] Piezoelectric energy harvester based on flag flutter was numerically and experimentally investigated by Macro et al. [83], [98] Junlei et al. explored the effect of Y-shaped attachments on the performance of piezoelectric energy harvested. [70], [99]

In this study, we experimentally investigate the effect of the wake produced due to two side by side (staggered) solid cylinders on energy harvesting when the energy harvesting eel is placed behind the solid cylinders by varying stream-wise distance. We further investigate the effect of

the center-to-center distance between staggered cylinders on the energy harvesting. All in all, we will focus on power response and amplitude response when the energy harvesting eel is placed at different points concerning two staggered cylinders, having specific center-to-center distance, and will compare the flapping behavior at each point.

CHAPTER 5: EXPERIMENTAL SETUP

This chapter deals with the experimental setup and methodology of the study. It provides a detailed description of the apparatus used in the experimentation, experimental setup, system parameters and experimental conditions and methodology of the work. It also includes the schematic description of the experimental setup and data acquisition setup highlighting the system parameters and the parameters to be measured.

5.1 Apparatus Description

5.1.1 Low-speed closed-circuit water channel

The hydrodynamic behavior of the objects submerged in water is studied in the water tunnel. It works on the same working principle as wind tunnel but have water as a working fluid instead of the air. It's most important application is its utility for visualizing the fluid flow over the submerged bodies. It can also be used to check the interaction of fluid with various structures and examining the boundary layer formation and processes such as flow separation and vortex shedding. As water is the working fluid in this apparatus, therefore, it is also very suitable for particle image velocimetry (PIV). Oil is used as a working fluid inside the tunnel instead of the water for the low Reynold's number (Re) ranges. It is because of the reason that the higher kinematic viscosity of the oil results in the speedy flow at lower Reynold's numbers. [68], [69]

The important parts of water tunnel and their functionalities are explained below.

5.1.1.1 Test section

The section with the transparent walls where various tests on different objects are carried out and the fluid can be seen flowing over the body, is known as the test section of the water tunnel. It's one of the major parts of the water channel apparatus. Test section's walls are made up of 10 mm thick Acrylic glass. The cross-sectional dimensions of the section are 0.4×0.4 m and the length is 2 m. [69]

5.1.1.2 Inlet plenum

Inlet plenum is the largest part of the apparatus which is used as a reservoir for storing sufficient amount of fluid for testing. The fluid pumped out from inlet through piping system is collected in this reservoir. [69]

It is consisted of two important parts:

- First and the important part is an inlet tank with baffle plates fixed inside it to keep the reservoir from deforming due to higher hydrostatic forces. A 6 mm thick aluminum plate having 16 mm diameter holes, is installed inside it in order to reduce turbulence, increasing the uniformity of the fluid flow by decreasing its turbulence intensity. [69]
- Settling chamber is the second part which is used to reduce the intensity of turbulence and flow speed by giving space to the molecules of fluid (water). This is a rectangular chamber having the dimensions $L \times W \times H = 1.5 \times 1.85 \times 0.5 \text{ m}$. [69]

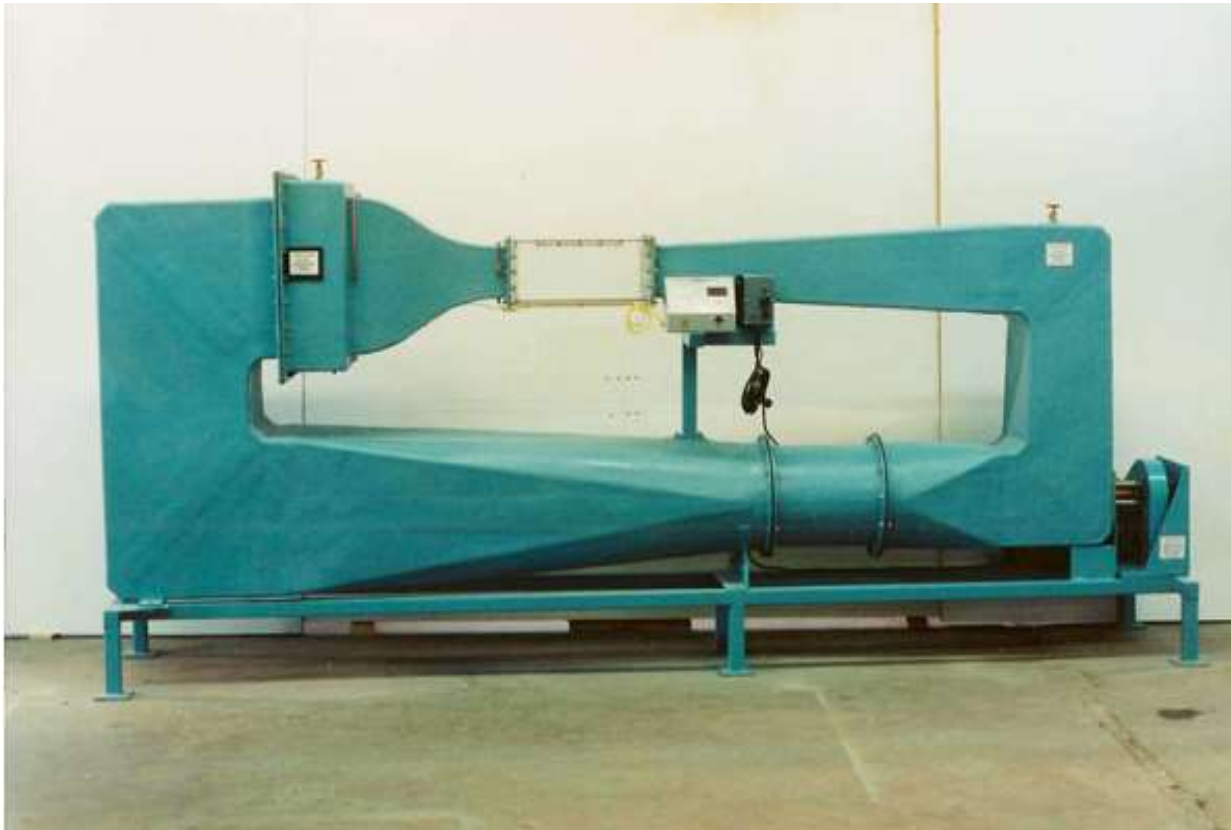


Figure 5.1: A closed loop water tunnel by *AEROLAB* with nominal speed 9.1 m/sec [100]

5.1.1.3 Honey comb

Honeycomb is the part of water tunnel which is used to convert the turbulence flow into the laminar flow by realizing the reduction in the transverse component of the fluctuating velocity. Free stream turbulence level and the liminality in the flow are required to the analysis. To get the fully laminar flow in the test section, the honeycomb is placed before converging section. Aluminum honeycombs with the hexagonal openings of the dimensions $1.83 \times 0.50 \times 0.025 \text{ m}$ ($L \times W \times H$) are used. [69]

5.1.1.4 Contraction chamber

A convergent section, known as contraction chamber is used after the honeycomb section to reduce the intensity of the turbulence and enhance the flow speed. The outlet of enhanced length is used to improve the flow uniformity. The ratio of contraction usually lies between 5 and 10.

The water tunnel at NUST have the contraction chamber of the contraction ratio equals to 5. Since the width of the test section is 0.4 m , therefore the width of $0.4 \times 5 = 2 \text{ m}$ at the contraction chamber's inlet is used. The height of chamber with rectangular cross-section is 0.5 m which is uniform along the length. [69]

5.1.1.5 Side walls

The side walls of the water channel are made of aluminum sheet and have a curvature to ensure streamline and smooth flow. [69]

5.1.1.6 Diffuser

The pressure of fluid (water or air) flowing through pipes or ductwork is increased using diffusers. In diffuser, it is important to ensure that the flow is steady and uniform at its outlet as it affects the main components' execution in downstream. Circular, square or rectangular cross-section can be used in diffusers. Straight or bell shaped (in order to guide the flow by making it more streamlined) diverging sections can be used in them. As water expands differently from gases, therefore lower diverging angles with longer lengths are used. The water tunnel facility at NUST have the diffuser of rectangular cross-section. Its divergence ratio is 0.67 while the angle

of semi-vertex is 11° . Its length is 0.5 m . Its cross-sectional area at inlet is equal to the test section's cross-sectional area. [69]

5.1.1.7 Outlet plenum

The wide-angle diffuser of the water tunnel is connected with the piping system to get its flow drained out, using the outlet plenum. The outlet plenum of the water tunnel should not cause any sort of irregularity leading to the back pressure or flow reversal, which may affect the results obtained in the test section. To avoid any reverse flow, back pressure and to ensure the smooth flow in the system, the outlet is consisted of two openings to allow the water to get distributed equally at the exit. To keep any sort of impurities from entering into the pump, a strainer is used between diffuser and outlet plenum. Its cross-sectional dimensions are $0.79 \times 0.79\text{ m}$ with the height of 1.5 m . [69]

5.1.1.8 Supporting table

The part of the water tunnel present between inlet and outlet, totally filled with water, is usually suspended freely in air. The model cannot bear the forces and the weight of the water. Therefore, usually a frame structure, supporting the whole water channel is used. NUST's water tunnel have supporting table made of 2 in squared mild steel pipes, which distributes the water's load and provide a support for the channel properly. [69]

5.1.1.9 Plumbing system

Flexible green pipes are used to connect the pump to inlet and outlet. Piping with a little bit of flexibility reduces the vibrations in the system. A 6 in diameter pipe is used for the suction at the pump's inlet while a 5 in diameter pipe is used at the outlet. Pump's outlet pipe provides water to the inlet container which then recirculate it through the system. To keep the piping system from leaking M-seals are used at the joints. [69]

5.1.1.10 The pump

A centrifugal pump with a 10 hp motor is used to pump the water through the system. It can deliver water to the test section up to the maximum flow speed of 0.5 ms^{-1} , while the minimum

flow speed is 0.2 ms^{-1} . It can be controlled by a voltage regulator. It provides a laminar flow by minimizing the turbulence. The flow speed can be controlled by using a ball valve in conjunction with a variable speed AC-controller. [69]

5.1.2 Data acquisition

Data acquisition (DAQ) is the process of measuring an electrical or physical phenomenon such as voltage, current, temperature, pressure, vibration or sound with a computer. A DAQ system consists of sensors, DAQ measurement hardware, and a computer with application software. [101]

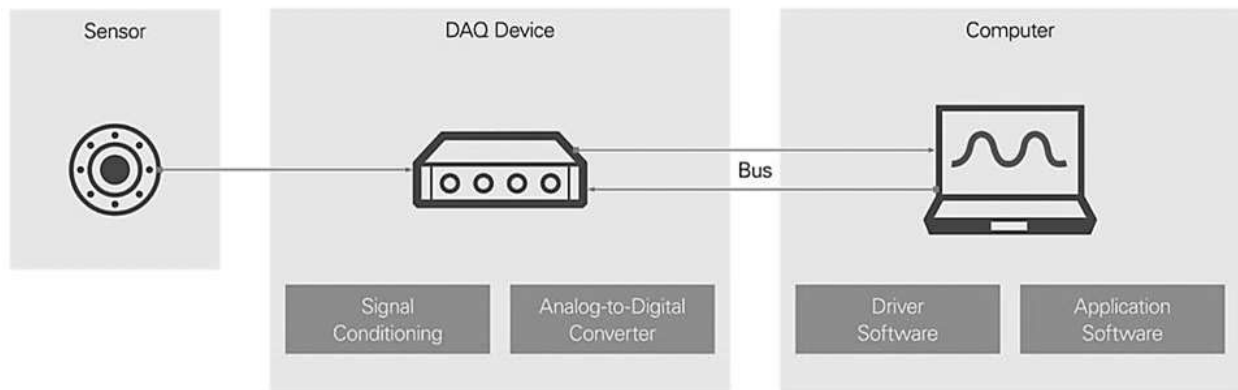


Figure 5.2: Schematic diagram of a simple data acquisition setup consisting of a sensor, DAQ device and a computer, by National Instruments (NI) [101]

5.1.2.1 Sensor

A sensor, also called a transducer, converts a physical phenomenon like temperature or vibration, into a measurable electrical signal like voltage or resistance. [101]

5.1.2.2 DAQ device

A DAQ device acts as the interface between a computer and signals from the outside world by digitizing incoming analog signals to be computer readable. DAQ devices include three key components: [101]

5.1.2.2.1 Signal conditioning circuitry

Transforms noisy real-world signals into forms that can be effectively and accurately measured.

5.1.2.2.2 Analog-to-digital converters (ADCs)

Digitize real-world analog data into digital representations that can be manipulated by computers.

5.1.2.2.3 Computer bus

Enables the DAQ device to transmit data to a computer. Examples include USB, PCIe, or Ethernet.

5.1.2.3 Computer and software

A computer with DAQ software is required to process, visualize, and store measurement data. DAQ software includes a driver, which is accessed by either application software or a development environment. [101]

5.1.2.3.1 Driver software

Gives application software the ability to control your DAQ device with menu-based configuration or a programmable API.

5.1.2.3.2 Application software

Gives the user a ready-made experience for acquiring, analyzing, and presenting data. Configuration is done using menu-based interfaces.

5.1.2.3.3 Programming environment

Allows users to develop their own application to acquire, analyze, and present data, using libraries of functions (APIs) to access and control their DAQ device.

5.2 Experimental Setup

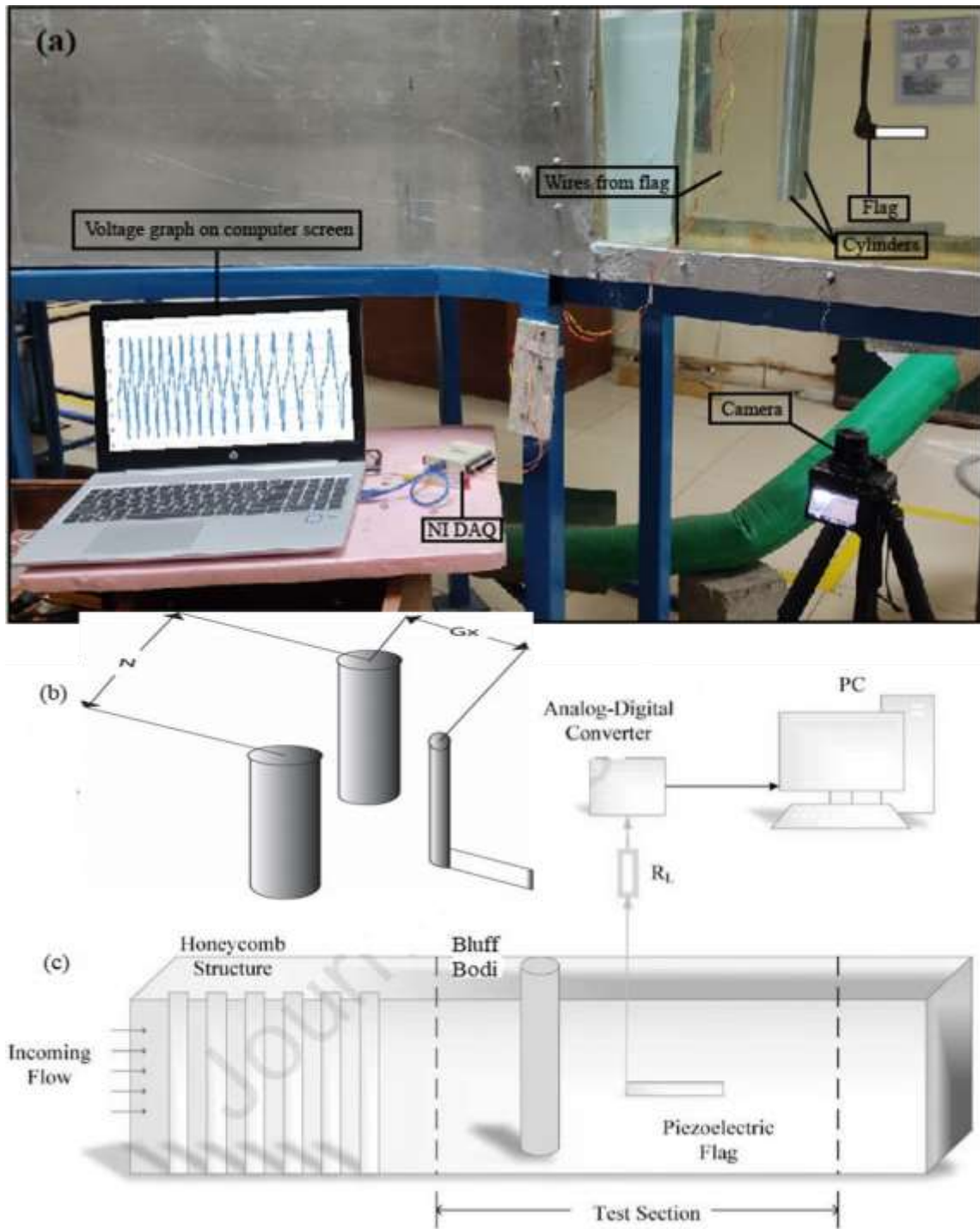


Figure 5.3: (a) Complete experimental setup, (b) Schematic diagram of the piezoelectric eel placed behind two staggered cylinders, and (c) Schematic diagram of the whole experimental setup [6]

Low-speed closed-circuit water channel facility available in the Department of Mechanical Engineering, School of Mechanical and Manufacturing Engineering at the National University of Sciences and Technology (NUST) is used for the experimentation. Test section of the water tunnel have a square cross-section and dimensions $(L \times W \times H) 2 \times 0.4 \times 0.4 \text{ m}$. To bring the uniformity in the flow, aluminum honeycombs with the hexagon openings having dimensions $1.83 \times 0.50 \times 0.025 \text{ m}$ ($L \times W \times H$) are used. The freestream velocity (U_∞) can be varied from 0 to 0.5 ms^{-1} (having maximum turbulence intensity less than 1%) using a variable frequency drive (VFD) motor. . [69] The experimental setup and schematic diagrams are shown in figure 5.3.

Improvement in energy harvesting by the flapping eel is examined by placing it behind two side by-side cylinders separated by the distance N in a staggered arrangement, as shown in figure 5.3 (b) and figure 5.4. To keep the test section from any kind of transverse motion or vibration, a frame fixed on the top of the test section is used to held aluminum rod, used to hold the eel from one end, and the cylinders tightly in the place. The setup for this experimentation is consisted of a sensor to measure the freestream velocity of the fluid, a slow-motion camera to capture the video shot of the eel's flapping, a data acquisition setup to record the output of eel, and a voltage measurement device to connect across the piezoelectric layer made of polyvinylidene-fluoride. Thin metalized layers having $54 \mu\text{m}$ thick piezoelectric layer packed inside them are connected to the built-in terminals and used to transport charges developed on piezoelectric layer. These layers are further covered with transparent, thin plastic layers, acting as a protection. Total thickness of piezoelectric eel is $64 \mu\text{m}$. The magnitude of the power produced by the eel depends on the applied force/pressure and the resulted deformation/strain in the piezoelectric layer. These layers can provide output voltage in the range of 10 mV to 100 V depending on the magnitude of applied force and total impedance of the circuit. For example, piezoelectric layers of PVDF-DT series usually produce voltage more than $10 \text{ mV}/\text{micro} - \text{strain}$.

A *DT2 – 052K/L PVDF* eel (P/N: 2 – 1003744 – 0) by *Measurement Specialties Inc.* with one end fixed on an aluminum rod (leading edge) of diameter, $\Phi = 4 \text{ mm}$ and the other end free to move (trailing edge), is used in the experimentation. The total length of the eel is 72 mm while its active length is 60 mm . The layers of eel have the thickness of $64 \mu\text{m}$ and the width of

12 mm. Complete set of properties of the eel and its material are given in table 5-1 while the system parameters of experimentation are given in table 5-2.

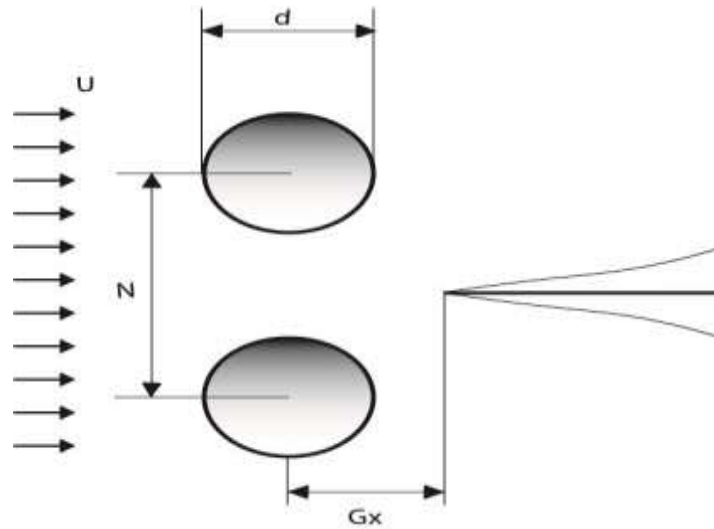


Figure 5.4: Arrangement of piezoelectric eel/flag behind two staggered cylinders of diameter D and separated by distance N , placed at the distance G_x^* in the fluid moving with the free stream velocity U_∞

Table 5-1: Physical properties of piezoelectric eel and its material [6]

Parameter	Value
Eel's total length (<i>mm</i>)	72
Eel's active length (<i>mm</i>)	60
Eel's width (<i>mm</i>)	16
Eel's material	<i>PVDF</i>
Density of eel (<i>kg/m³</i>)	1.78
Young's Modulus of eel (<i>10⁹ N/m²</i>)	2 – 4
Relative permittivity of eel (ϵ/ϵ_0)	12
d_{31} constant (<i>10⁻¹² C/N</i>)	23

g_{31} constant (10^{-3}Vm/N)	216
k_{31} constant (% at 1 kHz)	12
Capacitance of eel (nF)	1.44
Output voltage of eel (V)	0.01 – 100
Load resistor (M Ω)	2.5
Operational temperature (°C)	0 – 70

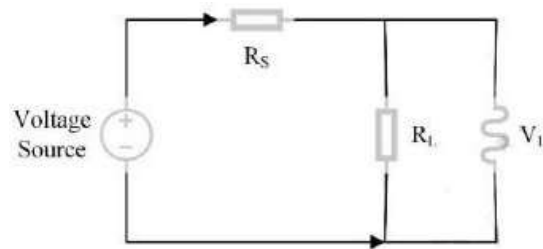


Figure 5.5: The circuit diagram showing a voltage source (piezoelectric eel/flag) connected with the load resistor R_L with the voltage drop V_L [6]

Table 5-0-2: Experimental system's parameters

Parameter	Value
Fluid	<i>Water</i>
Fluid density (kg/m^3)	998
Fluid velocity in tunnel (m/s)	0.31
Fluid temperature (°C)	25
Cylinder diameter (mm)	25
Number of cylinders	2
Rod diameter (mm)	4
Cylinder and rod material	<i>Aluminium</i>

The flapping of the piezoelectric eel is captured using *RX – 100 IV* high-speed camera by *Sony*. Figure 5.5 shows an external load resistance R_L ($2.5 M\Omega$) connected with the output wires of the PVDF eel. The frame rate of 50 frames/second and the resolution of 1920×1080 pixels is used to capture the video of each test for 120 seconds. *Mcopus TTV 204* LED lights positioned on both sides of the eel, are used to illuminate the piezoelectric layer for better visualization. Black paper is used to cover the test section to keep any background interference from the video. *MATLAB* codes are used for the post-processing of captured video shots to calculate the flapping frequency and amplitude of vibration of the eel. The *MATLAB* codes used to process the video to get the frequency and amplitude response, along with the flapping images, are given in the **Appendix A** of the thesis.

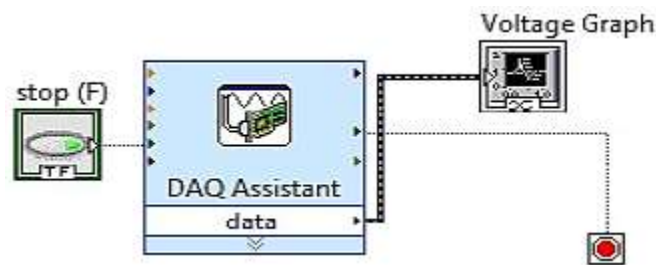


Figure 5.0.6: *LabVIEW* circuit of the data acquisition setup

Furthermore, the *NI – USB 6009*, multifunction I/O data acquisition card by *National Instruments*, is used to gather the data of the power generated by the piezoelectric eel using a *LabVIEW* model at 50 Hz for 120. The *LabVIEW* circuit of the data acquisition setup is given in the figure 5.6.

CHAPTER 6: RESULTS AND DISCUSSION

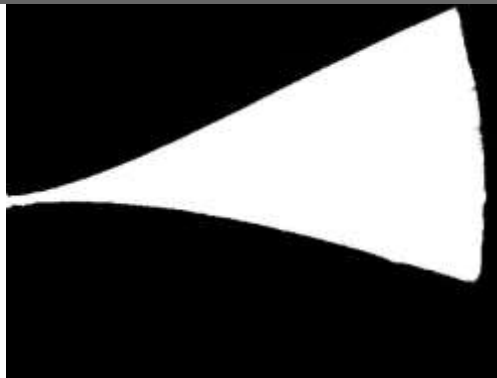
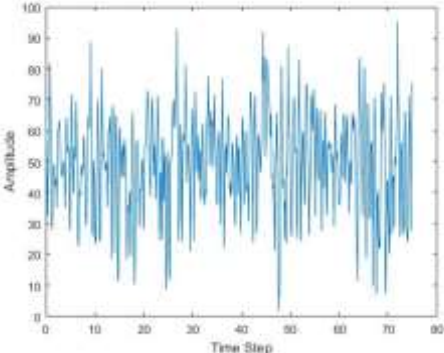
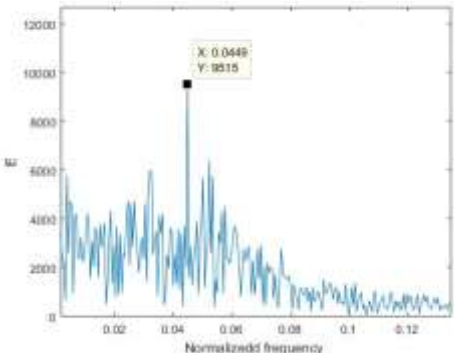
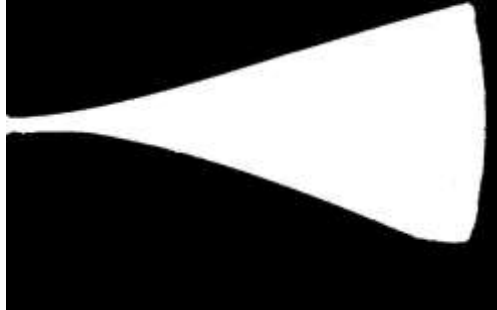
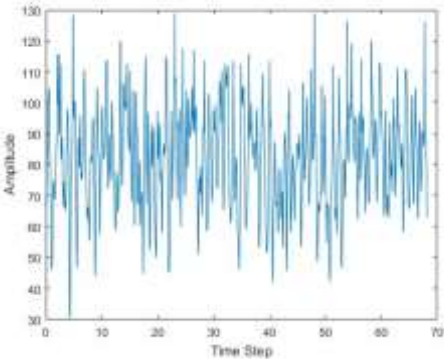
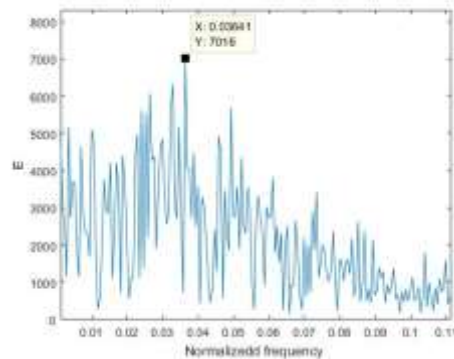
This chapter explains the measured results of experimentation and processed results of amplitude, voltage and power through *MATLAB* program and *Microsoft Excel* sheets, according to the methodology explained in the previous chapter. It also includes the graphical representation, plots of the results, and mainly focuses on discussing the obtained values of the parameters including frequency, amplitude, voltage and power under different testing conditions and scenarios, and explains the trends of the obtained graphs.

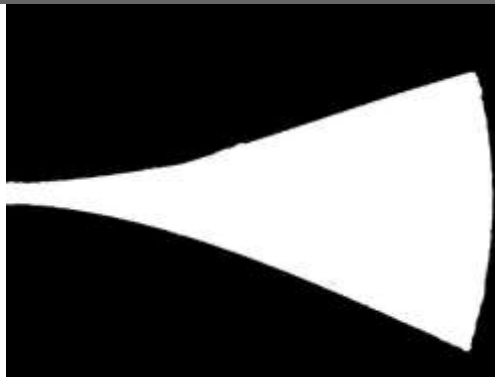
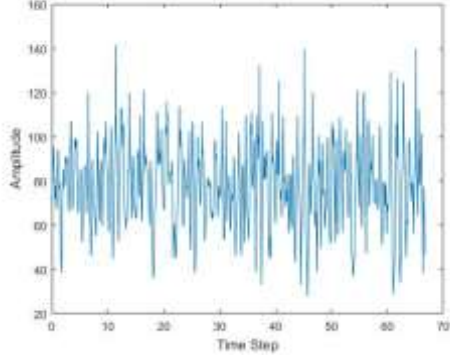
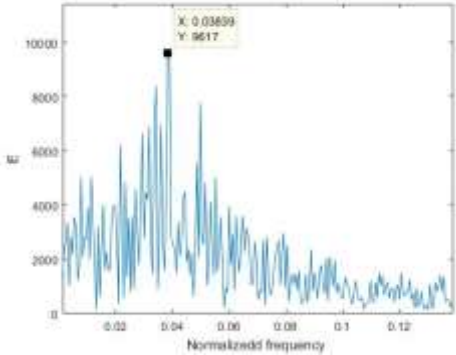
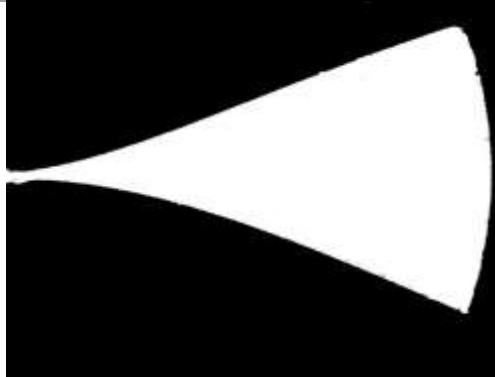
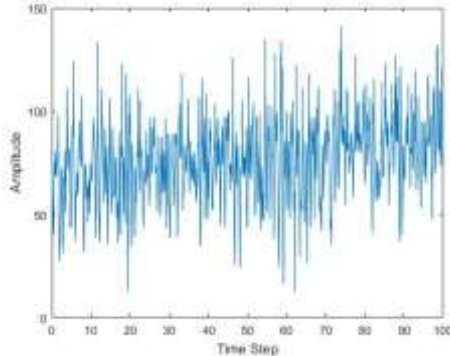
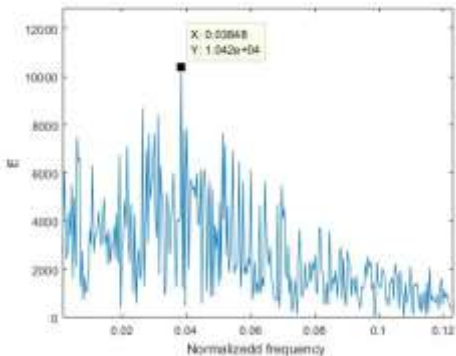
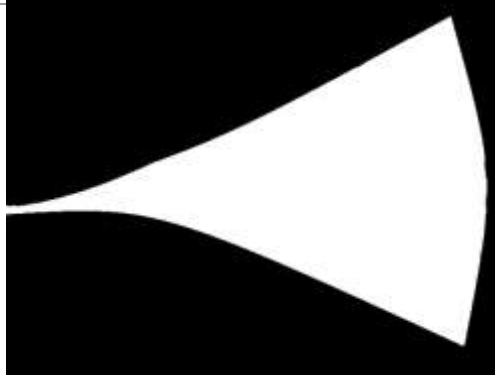
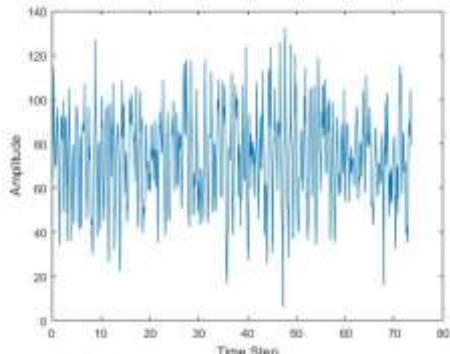
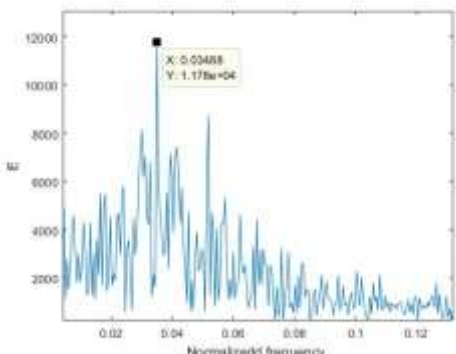
6.1 Piezoelectric Eel's Flapping, Amplitude and Frequency Response

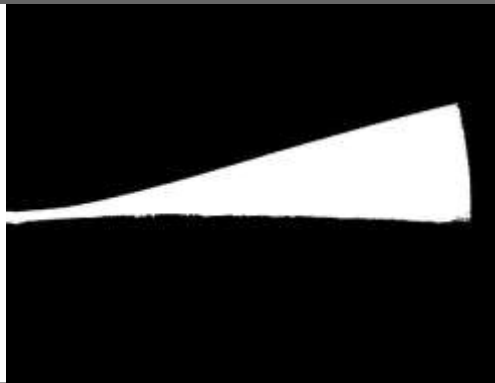
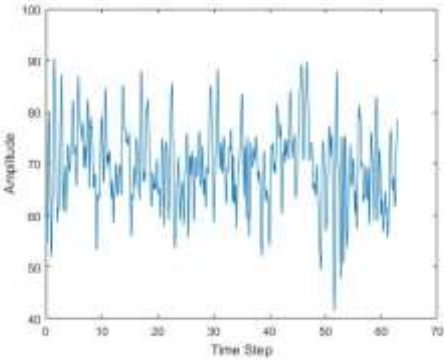
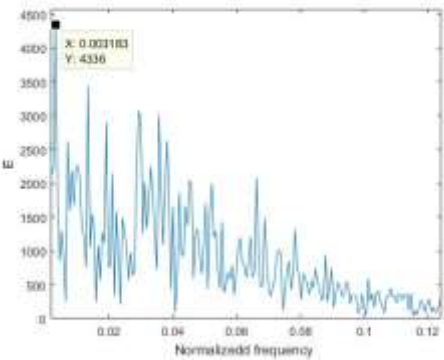
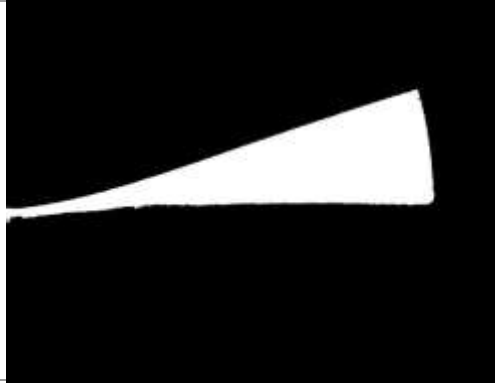
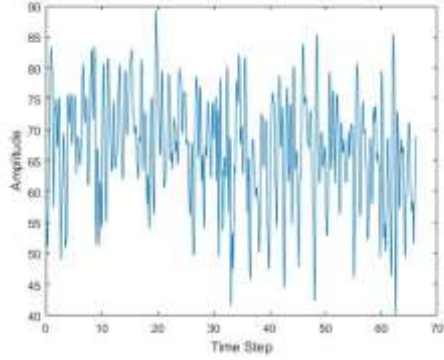
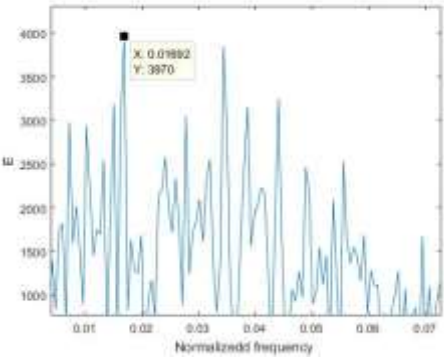

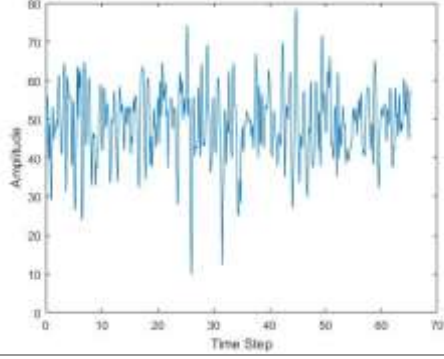
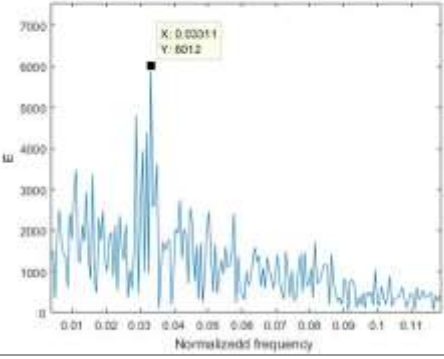
The piezoelectric flag/eel placed behind two side by side cylinders in a staggered arrangement is tested for 25 different cases. The technique is to vary the center-to-center gap between the staggered cylindrical bluff bodies, N , and stream-wise gap between eel's fixed end and the line joining the axes of the cylindrical, G_x^* . It is an important thing to note that the crosswise perpendicular distance between the center of the line joining the centers of cylinders and the fixed end of the eel remains unchanged, $G_y^* = 0$. Hence, the fixed end of the eel lies on the perpendicular bisector of the line joining the centers of both cylinders. Furthermore, both cylinders have equal and fixed diameters, $d = 25 \text{ mm}$. Therefore, the ratio, N/d , represents the direct relationship with the center-to-center gap between two cylindrical bluff bodies, N . Similarly, the ration, $G_x = G_x^*/d$, represents the direct relationship with the streamwise gap, G_x^* . The experimentation is done with some specific, fixed, N/d , while changing the value of, G_x , and then the experimentation is repeated for some other value of N/d . In this manner, the testing is done for five different values of $N/d = [1.00, 1.25, 1.50, 1.75, 2.00]$, each corresponding five different settings of $G_x = [2.0, 2.5, 3.0, 3.5, 4]$. The purpose is to get the flapping video of all these 25 cases, which then can be processed using the *MATLAB* code, given in **Appendix A**, to get the flapping image, amplitude and normalized frequency response over the time span for all cases.


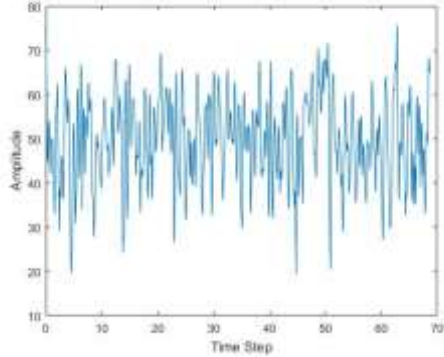
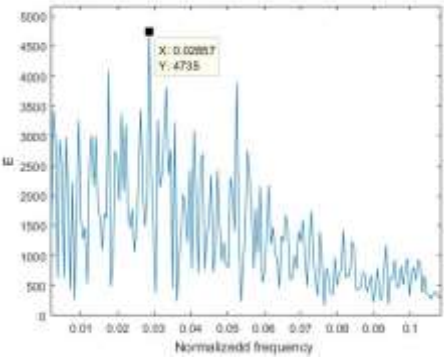
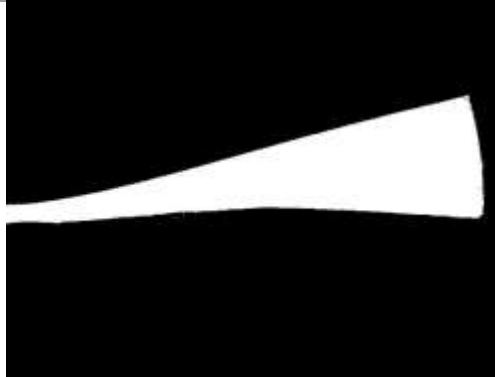
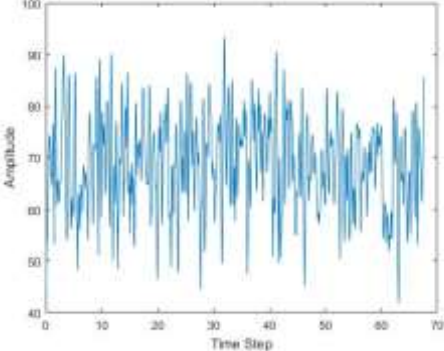
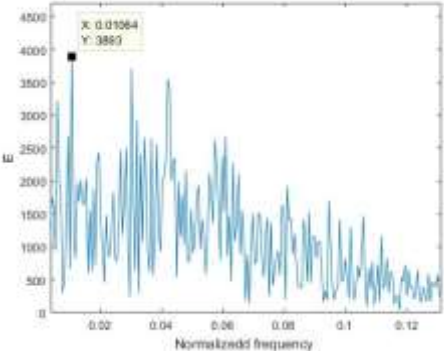

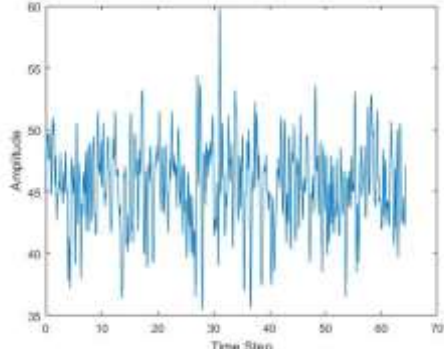
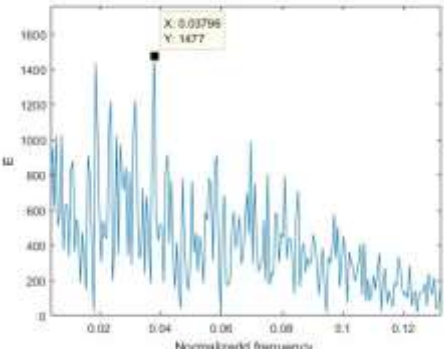
The results for flapping, amplitude and the normalized frequency response of the eel's vibration for all cases, obtained through the processing of captured videos of tests, are given below in the table 6-1.

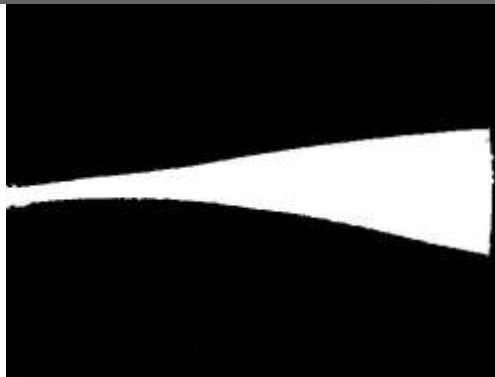
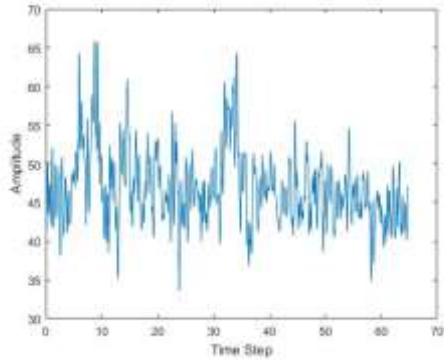
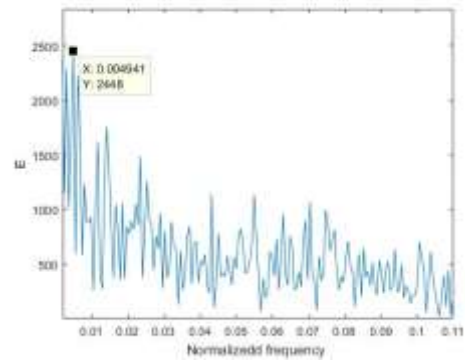
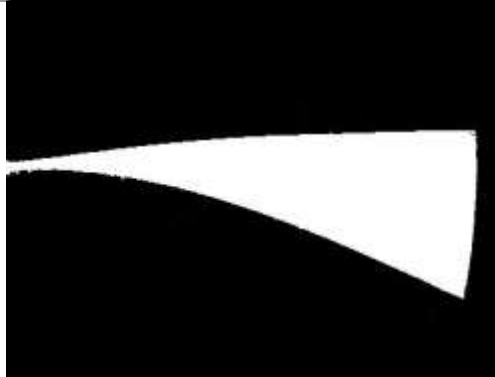
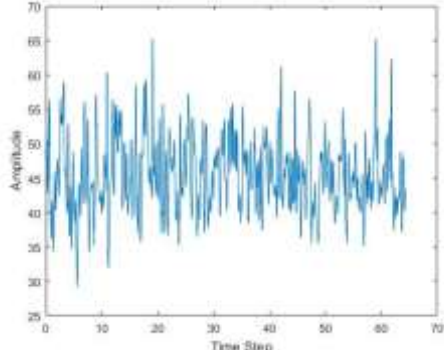
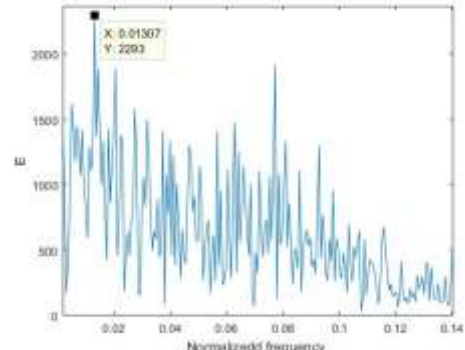
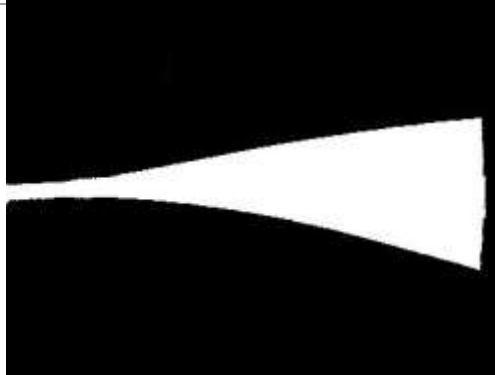
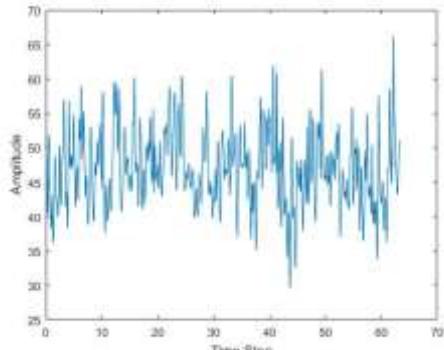
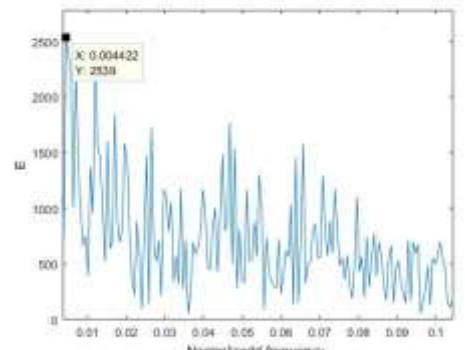
Table 6-1: The results for the flapping, amplitude and the normalized frequencies of the piezoelectric eel, obtained by processing the captured video shots of the different testing cases using the *MATLAB* codes available in the Appendix A

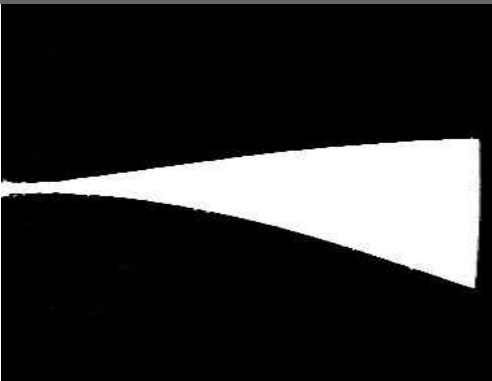
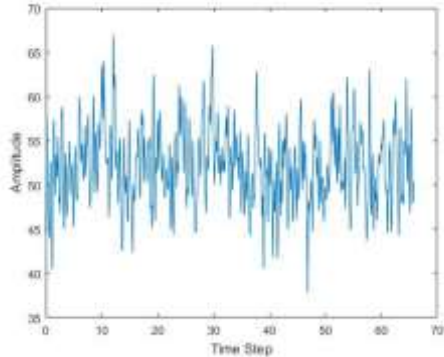
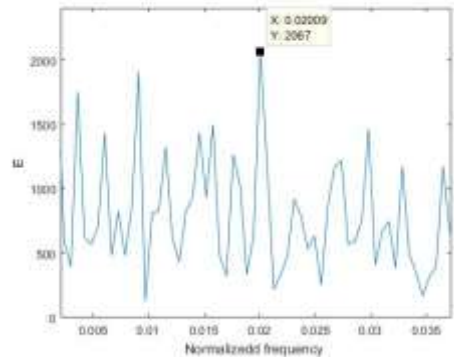
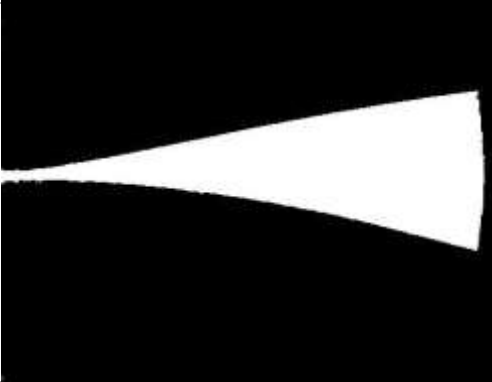
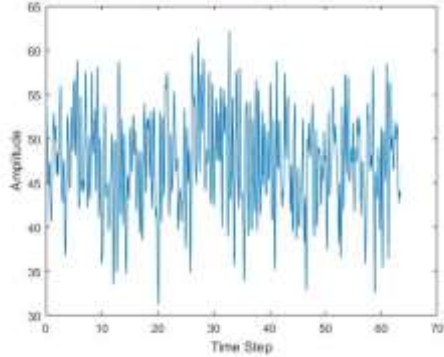
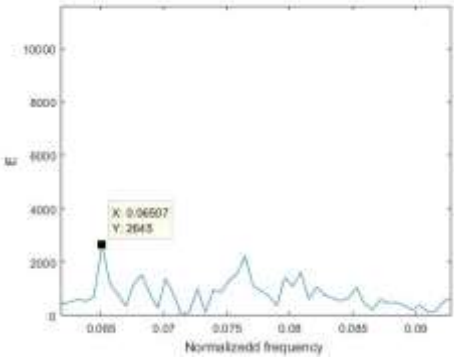

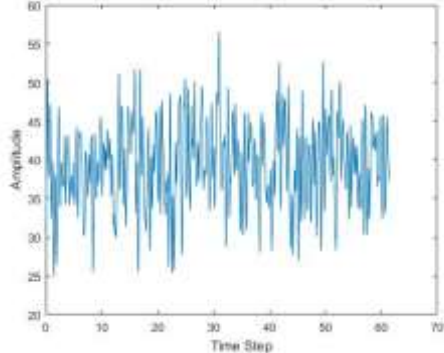
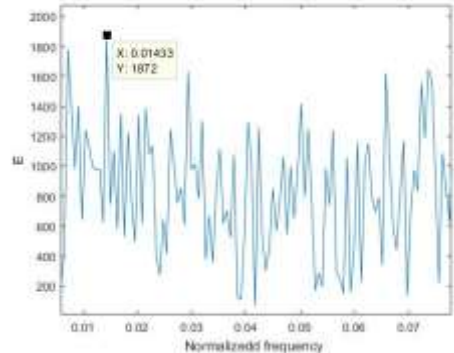
N/d	G_x	Flapping	Amplitude	Frequency
1.00	2.0			
1.00	2.5			

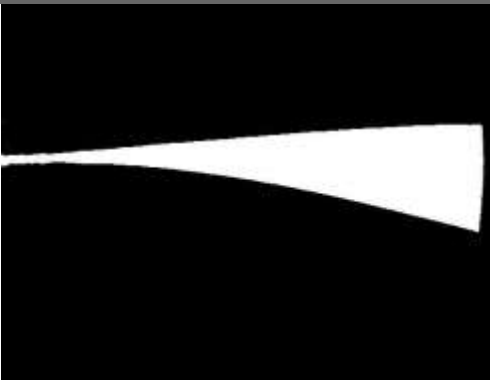
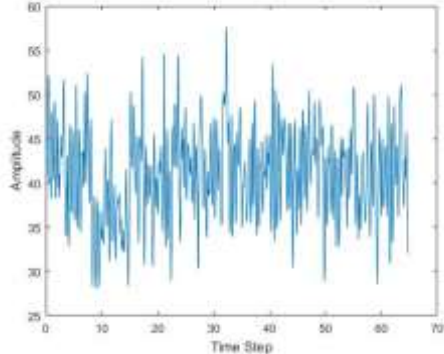
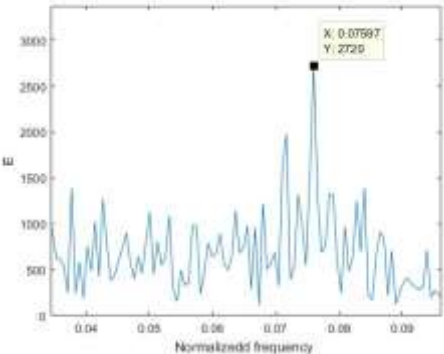
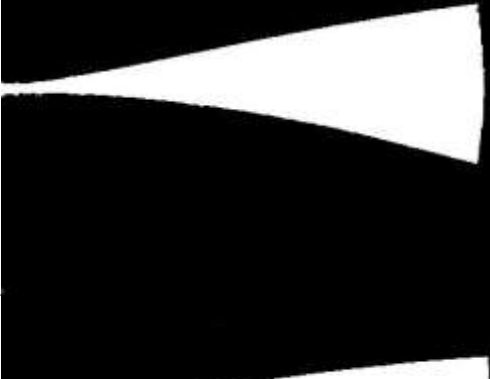
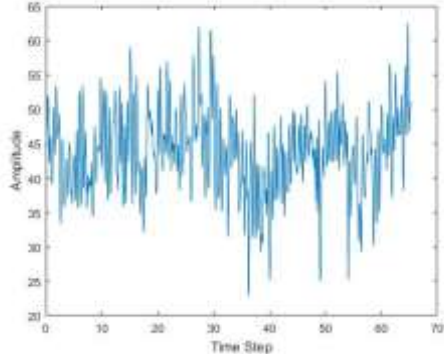
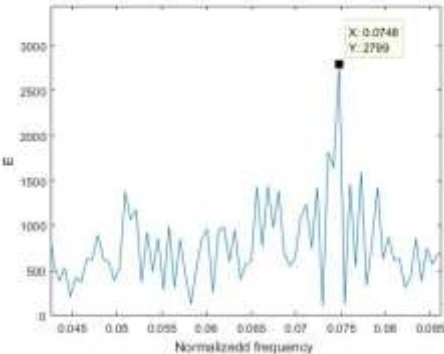

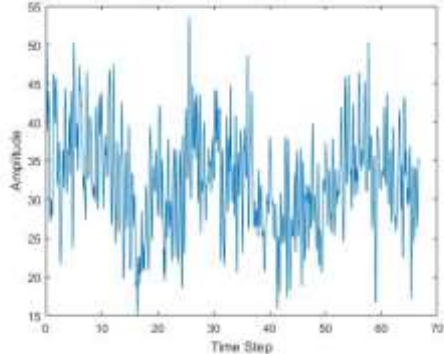
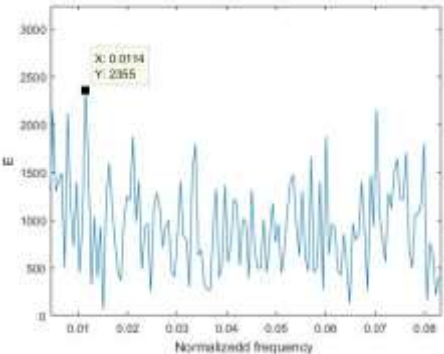
N/d	G_x	Flapping	Amplitude	Frequency
1.00	3.0			
1.00	3.5			
1.00	4.0			

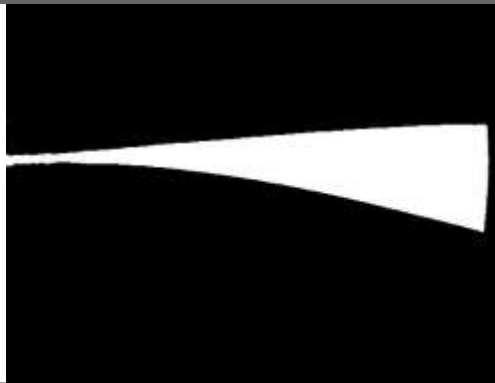
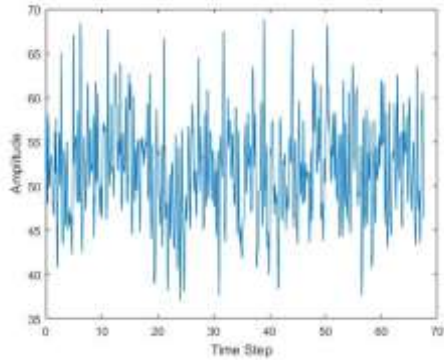
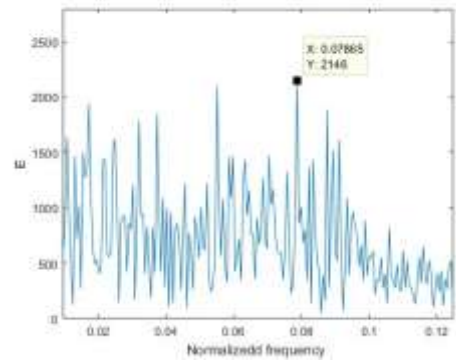
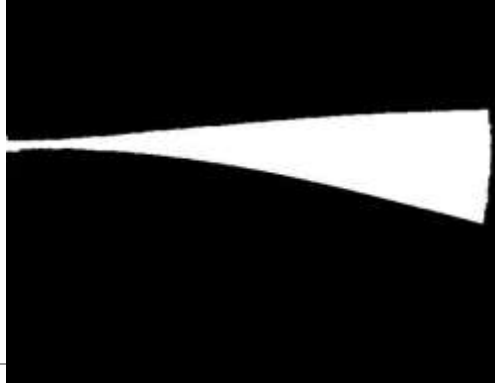
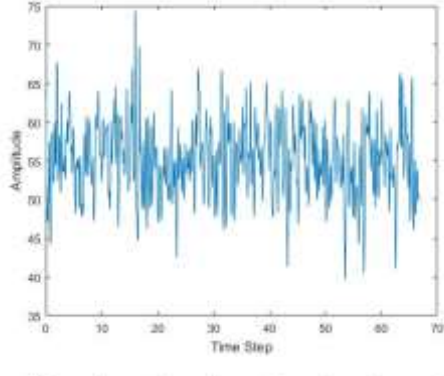
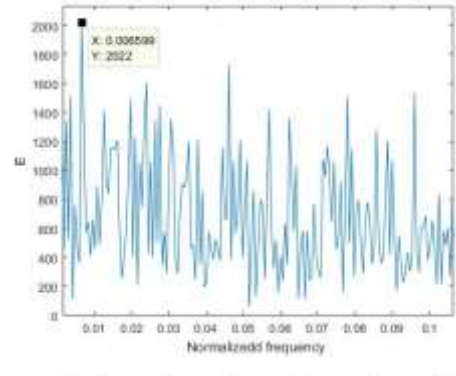

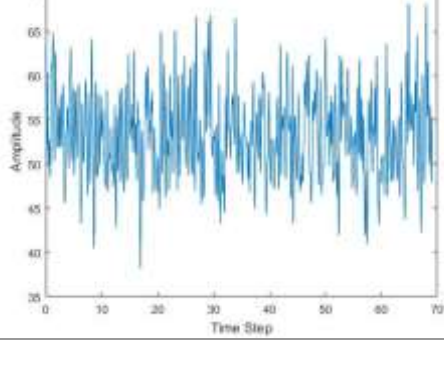
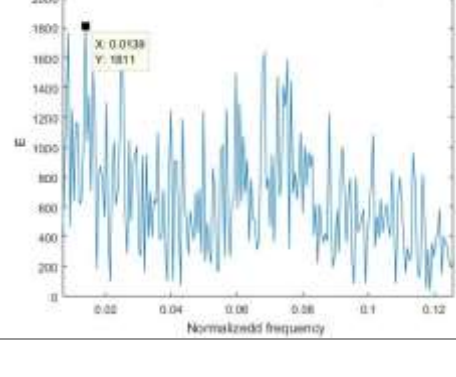
N/d	G_x	Flapping	Amplitude	Frequency
1.25	2.0			
1.25	2.5			
1.25	3.0			

N/d	G_x	Flapping	Amplitude	Frequency
1.25	3.5			
1.25	4.0			
1.50	2.0			

N/d	G_x	Flapping	Amplitude	Frequency
1.50	2.5			
1.50	3.0			
1.50	3.5			

N/d	G_x	Flapping	Amplitude	Frequency
1.50	4.0			
1.75	2.0			
1.75	2.5			

N/d	G_x	Flapping	Amplitude	Frequency
1.75	3.0			
1.75	3.5			
1.75	4.0			

N/d	G_x	Flapping	Amplitude	Frequency
2.00	2.0			
2.00	2.5			
2.00	3.0			

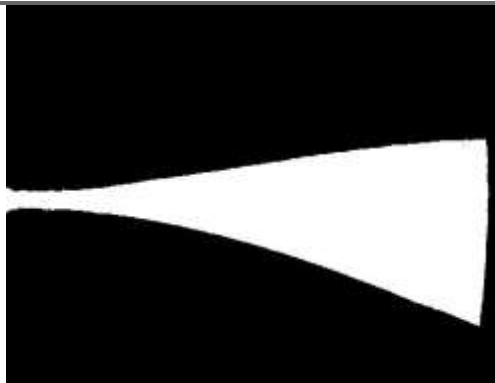
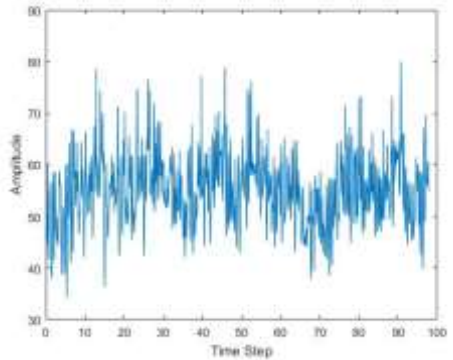
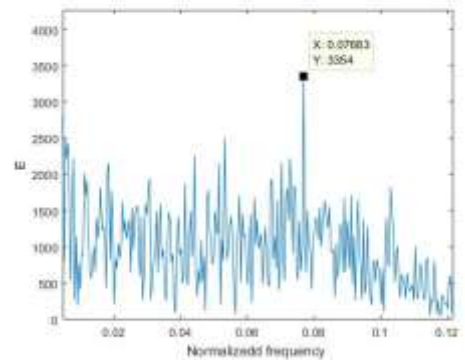
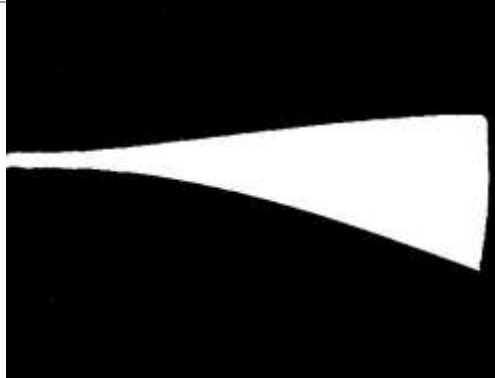
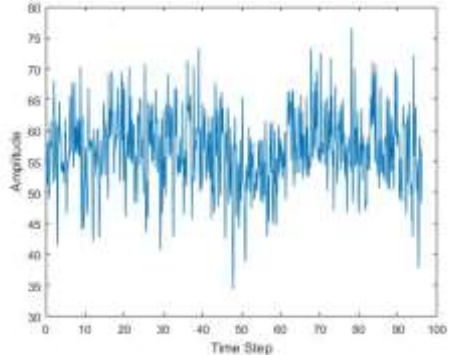
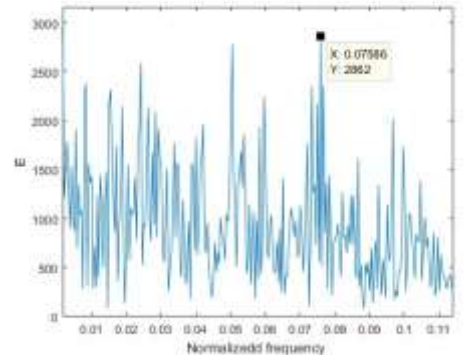
N/d	G_x	Flapping	Amplitude	Frequency
2.00	3.5			
2.00	4.0			

Table 6-1 represents the flapping, amplitude and frequency response of the piezoelectric eel, vibrating due to the vortices (turbulence) in the water, waked by the bluff bodies, over a certain time span. The trend can better be visualized by plotting the mean amplitude of vibration and the maximum frequency of flapping for each case against the respective N/d and G_x value for that case. The obtained plots along with their respective explanations for trends are given below.

6.2 Piezoelectric Eel's Non-Dimensional Amplitude and Frequency of Flapping

The amplitude of flapping, A , can be made dimensionless by dividing it by the length of the eel, L . Since, length of the eel is fixed, therefore, the dimensionless amplitude, A/L is in direct relationship with the actual amplitude, A of the flapping eel.

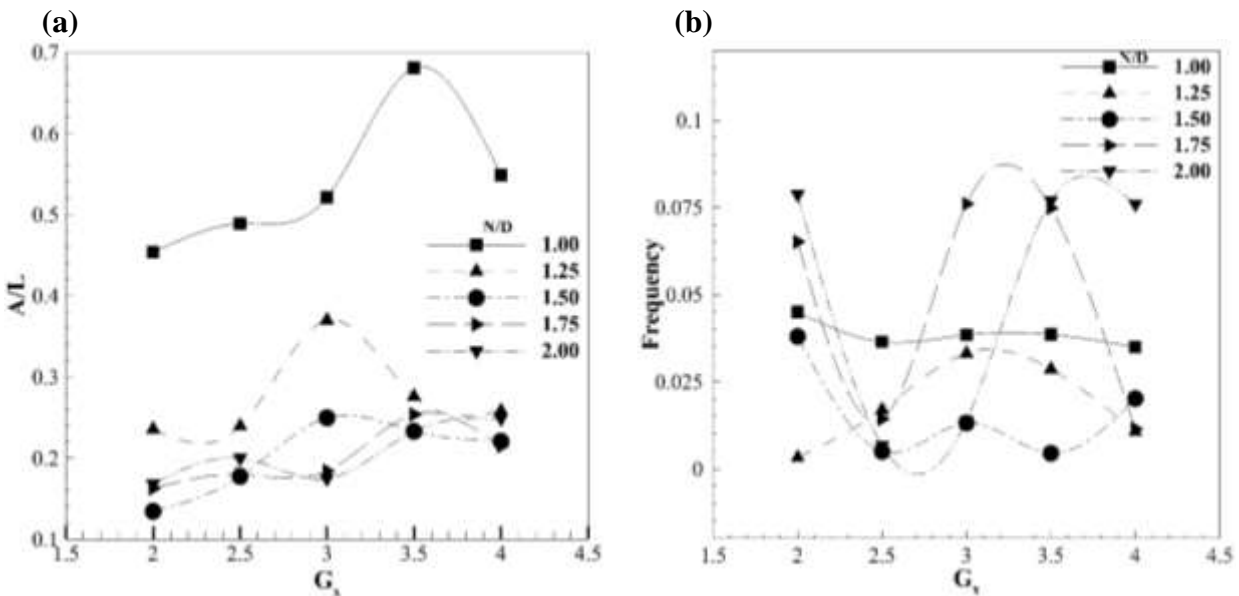


Figure 6.1: The results of the experimental cases for a range of G_x with different values of N/D ,
 (a) Non-dimensional amplitude of flapping (b) Normalized frequency of flapping

The plots of non-dimensional amplitude, A/L and normalized frequency versus G_x for different N/D values are shown in figure 6.1 (a) & (b), respectively. It can be seen from the plot that for $1.25 \leq N/D \leq 2.00$ and $2.0 \leq G_x \leq 4.0$, the value of A/L ranges from 0.12 to 0.25 with the

exception of $N/D = 1.25$ which corresponds to relatively higher value of $A/L = 0.375$ at $G_x = 3$. However, the case with the center-to-center distance between cylinders equals to the diameter of the cylinder i.e. $N/D = 1.00$, have relatively higher amplitude of flapping than other cases at all values of G_x . The case with $N/D = 1.00$ and $G_x = 3.5$ gives the highest amplitude of flapping i.e. $A/L = 0.68$. This is due to the fact that for $N/D = 1.00 \Rightarrow N = D$, there's no opening between two side by side arranged cylinders, hence it gives rise to the vortices of larger size which causes the eel to flap with the greater amplitude than previous cases.

As shown by figure 6.1 (b), the values of normalized frequency ranges from 0.005 to 0.08 for $1.00 \leq N/D \leq 2.00$ and $2.0 \leq G_x \leq 4.0$. The highest values are reported by the case with $N/D = 2.00$, $G_x = [2.0, 3.5, 4.0]$ and $N/D = 1.75$, $G_x = [3.0, 3.5]$. The cases with larger values of N/D generally reports the higher values of frequency because of the smaller vortices formed by both cylinders (bluff bodies separated by larger distance), at the both sides of the piezoelectric eel. The values of the frequencies reported by case with $N/D = 1.00 \Rightarrow N = D$ remains almost unaffected by the variation in G_x and are close to 0.0375.

6.3 Voltage and Power Produced by the Piezoelectric Eel's Flapping

As it is described earlier that the piezoelectric flag/eel used in the experiment generates an electric charge in response to applied mechanical stress. Hence, upon completing the circuit by connecting the impedance (load resistance), $R_L = 2.5 M\Omega$ the current starts to flow through the circuit and the potential different across the resistor can be measured. This measured value of voltage for any specific case is not some fixed/constant value, rather, it gives a complete alternating waveform. Although, neither this waveform represents a perfect sinusoidal waveform ($V = V_o \sin(\omega t)$) nor it's perfectly periodic, but this is an alternating wave which oscillates around the zero ($V = 0$), after some certain number of time steps. This is known as instantaneous voltages, as shown in the plot for the case with $N/D = 1.00$ and $G_x = 2.0$ in the figure 6.2. Similarly, the instantaneous voltages (set of voltage values against time steps) are measured for all cases to be tested. The root mean square (RMS) value of the voltages is a single value representing the whole wave form and can be obtained as follows:

$$V_{RMS} = \sqrt{\frac{1}{n} \sum_i V_i^2}$$

Where, V represents the instantaneous voltages, i is the instant (time step), n is the total number of instants (time steps) and V_{RMS} represents the root mean square value of the voltages.

In figure 6.2, the positive peak of the voltages lies at $V_{p+} = +6.368 \text{ mV}$, while the negative peak lies at $V_{p-} = -7.002 \text{ mV}$. However, the RMS value of the voltages, as calculated by the above formula, lies at $V_{RMS} = 3.615 \text{ mV}$.

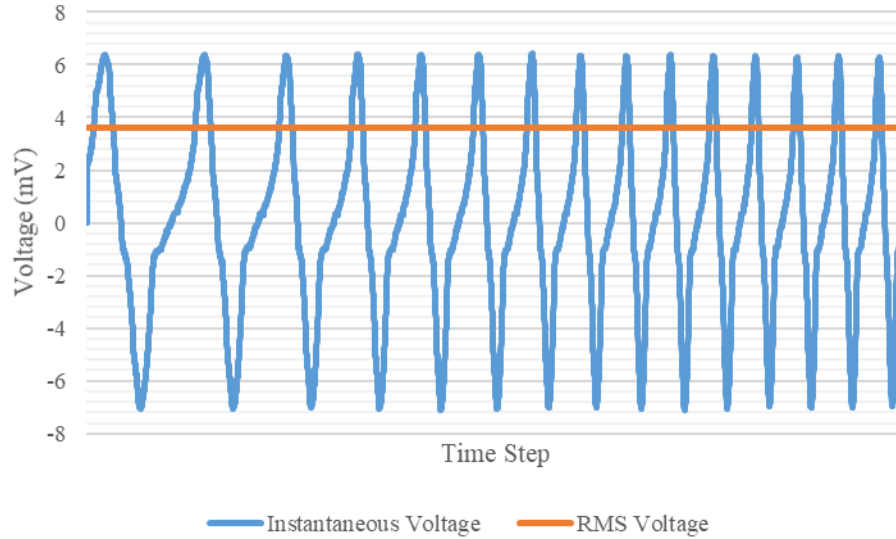


Figure 5.2: The instantaneous voltages produced by eel in the case with $N/D = 1.00$ and $G_x = 2.0$, as recorded by the DAQ setup

In the similar fashion, the root mean square values of voltages are calculated for all cases and plotted against the respective G_x values and specific N/D values of those cases, as shown in figure 6.3 (a).

Figure 6.3 (a) shows that the values of voltages ranges from 3.075 mV to 3.225 mV for $1.50 \leq N/D \leq 2.00$ and $2.0 \leq G_x \leq 4.0$. However, the cases with $1.00 \leq N/D \leq 1.25$ and $2.0 \leq G_x \leq 4.0$, gives particularly higher values of voltages than other cases. These values range from 3.525 mV to 3.675 mV . The reason behind these high values of voltages is the higher values of amplitude, A and hence the non-dimensional amplitude, A/L of flapping for these cases. Greater is the amplitude of flapping, higher would be the deformation in piezoelectric flag/eel and stronger would be the piezoelectric effect, hence greater would be the potential difference across the load resistor, R_L .

For the complete electric circuit having load resistor R_L , with the voltages across the resistor, V and the current flowing through the resistor, I , the electric power P is given as:

$$P = V \times I$$

As the Ohm's law states: $V = I \times R_L$, therefore,

$$P = I^2 \times R_L = \frac{V^2}{R_L}$$

The electric power generated (provided to the load resistor) by the flapping piezoelectric flag/eel is evaluated using the above formula for all cases and plotted against their respective parameters, N/D and G_x , as shown in figure 6.3 (b).

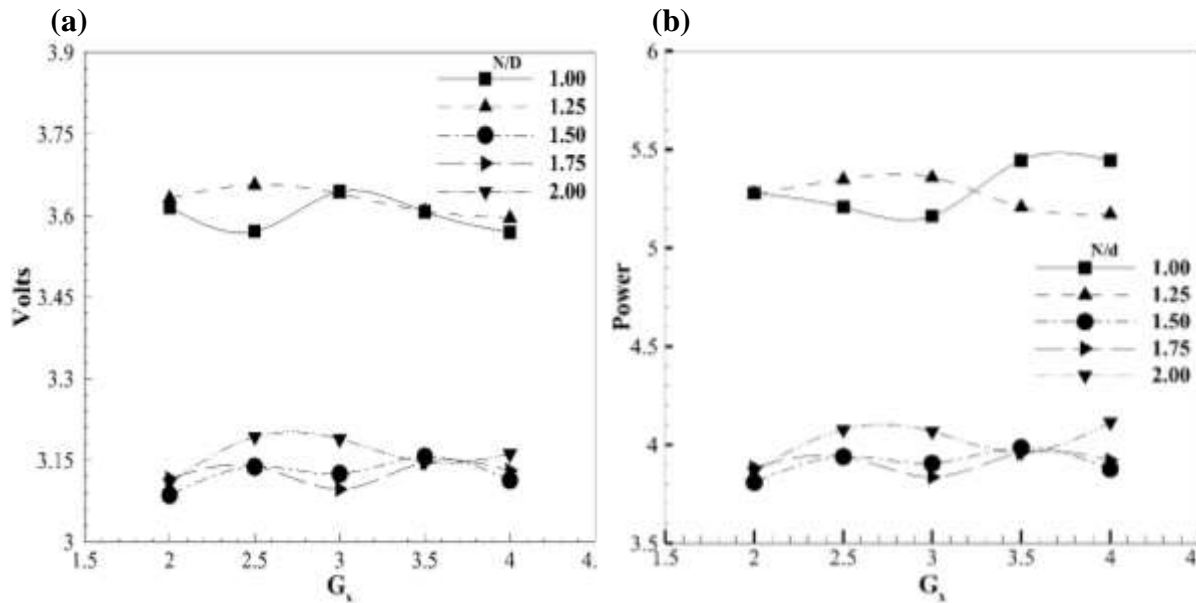


Figure 6.3: Voltages and power produced by the piezoelectric eel for the different cases of the experimentation

Figure 6.3 (b) shows the trend almost similar to that of voltages for all test cases. The values of power ranges from $3.75 \mu W$ to $4.25 \mu W$ for $1.50 \leq N/D \leq 2.00$ and $2.0 \leq G_x \leq 4.0$. However, the cases with $1.00 \leq N/D \leq 1.25$ and $2.0 \leq G_x \leq 4.0$, gives particularly higher values of power than other cases. These values range from $5.15 \mu W$ to $5.50 \mu W$. The reason behind these high values of power is the higher values of amplitude, A and hence the non-dimensional

amplitude, A/L of flapping for these cases. Greater is the amplitude of flapping, higher would be the deformation in piezoelectric flag/eel and stronger would be the piezoelectric effect, hence greater would be the potential difference V across the load resistor R_L and higher would be the power P provided to the resistor.

Hence, the values of voltages and generated power, as shown in figure 6.3 (a) & (b), are higher for the cases with $1.00 \leq N/D \leq 1.25$, because of their higher amplitude of flapping, as shown in figure 6.1 (a), and hence higher deformation in the eel and therefore the higher piezoelectric effect.

CHAPTER 7: CONCLUSION AND FUTURE RECOMMENDATIONS

This is the last chapter of the dissertation which concludes the whole study based on the concepts discussed in the previous chapters, reviewed literature, observations during experimentation and the results obtained. It also provides the future recommendations for further continuation and extension of the research work on the topic.

7.1 Conclusion

The improvement in power generation from the piezoelectric eel excited by striking vortices waked by two side by side cylindrical bluff bodies in a staggered arrangement has been explored and discussed, in this study. Though a single cylindrical bluff body can be used to get the continuous and stable power in the range $G_x = 0.5 - 2.0$ for the fluid velocity above $U_\infty = 0.23 \text{ m/s}$, but two side by side cylinders in staggered arrangement showed significant increase in the generated power for a broader range of $G_x = 2.0 - 4.0$ at the given velocity with high non-dimensional amplitude (A/L) and frequency (f). Different cases with varying N/D values from 1.00 to 2.00 were tested. The comparison of flapping and amplitude response at each point for all cases is made to understand the effects of system's variable parameters on the results and their trends. The power generated at each point was mainly focused for all cases and their comparative study to find optimal configuration. For the low given fluid speed and the cylinder arrangement with $N/D = 1.00 - 1.25$, the continuous oscillations and higher output power persisting for a wider range $G_x = 2.0 - 4.0$ was observed, which makes its application to the real-life systems feasible, as water and air usually flow at lower speeds. The study shows that the behavior of the fluid in the wake region of the system varies including formation length and the wake width with N/D that requires the variation in the inter-cylinder and streamwise distances for optimal synchronization for every case. Therefore, the arrangement with $N/D = 1$ roughly provided a 200 % higher amplitude of flapping due to its greater wake width and the frequency of flapping, which are the main factors responsible for energy harvesting, and leads to higher deformation in the piezoelectric layer. Experiments clearly showed that output power grows higher with the increase in the cylinders-eel's streamwise gap till $G_x = 4.0$, higher values were obtained at $G_x = 3.5 - 4.0$ for the velocity, $U_\infty = 0.31 \text{ m/s}$, with $N/D = 1.00 - 1.25$. The power generated by these configurations ranges from $5.15 \mu W$ to $5.50 \mu W$. Hence, the stated

configurations with $N/D = 1.00 - 1.25$ gives a significant advantage over other arrangements as a vibration source of energy harvesting from the flowing water, and the generated power would gradually increase with the stream-wise distance. The harvested power comes totally from the renewable sources of energy, does not have any harmful effect on the environment, atmosphere or ecosystem, and can replace small trickle charge and chemical batteries for powering micro electromechanical sensors like the sensors used for structural health monitoring in the remote areas. All in all, this study makes an effective contribution to the field of energy harvesting from striking vortices by setting the streamwise distance and center-to-center gap between the staggered cylindrical bluff bodies.

7.2 Future Recommendations

In this experimental study, the improvement in energy harvested using piezoelectric eel excited into vibrations by striking vortices waked by two side by side cylindrical bluff bodies in a staggered arrangement has been investigated and discussed. Different system configurations have been tested experimentally and compared with each other to find the optimal configuration. However, the future recommendations to continue the study, to improve the results of study or to enhance the scope of the study, are presented below.

- This study can be further continued by carrying out the water tunnel tests at different flow speed (or different Reynold's numbers, Re) to find the effect of flow speed on the overall power generation and to estimate the critical speed range resulting maximum and minimum power generation for all designs. This would help us further to come up with the better conclusion about the optimal designs and configuration's parameters.
- This study can be further extended by working on the visualization of flow field, turbulence around the cylinders and eel, and the vortices generated by different test case scenarios. The experimental technique of Particle Image Velocimetry (PIV) can employ to perform these tasks. The size of vortices and the profile of flow can be determined for all cases using PIV, and the results can be compared with each other to make inferences about the relationship between vortex's type and size, and the output power.
- Computational Fluid Dynamics (CFD) is the technique of solving the governing equations of fluid flow including velocity, momentum and energy equations, numerically by converting

the continuous fluid domain into finite number of cells (discretized domain) and applying Finite Volume Method (FVM) to approximate the solution. Many commercial and opensource CFD packages are available, including *ANSYS*, *OpenFOAM*, *PowerFLOW*, *SimScale*, *COMSOL Multiphysics*, *Autodesk CFD* etc. This study can be further extended and validated by modelling and simulating the simple fluid flow as well as the Fluid Solid Interaction (FSI) involved in the problem to validate the results obtained by water-tunnel experimentation and PIV.

- This experimental study can also be extended by using more staggered cylinders and multiple piezoelectric flags/eels to produce the power from the vortices waked by those staggered cylinders and study the increase in energy harvesting i.e. power generation.

Apart from these recommended task, further extensions and modifications can also be employed to improve the results and enhance the scope of this study. However, the main aim of every study would be to generate the power from renewable energy sources in an environment friendly and harmless way, so that the humanity may advance towards safe, sustainable and better future.

APPENDIX A

This appendix contains the important *MATLAB* codes used to process the data obtained through experimentation using data acquisition setup according to the methodology explained in Chapter 5 to get the results of different parameters, presented in Chapter 6.

A-1 Video Processing

The following code is used to process the captured video shot of the eel's flapping to get its processed image of flapping showing the amplitude of flapping, and the data files containing the information of flapping's frequency and amplitude.

```
clc;
clear ;
close all;
% Batch Processing
video_files = {'C0004.MP4'};
vidObj = VideoReader(video_files{1}); %
I = readFrame(vidObj);
[J, rect] = imcrop(I); % J is image and rect is coor
% Batch End
%Converting Vedio to a Array of Vector Frames
for vid = 1:length(video_files)
disp('Working on video')
vidObj = VideoReader(video_files{vid});
tip_pos = zeros(1,2);
cuurentframe = 1;
ss = zeros(size(J)); % For adding Images
vidObj.CurrentTime = 0.0;
while hasFrame(vidObj)
    F = readFrame(vidObj);
    fprintf('Current Processing Frame:\t %d\n', cuurentframe
%Converting from RGB to Grayscale and save them in Cell Array
    U = rgb2gray(F);
%Cropping frames to desire Workspace
    Q=imcrop(U, rect); %XY value to crop them in a desired workspace
% Converting Array of Crop Images into Binary Image
    W=Q>235; %threshold to remove unwanted region
    %W = imbinarize(Q);
% Image Dilation
    %se = strel('line',100,0); % 50 is length of line
    %gg = imdilate(W,se);
    %se = strel('line',105,0); % 50 is length of line
```

```

    %Wm = imerode(gg,se);
    ss=ss+W;
    %-----
    regionstats = regionprops(W, 'all');
    [~, largestidx] = max([regionstats.Area]); %find index of largest region
    %x=regionstats(largestidx).BoundingBox; %coordinate of bounding box of
largest region
    %y=regionstats(largestidx).PixelList; %coordinate of all pixels in
the region as a matrix
    h=regionstats(largestidx).Extrema; %coordinate of extreme axis
    pcoor = (h(3,:) + h(4,:)).*0.5;
    tip_pos(cuurentframe,:) = pcoor;
    cuurentframe = cuurentframe + 1;
% figure; imshow(Q)
% % figure; imshow(Wm)
% viscircles(pcoor,10);
% pause;
% close;close;
end
disp('Done')
xlswrite( strcat(video_files{vid} , '.xlsx'),tip_pos)
imwrite(double(ss),strcat (video_files{vid}, '.jpg'))
end % batch loop end
%%
S=double(ss);
imshow(S);
% rectangle('Position',regionstats(largestidx).BoundingBox, 'EdgeColor',
% 'r') %Rectangle to check if flap is detected properly
% imshow(W)
% viscircles(pcoor,10) TO plot a circle
%%
[temp,originalpos] = sort( h(:,1), 'descend' );
max_num = input('Ist ? max. values to read :');
n = temp(1:max_num); % ist three max values
p=originalpos(1:max_num); % idx in original array
% [v,idx] = max(h);
val = h(p,2);
fprintf('Ist three max values in ist col:\n');disp(n);
fprintf('Corresponding Values in 2nd col:\n');disp(val);
for aa =[1, 2, 3]
    disp(aa)
end

```

A-2 Frequency and Amplitude Response Visualization

The data files, obtained using the code given in A-1, containing the data points of the frequency and amplitude response of the vibrating eel can be further analyzed in and plotted in *Microsoft Excel* or *MATLAB*. The following code is used to import the data from the data files into the *MATLAB* and then plot them to visualize the frequency and amplitude response of the vibrating piezoelectric eel.

```

%% filtering matlab
clc
clear all
[v] = xlsread('C0016.MP4.xlsx', 'sheet1','D1:D3240');
dt= xlsread('C0016.MP4.xlsx', 'sheet1','C1:C3240');
figure(1)
plot(dt,v)
title ('')
xlabel('Time Step')
ylabel('Amplitude')
%% reading of excel file for specified column/values of peak and lower
position of flapping
    data = [v];
%A = [ 65 66 67 68 69 70];
%chr = mat2str ([data]);
A = data'
a = max(A);
b = min(A);
c = [a,b];
xlswrite('Delta-Y.xlsx',c);
%% plot magnitude spectrum of a signal
clc
X_mags=abs(fft(v))
figure(2)
plot(X_mags)
xlabel('DFT Bins')
ylabel('Magnititude')
%% filter
%plot the first half of normalized frequency
%num_bins = length(X_mags);
num_bins = length(X_mags);
figure(3)
plot ([0:1/(num_bins/2 -1):1] , X_mags(1:num_bins/2))
xlabel('Normalizedd frequency ') %(\pi rads/sample)
ylabel('E')
%% reading of excel file for specified column/values of voltages
    data = X_mags;
%A = [ 65 66 67 68 69 70];
%chr = mat2str ([data]);
B = data'
C =(B(1,5:end))
d = max(C);
e = min(C);
f = [d,e];
xlswrite('Energy Spectra.xlsx',f);
%%
[b_cheby,a_cheby] = cheby1(9, 0.9, 0.02, 'low');
H_cheby = freqz(b_cheby, a_cheby);
%plot filter

```

```
norm_freq_axis = [0:1/(512 -1):1];  
figure(4)  
plot(norm_freq_axis, abs(H_cheby), 'r')  
legend('Chebyshev')  
xlabel('Normalised Frequency'); ylabel('Magnitude')
```

A-3 Measurement of Flapping Amplitude

The following code is used to import the processed image of the eel's flapping, obtained by using the code given in A-1, and measure the length of eel and the maximum amplitude of its flapping.

```
clc  
clear all  
close all  
I = imread('C0011.MP4.jpg');  
imshow(I)
```


REFERENCES

- [1] “Key World Energy Statistics,” 2019. [Online]. Available: https://webstore.iea.org/download/direct/2831?filename=key_world_energy_statistics_2019.pdf.
- [2] M. Sato, “Thermochemistry of the formation of fossil fuels.,” *Spec. Publ. - Geochemical Soc.*, vol. 2, no. Fluid-Miner. Interact., pp. 271–283, 1991.
- [3] M. E. Karim *et al.*, “Energy revolution for our common future: An evaluation of the emerging international renewable energy law,” *Energies*, vol. 11, no. 7, 2018, doi: 10.3390/en11071769.
- [4] M. M. Bernitsas, K. Raghavan, Y. Ben-Simon, and E. M. H. Garcia, “VIVACE (Vortex Induced Vibration Aquatic Clean Energy): A new concept in generation of clean and renewable energy from fluid flow,” *J. Offshore Mech. Arct. Eng.*, vol. 130, no. 4, pp. 1–19, 2008, doi: 10.1115/1.2957913.
- [5] H. Mutsuda, R. Watanabe, S. Azuma, Y. Tanaka, and Y. Doi, “Omae2013-10078,” *Ocean Power Gener. Using Flex. Piezoelectric Device*, pp. 1–9, 2014.
- [6] U. Latif *et al.*, “Experimental investigation of energy harvesting behind a bluff body,” *J. Renew. Sustain. Energy*, vol. 12, no. 3, 2020, doi: 10.1063/1.5144347.
- [7] G. R. Center, “First Law of Thermodynamics,” NASA. <https://www.grc.nasa.gov/www/k-12/airplane/thermo1.html>.
- [8] B. T. L. App, “Energy Conversion.” <https://byjus.com/physics/energy-conversion>.
- [9] Learn with Kassia, “Forms of Energy.” <https://mskuksclass.weebly.com/lesson-2-forms-of-energy.html>.
- [10] Energy Education, “Efficiency.” <https://energyeducation.ca/encyclopedia/Efficiency>.
- [11] Siyavula, “Renewable and non-renewable energy.” <https://intl.siyavula.com/read/science/grade-7/sources-of-energy>.

- [12] AWEA, “Basics of Wind Energy.” <https://www.awea.org/wind-101>.
- [13] OpenEI, “Wind Energy,” [Online]. Available: https://openei.org/wiki/Wind_energy.
- [14] GE Renewable Energy, “What is Wind Power.” <https://www.ge.com/renewableenergy>.
- [15] Wikipedia, “Wind Turbine.” https://en.wikipedia.org/wiki/Wind_turbine.
- [16] Energy Education, “Types of Wind Turbines.” https://energyeducation.ca/encyclopedia/Types_of_wind_turbines.
- [17] P. A. Kozak, “Effects of Unsteady Aerodynamics on Vertical-Axis Wind Turbine Performance,” no. July, 2014.
- [18] Dolcera, “Different Types and Parts of a Horizontal Axis Wind Turbines.” <https://dolcera.com/wiki/index.php>.
- [19] Electrical Academia, “Horizontal-Axis Wind Turbine (HAWT) Working Principle | Single Blade, Two Blade, Three-Blade Wind Turbine.” <https://electricalacademia.com/renewable-energy>.
- [20] Office of Energy Efficiency and Renewable Energy, “Advantages and Challenges of Wind Energy,” [Online]. Available: <https://www.energy.gov/eere/wind>.
- [21] Wikipedia, “Hydropower.” <https://en.wikipedia.org/wiki/Hydropower>.
- [22] U.S. Energy Information Administration, “Hydropower Explained.” <https://www.eia.gov/energyexplained/hydropower/>.
- [23] Office of Energy Efficiency and Renewable Energy, “Types of Hydropower Plants,” [Online]. Available: <https://www.energy.gov/eere/water/types-hydropower-plants>.
- [24] The Editors of Encyclopaedia Britannica, “Waterwheel,” *Encyclopædia Britannica*. <https://www.britannica.com/technology/waterwheel-engineering>.
- [25] OpenLearn, “Types of hydroelectric plant,” *Open University*. <https://www.open.edu/openlearn/ocw>.

- [26] Hydropower Learning Centre, “Hydropower,” *Renewables First*.
<https://www.renewablesfirst.co.uk/hydropower/hydropower-learning-centre>.
- [27] SSWM, “Water Energy,” SSWM. <https://sswm.info/water-nutrient-cycle/water-use/hardwares/water-energy>.
- [28] GreenBug Energy, “Types of Turbines.” <https://greenbugenergy.com/get-educated-knowledge/types-of-turbines>.
- [29] J. Chen, J. Chen, H. X. Yang, C. P. Liu, C. H. Lau, and M. Lo, “A novel vertical axis water turbine for power generation from water pipelines,” no. November, 2016, doi: 10.1016/j.energy.2013.01.064.
- [30] Hydro Quebec, “The Advantages of Hydropower.”
<http://www.hydroquebec.com/learning/hydroelectricite>.
- [31] Department of Ocean Engineering, “Marine Hydrodynamics,” MIT.
http://web.mit.edu/fluids-modules/www/potential_flows/LecturesHTML/lec01/lecture1.html.
- [32] Lumen Learning, “Solid, Liquid and Gas.”
<https://courses.lumenlearning.com/cheminter/chapter/solid-liquid-and-gas/>.
- [33] The Editors of Encyclopaedia Britannica, “Density,” *Encyclopædia Britannica*, 2020.
<https://www.britannica.com/science/density>.
- [34] Glenn Research Center, “Fluids Pressure and Depth,” NASA, 1996.
https://www.grc.nasa.gov/www/k-12/WindTunnel/Activities/fluid_pressure.html.
- [35] Mecholic, “Absolute Pressure, Gauge Pressure and Vacuum Pressure,” *Mecholic*, 2018.
<https://www.mecholic.com/2018/06/absolute-pressure-gauge-pressure.html>.
- [36] Princeton University, “What is viscosity?,” *Princeton University*.
https://www.princeton.edu/~gasdyn/Research/T-C_Research_Folder/Viscosity_def.html.
- [37] NPTEL, “Cause of Viscosity,” *National Programme on Technology Enhanced Learning*.

- <https://nptel.ac.in/content/storage2/courses/112104118/lecture-1/1-11-cause-of-viscosity.htm>.
- [38] Multidisciplinary Design Project (MDP), “Flow Description, Streamline, Pathline, Streakline and Timeline,” *Cambridge-MIT Institute*. <http://www-mdp.eng.cam.ac.uk>.
- [39] eCourses, “Streamline, Streakline and Pathline,” *The University of Oklahoma*. <https://www.ecourses.ou.edu>.
- [40] Multidisciplinary Design Project (MDP), “One, Two and Three Dimensional Flows,” *Cambridge-MIT Institute*. <http://www-mdp.eng.cam.ac.uk>.
- [41] J. M. C. Yunus A. Çengel, *Fluid Mechanics: Fundamentals and Applications*. 2006.
- [42] F. M. White, *Fluid Mechanics*. McGraw Hill, 2011.
- [43] T. H. O. Bruce R. Munson, Alric P. Rothmayer, *Fundamentals of Fluid Mechanics*, 7th ed. Wiley, 2012.
- [44] J. Liburdy, *Intermediate Fluid Mechanics*, 1st ed. Oregon State University.
- [45] Glenn Research Center, “Boundary Layer,” *NASA*. <https://www.grc.nasa.gov/www/k-12/airplane/boundlay.html>.
- [46] R. Fitzpatrick, “Boundary Layer on a Flat Plate,” *The University of Texas at Austin*, 2018. <http://farside.ph.utexas.edu/teaching/336L/Fluidhtml/node113.html>.
- [47] “Bicycle Aerodynamics: Drag of Blunt Bodies and Streamlined Bodies,” *Princeton University*, 2007. https://www.princeton.edu/~asmits/Bicycle_web/blunt.html.
- [48] G. Buresti, “Bluff-Body Aerodynamics.” Department of Aerospace Engineering, University of Pisa, Italy, 2000, [Online]. Available: <https://www.mech.kth.se/courses/5C1211/BluffBodies.pdf>.
- [49] M. Perez, S. Boisseau, P. Gasnier, J. Willemin, and J. L. Reboud, “An electret-based aeroelastic flutter energy harvester,” *Smart Mater. Struct.*, vol. 24, no. 3, p. 35004, 2015,

doi: 10.1088/0964-1726/24/3/035004.

- [50] F. Candelier, M. Porez, and F. Boyer, “Note on the swimming of an elongated body in a non-uniform flow,” *J. Fluid Mech.*, vol. 716, pp. 616–637, 2013, doi: 10.1017/jfm.2012.560.
- [51] R. Fitzpatrick, “Fluid Mechanics: Vortex Lines, Vortex Tubes, and Vortex Filaments,” *The University of Texas at Austin*, 2016. <http://farside.ph.utexas.edu/teaching/336L/Fluidhtml/node61.html>.
- [52] C. H. K. Williamson and R. Govardhan, “Vortex-induced vibrations,” *Annu. Rev. Fluid Mech.*, vol. 36, no. 1982, pp. 413–455, 2004, doi: 10.1146/annurev.fluid.36.050802.122128.
- [53] H. L. Dai, A. Abdelkefi, and L. Wang, “Theoretical modeling and nonlinear analysis of piezoelectric energy harvesting from vortex-induced vibrations,” *J. Intell. Mater. Syst. Struct.*, vol. 25, no. 14, pp. 1861–1874, 2014, doi: 10.1177/1045389X14538329.
- [54] C. B. Williams and R. B. Yates, “Analysis of a micro-electric generator for microsystems,” *Sensors Actuators, A Phys.*, vol. 52, no. 1–3, pp. 8–11, 1996, doi: 10.1016/0924-4247(96)80118-X.
- [55] R. Caliò *et al.*, “Piezoelectric energy harvesting solutions,” *Sensors (Switzerland)*, vol. 14, no. 3, pp. 4755–4790, 2014, doi: 10.3390/s140304755.
- [56] J. A. C. Dias, C. De Marqui, and A. Erturk, “Hybrid piezoelectric-inductive flow energy harvesting and dimensionless electroaeroelastic analysis for scaling,” *Appl. Phys. Lett.*, vol. 102, no. 4, pp. 1–6, 2013, doi: 10.1063/1.4789433.
- [57] F. U. Khan and I. Ahmad, “Review of Energy Harvesters Utilizing Bridge Vibrations,” vol. 2016, 2016.
- [58] P. A. Kumar, P. S. S. Balpande, and P. S. C. Anjankar, “Electromagnetic Energy Harvester for Low Frequency Vibrations using MEMS,” *Procedia - Procedia Comput. Sci.*, vol. 79, pp. 785–792, 2016, doi: 10.1016/j.procs.2016.03.104.

- [59] S. Boisseau, G. Despesse, and B. A. Seddik, “Electrostatic Conversion for Vibration Energy Harvesting.”
- [60] S. Boisseau, G. Despesse, and B. A. Seddik, “Electrostatic Conversion for Vibration Energy Harvesting,” pp. 1–39, 2012.
- [61] S. Pobering and N. Schwesinger, “A novel hydropower harvesting device,” *Proc. - 2004 Int. Conf. MEMS, NANO Smart Syst. ICMENS 2004*, pp. 480–485, 2004, doi: 10.1109/icmens.2004.1332349.
- [62] K. S. Ramadan, D. Sameoto, and S. Evoy, “A review of piezoelectric polymers as functional materials for electromechanical transducers,” *Smart Mater. Struct.*, vol. 23, no. 3, 2014, doi: 10.1088/0964-1726/23/3/033001.
- [63] C. De Marqui, *Piezoelectric energy harvesting*. 2016.
- [64] O. Doaré and S. Michelin, “Piezoelectric coupling in energy-harvesting fluttering flexible plates: Linear stability analysis and conversion efficiency,” *J. Fluids Struct.*, vol. 27, no. 8, pp. 1357–1375, 2011, doi: 10.1016/j.jfluidstructs.2011.04.008.
- [65] F. Pan, Z. Xu, L. Jin, P. Pan, and X. Gao, “Designed Simulation and Experiment of a Piezoelectric Energy Harvesting System Based on Vortex-Induced Vibration,” *IEEE Trans. Ind. Appl.*, vol. 53, no. 4, pp. 3890–3897, 2017, doi: 10.1109/TIA.2017.2687401.
- [66] S. Roundy *et al.*, “Improving power output for vibration-based energy scavengers,” *IEEE Pervasive Comput.*, vol. 4, no. 1, pp. 28–36, 2005, doi: 10.1109/MPRV.2005.14.
- [67] C. Grouthier, S. Michelin, R. Bourguet, Y. Modarres-Sadeghi, and E. de Langre, “On the efficiency of energy harvesting using vortex-induced vibrations of cables,” *J. Fluids Struct.*, vol. 49, pp. 427–440, 2014, doi: 10.1016/j.jfluidstructs.2014.05.004.
- [68] U. Latif *et al.*, “Experimental electro-hydrodynamic investigation of flag-based energy harvesting in the wake of inverted C-shape cylinder,” *Energy*, vol. 215, 2021, doi: 10.1016/j.energy.2020.119195.

- [69] M. Saeed, E. Uddin, A. Mubashar, S. U. Zahir, and A. A. Zaidi, "Design and development of low-speed water tunnel," *Proc. 2018 15th Int. Bhurban Conf. Appl. Sci. Technol. IBCAST 2018*, vol. 2018-January, pp. 614–619, 2018, doi: 10.1109/IBCAST.2018.8312288.
- [70] J. Wang, L. Geng, L. Ding, H. Zhu, and D. Yurchenko, "The state-of-the-art review on energy harvesting from flow-induced vibrations," *Appl. Energy*, vol. 267, no. March, p. 114902, 2020, doi: 10.1016/j.apenergy.2020.114902.
- [71] E. Lefevre, A. Badel, C. Richard, L. Petit, and D. Guyomar, "A comparison between several vibration-powered piezoelectric generators for standalone systems," *Sensors Actuators, A Phys.*, vol. 126, no. 2, pp. 405–416, 2006, doi: 10.1016/j.sna.2005.10.043.
- [72] C. De Marqui, W. G. R. Vieira, A. Erturk, and D. J. Inman, "Modeling and analysis of piezoelectric energy harvesting from aeroelastic vibrations using the doublet-lattice method," *J. Vib. Acoust. Trans. ASME*, vol. 133, no. 1, pp. 1–9, 2011, doi: 10.1115/1.4002785.
- [73] C. K. ee and F. C. Moon, "Laminated piezopolymer plates for torsion and bending sensors and actuators," *J. Acoust. Soc. Am.*, vol. 85, no. 6, pp. 2432–2439, 1989, doi: 10.1121/1.397792.
- [74] L. B. Zhang, H. L. Dai, A. Abdelkefi, and L. Wang, "Experimental investigation of aerodynamic energy harvester with different interference cylinder cross-sections," *Energy*, vol. 167, pp. 970–981, 2019, doi: 10.1016/j.energy.2018.11.059.
- [75] A. H. Techet, J. J. Allen, and A. J. Smits, "Piezoelectric Eels for Energy Harvesting in the Ocean," *Proc. Int. Offshore Polar Eng. Conf.*, vol. 12, pp. 713–718, 2002.
- [76] G. W. Taylor, J. R. Burns, S. M. Kammann, W. B. Powers, and T. R. Welsh, "The energy harvesting Eel: A small subsurface ocean/river power generator," *IEEE J. Ocean. Eng.*, vol. 26, no. 4, pp. 539–547, 2001, doi: 10.1109/48.972090.
- [77] G. Taylor and P. R. S. L. A, "Analysis of the swimming of long and narrow animals," *Proc. R. Soc. London. Ser. A. Math. Phys. Sci.*, vol. 214, no. 1117, pp. 158–183, 1952,

doi: 10.1098/rspa.1952.0159.

- [78] D. N. Beal, F. S. Hover, M. S. Triantafyllou, J. C. Liao, and G. V. Lauder, “Passive propulsion in vortex wakes,” *J. Fluid Mech.*, vol. 549, pp. 385–402, 2006, doi: 10.1017/S0022112005007925.
- [79] S. Alben, “Flag flutter in inviscid channel flow,” *Phys. Fluids*, vol. 27, no. 3, 2015, doi: 10.1063/1.4915897.
- [80] S. Chad Gibbs, I. Wang, and E. Dowell, “Theory and experiment for flutter of a rectangular plate with a fixed leading edge in three-dimensional axial flow,” *J. Fluids Struct.*, vol. 34, pp. 68–83, 2012, doi: 10.1016/j.jfluidstructs.2012.06.009.
- [81] L. Schouveiler and C. Eloy, “Coupled flutter of parallel plates,” *Phys. Fluids*, vol. 21, no. 8, pp. 1–5, 2009, doi: 10.1063/1.3204672.
- [82] C. Eloy, N. Kofman, and L. Schouveiler, “The origin of hysteresis in the flag instability,” *J. Fluid Mech.*, vol. 691, no. December 2011, pp. 583–593, 2012, doi: 10.1017/jfm.2011.494.
- [83] C. Eloy, R. Lagrange, C. Souilliez, and L. Schouveiler, “Aeroelastic instability of cantilevered flexible plates in uniform flow,” *J. Fluid Mech.*, vol. 611, pp. 97–106, 2008, doi: 10.1017/S002211200800284X.
- [84] J. A. Dunnmon, S. C. Stanton, B. P. Mann, and E. H. Dowell, “Power extraction from aeroelastic limit cycle oscillations,” *J. Fluids Struct.*, vol. 27, no. 8, pp. 1182–1198, 2011, doi: 10.1016/j.jfluidstructs.2011.02.003.
- [85] D.-A. Wang, H.-T. Pham, C.-W. Chao, and J. M. Chen, “A Piezoelectric Energy Harvester Based on Pressure Fluctuations in Karman Vortex Street,” *Proc. World Renew. Energy Congr. – Sweden, 8–13 May, 2011, Linköping, Sweden*, vol. 57, pp. 1456–1463, 2011, doi: 10.3384/ecp110571456.
- [86] J. Curie and P. Curie, “Development by Pressure of Polar Electricity in Hemihedral Crystals with Inclined Faces,” *Bull. la Société minéralogique Fr.*, vol. 3, no. 4, pp. 90–93,

1880, [Online]. Available: https://www.persee.fr/doc/bulmi_0150-9640_1880_num_3_4_1564.

- [87] D. Kim, J. Cossé, C. Huertas Cerdeira, and M. Gharib, “Flapping dynamics of an inverted flag,” *J. Fluid Mech.*, vol. 736, pp. 1–12, 2013, doi: 10.1017/jfm.2013.555.
- [88] H. Kim, S. Kang, and D. Kim, “Dynamics of a flag behind a bluff body,” *J. Fluids Struct.*, vol. 71, pp. 1–14, 2017, doi: 10.1016/j.jfluidstructs.2017.03.001.
- [89] B. Zhang, B. Song, Z. Mao, W. Tian, and B. Li, “Numerical investigation on VIV energy harvesting of bluff bodies with different cross sections in tandem arrangement,” *Energy*, vol. 133, pp. 723–736, 2017, doi: 10.1016/j.energy.2017.05.051.
- [90] F. R. Liu, H. X. Zou, W. M. Zhang, Z. K. Peng, and G. Meng, “Y-type three-blade bluff body for wind energy harvesting,” *Appl. Phys. Lett.*, vol. 112, no. 23, pp. 1–6, 2018, doi: 10.1063/1.5029415.
- [91] J. W. Moon *et al.*, “Optimal design and application of a piezoelectric energy harvesting system using multiple piezoelectric modules,” *J. Electroceramics*, vol. 32, no. 4, pp. 396–403, 2014, doi: 10.1007/s10832-014-9934-0.
- [92] G. J. Song *et al.*, “Development of a pavement block piezoelectric energy harvester for self-powered walkway applications,” *Appl. Energy*, vol. 256, no. April, p. 113916, 2019, doi: 10.1016/j.apenergy.2019.113916.
- [93] M. Usman, A. Hanif, I. H. Kim, and H. J. Jung, “Experimental validation of a novel piezoelectric energy harvesting system employing wake galloping phenomenon for a broad wind spectrum,” *Energy*, vol. 153, pp. 882–889, 2018, doi: 10.1016/j.energy.2018.04.109.
- [94] R. Song, X. Shan, F. Lv, and T. Xie, “A study of vortex-induced energy harvesting from water using PZT piezoelectric cantilever with cylindrical extension,” *Ceram. Int.*, vol. 41, no. S1, pp. S768–S773, 2015, doi: 10.1016/j.ceramint.2015.03.262.
- [95] X. Shan, R. Song, M. Fan, and T. Xie, “Energy-harvesting performances of two tandem

- piezoelectric energy harvesters with cylinders in water,” *Appl. Sci.*, vol. 6, no. 8, 2016, doi: 10.3390/app6080230.
- [96] K. Shoele and R. Mittal, “Energy harvesting by flow-induced flutter in a simple model of an inverted piezoelectric flag,” *J. Fluid Mech.*, vol. 790, pp. 582–606, 2016, doi: 10.1017/jfm.2016.40.
- [97] Y. Tanaka, T. Oko, H. Mutsuda, R. Patel, S. McWilliam, and A. A. Popov, “An experimental study of wave power generation using a flexible piezoelectric device,” *J. Ocean Wind Energy*, vol. 2, no. 1, pp. 28–36, 2015.
- [98] D. Dessi and S. Mazzocconi, “Aeroelastic behavior of a flag in ground effect,” *J. Fluids Struct.*, vol. 55, pp. 303–323, 2015, doi: 10.1016/j.jfluidstructs.2015.03.006.
- [99] J. Wang, S. Zhou, Z. Zhang, and D. Yurchenko, “High-performance piezoelectric wind energy harvester with Y-shaped attachments,” *Energy Convers. Manag.*, vol. 181, no. September 2018, pp. 645–652, 2019, doi: 10.1016/j.enconman.2018.12.034.
- [100] AEROLAB, “Water Tunnels & Channels,” *AEROLAB*. <https://www.aerolab.com/products/water-tunnels-channels/>.
- [101] “Data Acquisition (DAQ),” *National Instruments*. <https://www.ni.com/en-lb/shop/data-acquisition.html>.